PHYSICS-BASED DIESEL ENGINE MODEL DEVELOPMENT CALIBRATION AND VALIDATION FOR ACCURATE CYLINDER PARAMETERS AND NOX PREDICTION

by

Vaibhav Kailas Ahire

A Thesis

Submitted to the Faculty of Purdue University

In Partial Fulfillment of the Requirements for the degree of

Master of Science in Mechanical Engineering

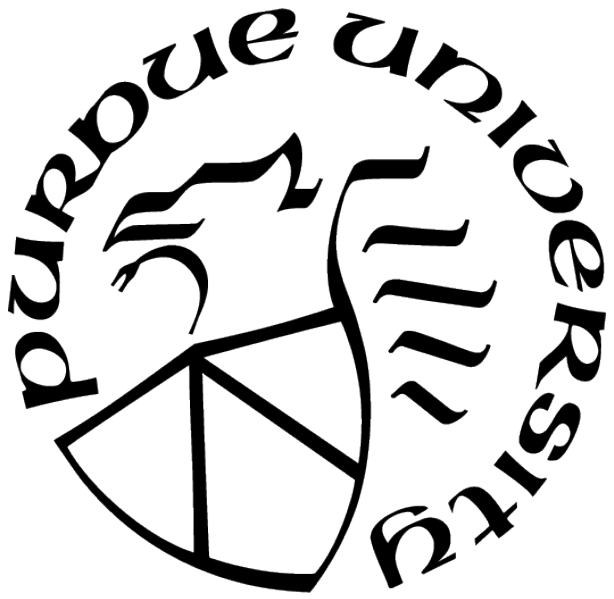

Department of Mechanical and Energy Engineering

Indianapolis, Indiana

May 2021

THE PURDUE UNIVERSITY GRADUATE SCHOOL
STATEMENT OF COMMITTEE APPROVAL

Dr. Ali Razban, Chair

Department of Mechanical and Energy Engineering

Dr. Sohel Anwar

Department of Mechanical and Energy Engineering

Dr. Hazim El-Mounayri

Department of Mechanical and Energy Engineering

Approved by:

Dr. Jie Chen

Dedicated to my mentors

ACKNOWLEDGMENTS

I am really thankful to Dr. Ali Razban for providing me an opportunity to work with him in this research and offering me a Research Assistant position. His guidance and support made this project to reach its conclusion.

I am grateful to the Department of Mechanical and Energy Engineering for providing all resources to work on the this project.

I am thankful to the research committee members, Dr. Sohel Anwar and Dr. Hazim El-Mounayri provided timely feedback for the work that helped it adding more value.

I am also thankful to my academic advisor Jerry Mooney, office administrators Linda Wright and Susan James for their support and advises throughout the program.

I would like to thank my colleague Mahesh Shewale for his endless support in making this research successful by providing the required technical support. Also thankful to Omkar Parker for his assistance in various technical hurdles this project went through.

Extremely thankful to my friend Sanket Joshi to supporting me through the entire journey. This journey wouldn't have been possible without the help of all of my friends, family and colleagues.

TABLE OF CONTENTS

LIST OF TABLES

LIST OF FIGURES

LIST OF SYMBOLS

Notation:

A	mass (m^2)
BSR	Blade speed ratio
c_p	Specific heat capacity at constant pressure (J/kgK)
c_v	Specific heat capacity at constant volume (J/kgK)
J	inertia ($kg\ m^2$)
n_{cyl}	Number of cylinders
n_e	Engine rotational speed (rpm)
n_t	Turbine rotational speed (rpm)
$(O/F)_s$	Stoichiometric oxygen-to-fuel ratio
p	Pressure (Pa)
P	Power (W)
q_{HV}	Heating value of fuel (J/kg)
r_c	compression ratio
R	Gas constant ($J/kg\mathbf{K}$)
R	Radius (m)
T	Temperature (K)
u	Control input
V	Volume (m^3)
W	Mass flow (kg/s)
x_{egr}	EGR fraction
X_O	Oxygen mass fraction
γ	Specific heat capacity ratio
η	Efficiency
λ_O	Oxygen-to-fuel ratio
Π	Pressure ratio
ρ	Density (kg/m_3)
τ	Time constant (s)

ϕ_c	Volumetric flow coefficient
ψ_c	Energy transfer coefficient
ω	Rotational speed (rad/s)
z	Piston position from TDC (m)
l	Length of connecting rod (m)
a	Crank radius (m)
θ	Crank angle rad $(degrees)$
s	Instantaneous pin position (m)
V_c	Clearance volume (m^3)
B	Cylinder bore diameter (m)
P_{motor}	Motoring pressure (Pa)
T_{motor}	Motoring Temperature (K)
x_b	Mass burnt fraction
$\tau_{\mathrm{i}g}$	Ignition delay (s)
ϕ	Equivalence Ratio
Q_{hr}	Total heat release (kJ)
Q_{ht}	Heat transferred (kJ)
U	Internal energy (kJ)
h	Enthalpy (kJ)
$V_{b,\mathrm{i}}$	Reaction zone volume (m^3)
$m_{b,\mathrm{i}}$	Burnt stoichiometry mass (kg)
C_{rad}	Radiation constant

Subscripts:

a	air
amb	ambient
c	compressor
d	displaced

e	engine
egr	exhaust gas recirculation
ei	engine cylinder in
em	exhaust manifold
eo	engine cylinder out
f	fuel
ig	indicated gross
im	intake manifold
m	mechanical
t	turbine
$totem$	total exhaust manifold
$totim$	total intake manifold
vgt	variable geometry turbine
vol	volumetric
δ	fuel injection
rad	radiation
ad	adiabatic
NO	NOx
$comb$	combustion
$motor$	motoring
hr	heat release
ht	heat transfer

ABBREVIATIONS

AHRR	Apparent Heat Release Rate
ANN	Artificial Neural Network
ATS	After Treatment System
BTS	After Treatment System
CAA	Clean Air Act
CAD	Crank Angle Degrees
CI	Compression Ignition
CO	Carbon Monoxide
DPF	Diesel Particulate Filter
ECU	Engine Control Unit
EGR	Exhaust Gas Recirculation
EO	Engine Out
EOI	End of Injection
EPA	Environmental Protection Agency
ESC	European Steady State Cycle
ETC	European Transient Cycle
FHWA	Federal Highway Administration
FTP	Federal Test Procedures
GT Suite	Gamma Technologies Suite
HC	Hydrocarbon
HCN	Hydrogen Cyanide
HDE	Heavy Duty Engines
HDV	Heavy Duty Vehicles
HiL	Hardware in Loop
HRR	Heat Release Rate
IC	Internal Combustion
IMEP	Indicated Mean Effective Pressure
IVC	Intake Valve Close

IVO	Intake Valve Open
JANAF	Joint Army-Navy-NASA-Air Force
LL	Liquid Length
LOL	Lift-Off Length
LPF	Low Pass Filter
MARE	Mean Absolute Relative Error
MFB	Mass Fractions Burnt
MiL	Model in Loop
N2	Nitrogen molecule
N2O	Nitrous Oxide
NASA	National Aeronautics and Space Administration
NO	Nitric Oxide
NOx	Nitrogen Oxides
OBD	On-board Diagnosis
OH	Hydroxide
OICA	Organisation Internationale des Constructeurs d'Automobiles
ROHR	Rate of Heat Release Rate
SCR	Selective Catalytic Reduction
SiL	Software in Loop
SOC	Start of Combustion
SOI	Start of Injection
TDC	Top Dead Center
UHC	Unburnt Hydrocarbon
UN ECE	United Nations Economic Commission for Europe
US	United States
VGT	Variable Geometry Turbine
VMT	Vehicle Miles Travelled
VNT	Variable Nozzle Turbine
VOCs	Volatile Organic Compounds

VVA	Variable Valve Actuation
VVT	Variable Valve Turbine
WHSC	World Harmonized Stationary Cycle

ABSTRACT

Stringent regulatory requirements and modern diesel engine technologies have engaged automotive manufacturers and researchers in accurately predicting and controlling diesel engine-out emissions. As a result, engine control systems have become more complex and opaquer, increasing the development time and costs. To address this challenge, Model-based control methods are an effective way to deal with the criticality of the system study and controls. And physics-based combustion engine modeling is a key to achieve it. This thesis focuses on development and validation of a physics-based model for both engine and emissions using model-based design tools from MATLAB & Simulink. Engine model equipped with exhaust gas circulation and variable geometry turbine is adopted from the previously done work which was then integrated with the combustion and emission model that predicts the heat release rates and NOx emission from engine. Combustion model is designed based on the mass fraction burnt from CA10 to CA90 and then NOx predicted using the extended Zeldovich mechanism. The engine models are tuned for both steady state and dynamics test points to account for engine operating range from the performance data. Various engine and combustion parameters are estimated using parameter estimation toolbox from MATLAB & Simulink by applying least squared solver to minimize the error between measured and estimated variables. This model is validated against the virtual engine model developed in GT-power for Cummins 6.7L turbo diesel engine. To account the harmonization of the testing cycles to save engine development time globally, a world harmonized stationary cycle (WHSC) is used for the validation. Sub-systems are validated individually as well as in loop with a complete model for WHSC. Engine model validation showed promising accuracy of more than 88.4 percent in average for the desired parameters required for the NOx prediction. NOx estimation is accurate for the cycle except warm up and cool down phase. However, NOx prediction during these phases is limited due to actual NOx measured data for tuning the model for real time NOx estimation. Results are summarized at the end to compare the trend of NOx estimation from the developed combustion and emission model to show the accuracy of in-cylinder parameters and required for the NOx estimation.

1. INTRODUCTION

Over the last few decades, the number of registered on-road vehicles in the United States has risen from 8000 to 268 million (Bureau of Transportation Statistics [BTS] 2016; Federal Highway Administration [FHWA] 1997) [1] . As a result, between 1950 and 2016, vehicle miles traveled (VMT) increased by nearly 690 percent while road miles built increased by just 25 percent in the United States (US) [2]. Despite the fact that the rise in road miles has been modest, technical advancements in fuel economy have led to a substantial increase in the number of global on-road operating vehicles to nearly 1.3 billion in the last few decades. According to the International Organization of Motor Vehicle Manufacturers' [OICA] survey from 2015, there were 821 motor vehicles registered per 1000 people in the United States [3].

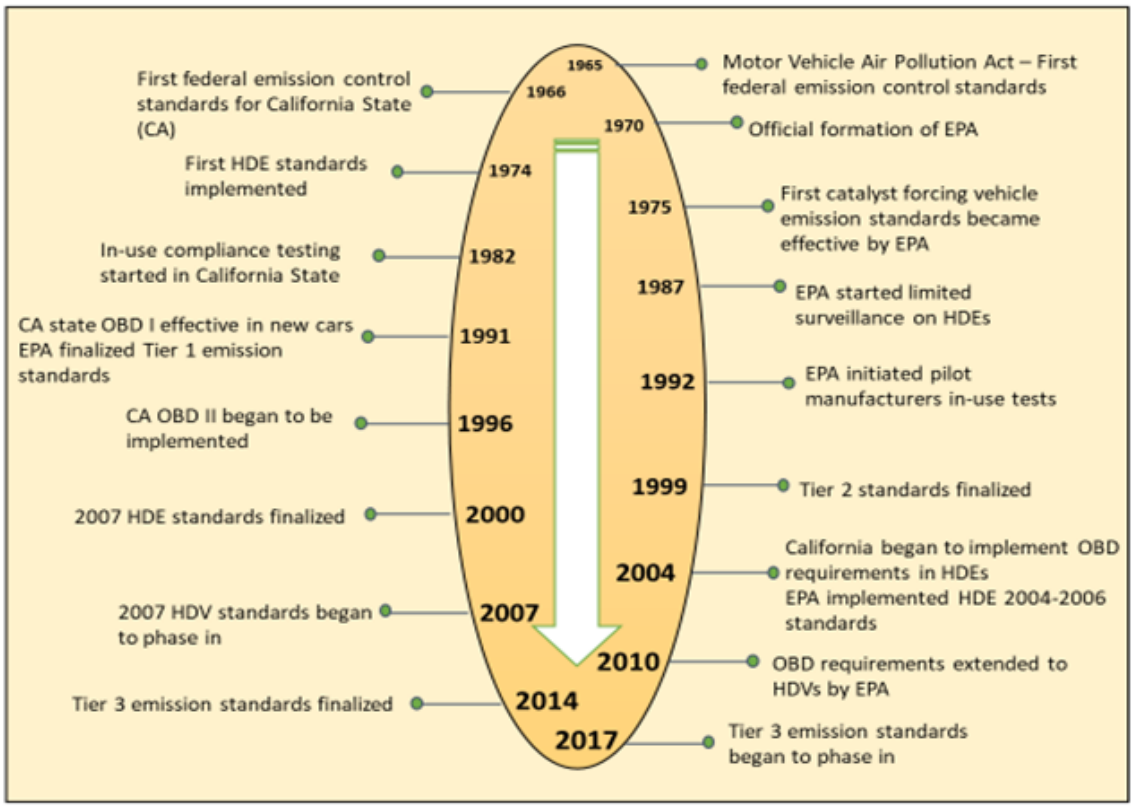

Figure 1.1. History of the U.S. Emissions Compliance and Control Programs

The number of on-road vehicles, on the other hand, grows in lockstep with the number of toxic by-products released by internal combustion (IC) engine vehicles known as emissions.

By 1970, on-road vehicles were responsible for 35 percent of nitrogen oxides (NOx), 68 percent of carbon monoxide (CO), and 42 percent of volatile organic compounds (VOCs) in the United States [4]. This had a detrimental effect on air quality, resulted in the rise of many respiratory diseases, and causing premature deaths in some cases. As a response, the Environmental Protection Agency (EPA) mandated the first national vehicle emissions standards in the 1970 Clean Air Act (CAA). From 1990 to 2017, the EPA continued to impose strict regulations on tail-pipe pollution from gasoline and diesel engines [5]. The evolution of the United States' automotive pollution enforcement and control policy is illustrated in Figure 1.1 [6], [7].

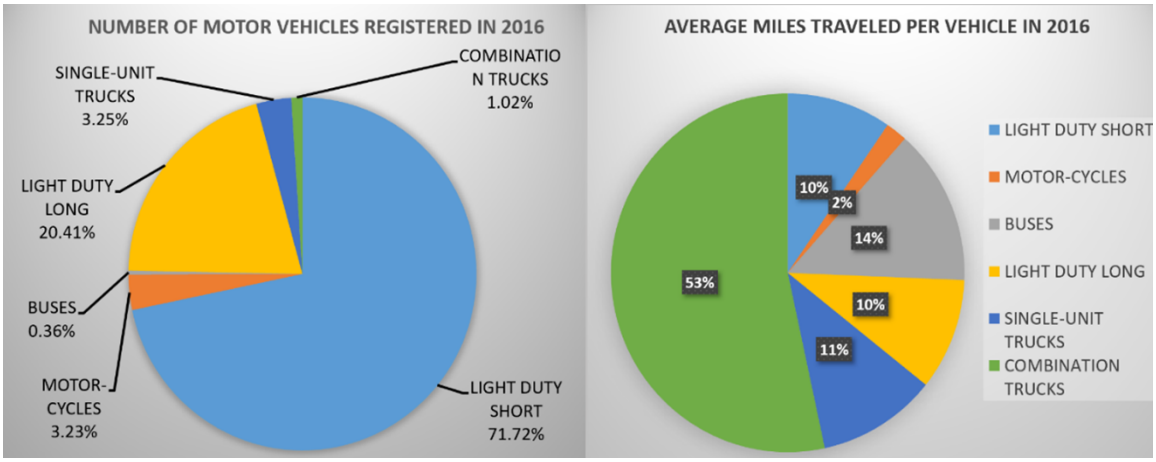

Figure 1.2. Annual Vehicle Registered and Distance Traveled in Miles and Related Data – 2016 FHWA

Because of the added infrastructure and business needs in the US, road transportation is the primary mode of moving the goods around the states. Figure 1.2 shows that, considering the millions of gasoline-powered vehicles on the road, diesel-powered vehicles contribute more VMT than gasoline vehicles resulting in more pollutants in air [8]. The VMT number for diesel engines shows the need for further improvement in terms of fuel efficiency. As a result, automakers are attempting to comply with EPA pollution regulations by implementing new emission reduction methods that also increase fuel economy. Vehicle manufacturers have implemented some of the technologies, like electronically controlled fuel injection, exhaust gas recirculation (EGR), catalytic converters, and particle filters [9]. Further, on-board

diagnosis (OBD) devices/systems were mandated by EPA to ensure the emission control and other engine control devices to monitor the faults during the real-time operation.

Engine production and control has become a complicated process as a result of these new technologies. In addition, to cope up with the emerging solution for the engine control, hardware needed to achieve the targets complying with the regulation are also evolving. To address this, different strategies are discussed in this chapter later that include both engine modeling and controlling strategies that are contributing to achieve less tail pipe emission and better fuel economy. These new strategies put great demands on in-cylinder charge condition and combustion control.. Increased complexity in engine development due to the issues mentioned above has increased the time and cost for the same.

In order to address this, one need to come up with a development of integrated system which includes sub-models predicting the in-cylinder parameters like temperature, pressure, charge composition. This work focuses on the development and validation of the physics-based in-cylinder diesel combustion model comprising of a complete engine air-path model, combustion model integrated with the emission model. A physics-based diesel engine model is developed for a compression ignition (CI) engine equipped with exhaust gas recirculation (EGR) and variable geometry turbine (VGT) that depicts the engine operation considering the ideal gas laws and first law of thermodynamics for conservation of mass. An extended NOx emission prediction model is also developed based on the rate of heat release from the diesel combustion in cylinder. This model is then optimized for both stationary and dynamic tests to tune the engine parameters using non-linear optimization techniques. This model is then validated for the world harmonized stationary cycle. Predicted results are validated against the virtual engine developed in GT-power for a light duty benchmark – Cummins 6.7L Turbo Diesel Engine. Details of the engine model development, tuning and validation are elaborated in the chapters 2 and 3. A background study of the diesel engine combustion and controlling strategies is given in this chapter in the following sections.

1.1 Background Study of Diesel Engine Combustion and Engine Out Emissions

Combustion Modeling is explored in depth in this section. Thanks to advanced technology, detailed combustion simulation aids in understanding the various degrees of freedom involved in modern engines. As illustrated in the following sections, different methods are based on approaches developed for various applications.

1.1.1 Need for Combustion Modeling

Diesel combustion is a heterogeneous chemical reaction in which a liquid fuel containing hundreds of hydrocarbon species reacts with a gaseous in-cylinder charge (air) to produce heat and emissions. Several factors affect these thermal reactions, including engine geometry, state of charge mixing with fuel, and combustion residues. Based on this combustion principle, engine manufacturers have developed such technologies such as Variable Valve Technology (VVT), Electronics Fuel Injection Systems, Turbochargers, Superchargers, EGR, and After Treatment Systems. Engine control is complicated by these methods, which aim for optimum fuel consumption and emission reduction in both the tailpipe and the cylinder. As a result, developers have a new task: the need to understand this complex phenomenon. Combustion models proved to be effective tools for better understanding the combustion process, and they have contributed to new technical breakthroughs that have resulted in improved fuel efficiency and lower emissions. Over the last few decades, new innovations with several degrees of freedom have been added to satisfy both driver and legislative demands, as shown in Figure 1.3 [10].

Due to several degrees of freedom and the inevitability of time and cost constraints for controller design and development cycles, the sophistication of engine control strategies has skyrocketed. Engine Models accelerate the engine development cycles since components or systems can be modeled in early phases and can then be optimized by testing these virtual engines without costly test cells [11]. Model-Based Control saves calibration and testing time by using real-time combustion models in transient engine control [12] [13]. Isermann et al. defined a systematic process for model-based design of the multi-variable control mechanism of IC engines that considers both steady-state and transient behaviors, resulting

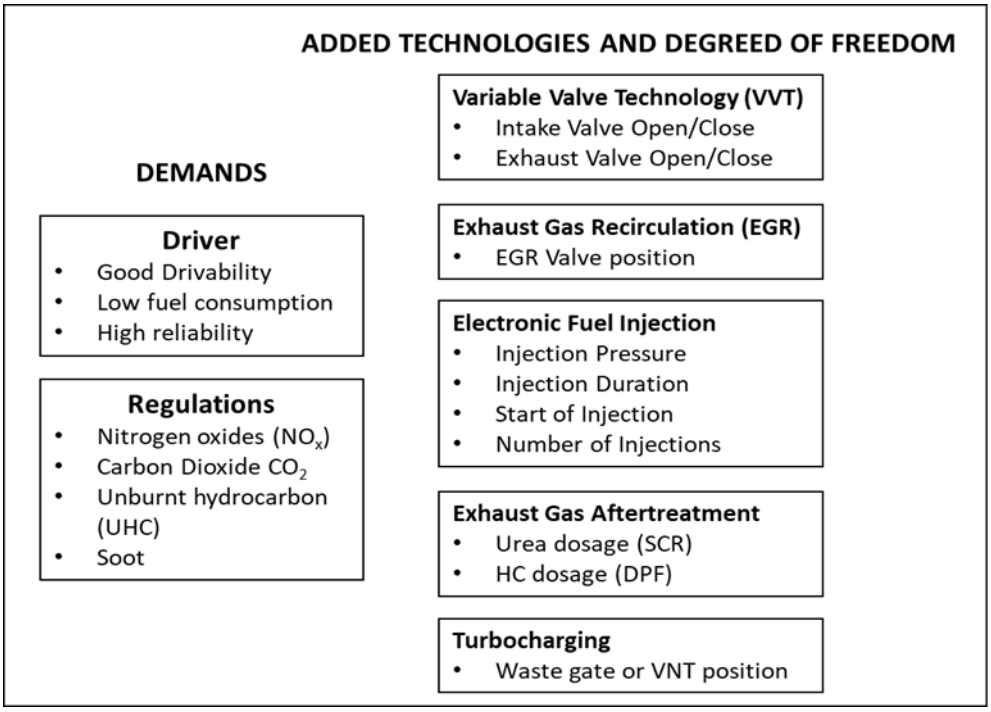

Figure 1.3. Overview - Demands Placed on the Compression Ignition (CI) Engine and Added New Technologies

in optimal fuel consumption and emissions control. The models are validated by using the Global Optimization approach to reduce model uncertainty and smoothing the local optimal setpoints [14]. According to Isermann and his colleagues, engine control system was divided into two parts: function creation and function calibration. Based on the functional requirements, systems are modeled using different approaches as discussed in combustion models section 1.1.2.

The preliminary fitness of these models is measured in the loop (model in loop - MiL) with the actual system. The developed functions serve as a starting point for controller design and simulation, which can then be calibrated. Models that have been successfully calibrated include the source codes for the engine control unit (ECU), which are then tested in real-time simulations before being deployed to the system. The workflow of model-based design is formulated in Figure 1.4 and indicates that the system modeling is the first milestone in engine development and testing [14]. An important component of function development requires the fundamental understanding of diesel engine combustion that involves various

systems depending on the type and application. To comprehend diesel engine combustion, one must first comprehend numerous methods of modeling combustion phenomena, engine operations that regard both inputs and outputs, and complexity based on technical advances over the years. The next section gives an overview of engine modeling techniques for better understanding.

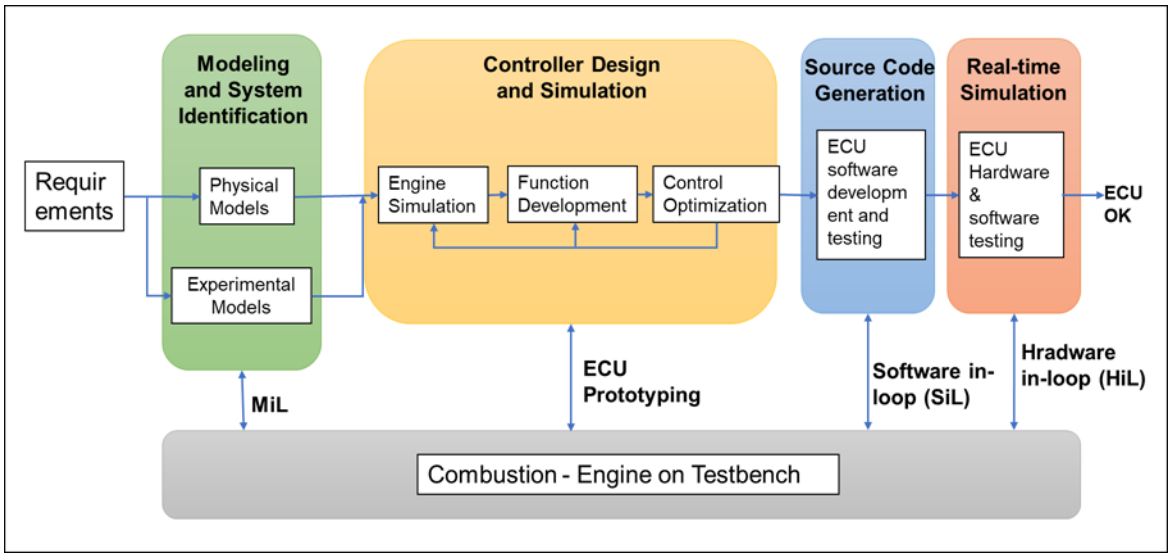

Figure 1.4. The workflow of Model-Based Design

1.1.2 Combustion Models

One of the major challenges in Diesel Engine Combustion is estimation and control of combustion characteristics which are affected by multiple factors: fuel-air properties, crank angle-based events like intake valve closing (IVC), intake valve opening (IVO), start of injection (SOI), end of injection (EOI), start of combustion (SOC), etc., and additional engine-dependent parameters such as geometry and specification [15] [16]. The number of these parameters involved in the modeling dictates the complexity and computational effort. As a consequence, comprehensive and accurate diesel engine modeling is important. These models are categorized into three types:

1. Empirical Combustion models
2. Phenomenological Combustion models
3. Physics-based Combustion models

Empirical Combustion Models

This approach treats combustion as a "Black Box" and is based on data obtained from experiments under complex operating conditions. Neural networks, correlations, and look-up tables are the hallmarks of the Empirical Model. Watson et al. (2010) conducted a series of tests on three separate engines to determine the relationship between engine operating parameters and apparent heat release rate (AHRR) [17]. The study included finding a correlation between engine operating parameters and respective heat release rates that are effective only for coarser crank angle (CAD) intervals. These models were adaptive for parametric changes in performance parameters like compression ratio, valve timing, valve areas, injection timing, aftercooling, ambient conditions, etc. but could not be used to predict the effect of the combustion chamber design changes. Weibe, Wolfer, and Woschni et al. established correlations between ignition delay and pressure, temperature, SOI, and EOI, which can be used to calculate the heat release rated using experimental data [18][19][20]. This method involves measuring mass burned fractions, which contributes to emission prediction. Based on specific operating conditions, they calculated shape factors and empirical constants

for their correlations. Look-up tables have been commonly used in the industry for engine calibration and control for the last couple of decades, and while they have proven to be efficient calibration models, they are not reliable in terms of handling uncertainties in real-world operating conditions. Artificial Neural Networks (ANN) are the most recent methods for predicting cylinder states and emissions using correlations obtained from real operating conditions. There are two types of ANN learning rules: supervised and unsupervised. The weights of the network are adjusted by supervised learning rules to reduce the error between the network output and the calculated output. Researchers developed a few approaches that resulted in cylinder state estimation and emission accuracy of up to 93 percent [21][22][23]. However, since the ANN approach was created for particular engines, relationships derived from it cannot be used for general operating conditions and are vulnerable to errors when extrapolated outside of the experimental conditions.

Phenomenological Combustion Models

Simple physical models that reproduce the physical and chemical phenomena occurring during the combustion process are used to predict combustion variables in this model type. Zero-dimensional and quasi-dimensional models are two types of phenomenological models. The model is divided into ”packages” or ”zones” in the case of fuel spray phenomena, which have no real spatial coordinates, hence the term ”quasi-dimensional” [24][25][26][27][28]. The zero-dimensional models are generally only able to predict the heat release rate [29] [30]. For emission formation prediction, at least two zones are required. In the earlier stage of this area, a few people studied the chemical phenomenon for nitric oxide (NO) and Soot formation:

1. Thermal NO proposed by Zeldovich Y, in 1946 [31] was later extended by Lavoie et. al. [32] and is now referred to as the extended “Zeldovich mechanism”.

2. NO formation via the prompt-NO mechanism also referred to as the Fenimore mechanism after Fenimore C [33], occurs when fuel-rich flames in the presence of hydrocarbon radicals react with nitrogen (N2) to form hydrocyanic acid (HCN).

3. Wolfrum, 1972, postulated the nitrous oxide (N2O) intermediate pathway [34]. This describes NO formation via nitrous oxide N2O as an intermediate species formed when nitrogen is attacked by atomic oxygen and a third-body molecule

Tree et al. [35], studied the soot formation process and discussed the effects of fundamental properties like temperature, pressure, stoichiometry, and fuel consumption. They revealed the complexity of the phenomenological models regarding the number of formation zones; this is a vital criterion for the accuracy of prediction algorithms. These models generally can predict heat release rates [30][35].

In comparison to empirical models, phenomenological models allow for (to a degree) extrapolation outside of the operational range for which they were built. Furthermore, if physical measurement is not feasible due to sensor limitations, the prediction of a specific phenomenon is dependent on a variety of driving inputs that must be modeled. The NOx model, for example, is based on the pressure and temperature traces within the cylinder. Predicting the heat release rates that drive combustion states in a cylinder requires an understanding of chemical kinetics within the cylinder. With the latest developments in diesel engine control, modeling these complex systems is important for better predictive accuracy. The following section focuses on certain Physics-Based models for modern diesel engines' various systems.

Physics-Based Mean Value Combustion Models

Physics-based models provide the most accurate depiction of the physical and chemical processes that occur during combustion with a microscopic level of detailing. The engine and combustion chamber are grouped into several local systems, each with its own dimensions and degrees of freedom. Full conservation equations for mass, energy, and momentum are solved for each local system. As a result, these models have the best predictive qualities: they can predict pollution formation and heat release rates, and they are generic. Guzzella, L. et al. [36] developed a comprehensive model for a diesel engine in 1998, considering the fuel injection system, EGR, and turbochargers. They were able to simulate the air-path with a EGR and turbo effect to assess optimal performance, fuel efficiency and emissions.

Figure 1.5 shows the various systems (cells) taken in the gas exchange model considering the EGR fraction effect [36]. The detailed factors considered as gas mixes in a running engine fitted with EGR are depicted in this same. The intake manifold (fresh gas mass), exhaust manifold (exhaust mass), fuel injection system (injected and burned fuel mass), combustion chamber (gas exchange within the combustion chamber), and EGR system are all related to account for recirculated masses in the cylinder. Depending on the phenomenon and its occurrence range, these local mechanisms may be cycle-to-cycle or CAD-based. For example, gas exchange processes are based on the combustion cycle, and the heat release rate for each combustion cycle is calculated using CAD. Guzzella's work, as groundbreaking as it was, was limited by technical limitations. Guzzella's work did not include many factors such as comprehensive NOx modeling based on newly added techniques, robust controls, and multipoint electronic fuel injection technology.

After including comprehensive combustion and emission models, the engine models become more complex. As a result, simple but detailed mean value models are developed. To put it another way, averaged states measured during each combustion cycle are used in mean value engine models. These models are more generalized to minimize uncertainty and are transient in macroscopic effects. Because of their simplicity, such models are easy to use in the online control of diesel engines. A practical online Engine Model that includes both combustion and gas (air-fuel mixture) exchange models has been developed by a few researchers as a feature of CAD (Crank Angle Degrees). This model has a 0.1 CAD resolution and 90 percent less computational time, and it was accurate in NO formation up to 10.4 percent mean relative error [37]. This modeling approach, when applied online in the electronic controller that directs the engine, offers flexibility in modifying local models to troubleshoot and enables researchers to investigate local systems in greater depth. Furthermore, data acquisition and post-processing tools such as MATLAB & Simulink, gamma technologies' GT Suite, Labview, dSPACE, and others allow for more detailed calibration and optimization of the models developed [38]. Durjarasan et al. developed a control-oriented physics-based model for predicting NOx emissions for a diesel engine with EGR in 2019 [39]. This model includes models for gas exchange, heat release rate, chemical equilibrium solver for adiabatic temperature, temperature compensator for losses, and a detailed NOx model to cover a detailed

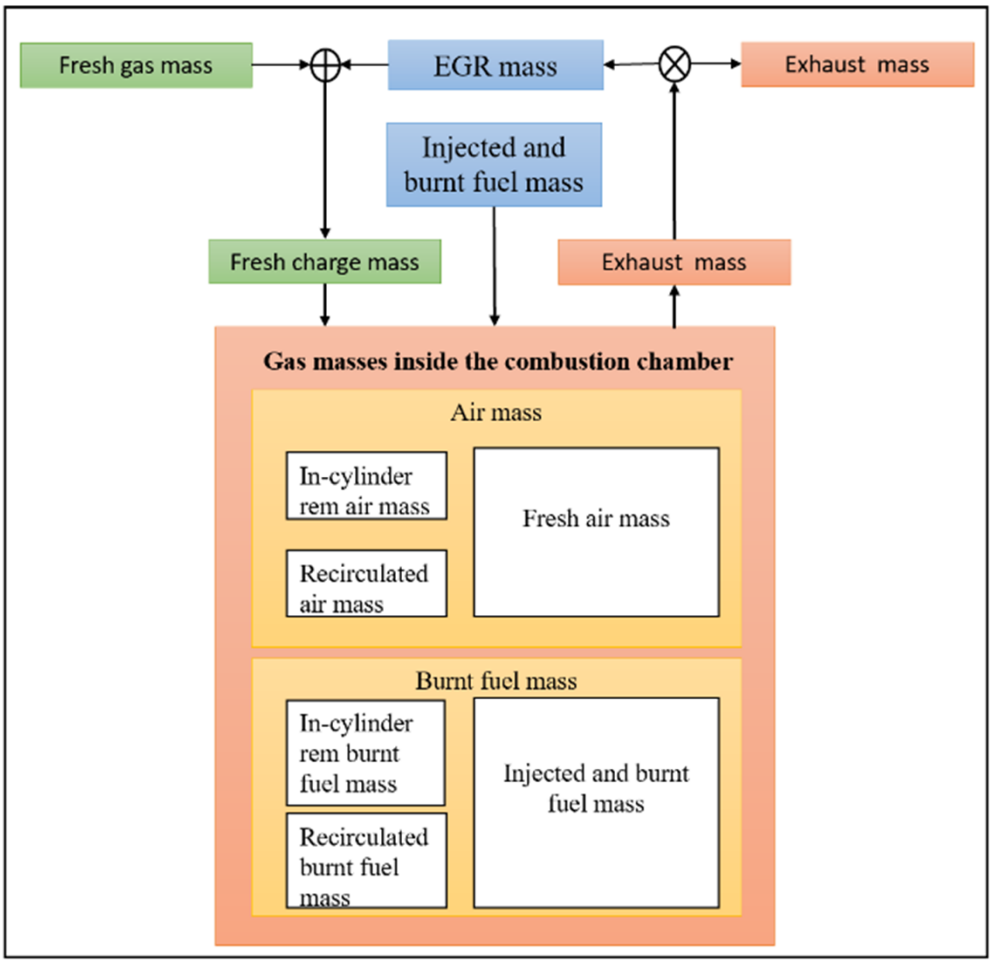

Figure 1.5. Basic Physics-based Air-path Model for an EGR Equipped Engine

phenomenon of NOx formation. Using generic model-based engine control techniques, these integrated accurate and detailed sub-models achieved a prediction accuracy of 93 percent.

Ultimately, physics-based models have an advantage in accurately predicting in-cylinder states, which is required for engine out (EO) emissions as well as performance estimation and control. Although model speed is of utmost concern, developing such local models and integrating them into the mean value engine models provides both high accuracy and faster prediction when embedded with real-time engine controllers.

1.2 Current State of the Art for Engine Control Strategies

A few challenges are linked to the existing state-of-the-art due to the added techniques for engine control as summarized by Ahire V. et al. in 2021 [6]. According to them, the method of defining control variables and plant states has an effect on controller robustness and stability. These variables may be sensor outputs or model outputs based on the combustion modeling techniques discussed earlier. Thus, following prerequisites are needed to address while developing the control systems for the emissions control for diesel engine:

- Accurate prediction models
- Controller design and optimization techniques
- Controller robustness and stability strategies
- Verification and validation through globally harmonized driving cycles

For advanced modern diesel engine control, accurate prediction of cylinder states and engine-out products based on detailed physical and chemical kinetics models is needed. To deal with these complex systems that are the product of comprehensive models, ease of controller design and model parametric reduction are needed. However, there are a few challenges in measuring the engine parameters with the existing sensing techniques available that are discussed in the next section 1.2.1. A comprehensive study on recent diesel engine control strategies by Ahire V. et al. discusses about new techniques such as cylinder deactivation and variable valve actuation (VVA) that needs an estimation and prediction of cylinder parameters and emissions [6]. They have also discussed the need for the world harmonized cycles for vehicle testing that includes both urban and highway condition for different regions in the world. This harmonization will reduce the time and cost spent on the engine development by manufacturers.

1.2.1 Limitations to Measure In-cylinder Parameters and Emissions

As discussed previously, accurate measurements of the engine parameters are key to control engine emissions and combustion control. A study by Eriksson L et al. [40] shows

that Pressure-based combustion control systems have been viewed as a possible benefit for future engines as emission and efficiency standards have become more stringent. These systems primarily rely on pressure-extracted data including indicated mean effective pressure (IMEP), heat release rate, combustion length, compression state, and so on. Both the pressure and the crank angle (CAD) must be calculated with high precision to ensure the precision of the derived parameters.

Piezoelectric pressure transducers mounted on the cylinder walls are used to measure cylinder pressure. An encoder mounted on a flywheel casing, which also tests engine speeds, is used to measure CAD. However, the accuracy and sensitivity of these two sensors are limited. Thermal shocks, signal drifts, and sensitivity variance are all caused by piezoelectric pressure transducers' sensitivity to temperature. Therefore, a variation in pressure measurement may result in major differences in heat release rates [41]. These deviations influence the engine calibration process, which causes measurement uncertainty. As a result, one of the crucial tasks for future engines is CAD-based precise measurement of pressure and heat release rates.

In case of EGR control, the input from the lambda (oxygen) sensor and NOx sensors mounted after the exhaust manifold controls the actuation of the EGR valve. The input from NOx sensors mounted before and after treatment systems (ATS) such as catalytic converters (Selective Catalytic Reduction- SCR), diesel oxidation catalyst (DOC), and diesel particulate filter (DPF) is also used to monitor them. The temperature-dependent electrochemical theory is used in today's NOx sensors. The temperature at which a sensor begins to operate, or when it undergoes the electrochemical phase, is referred to as the light off temperature. It ranges from 450^oC to 800^oC depending on the makers and its specification. Additionally, measurement range, accuracy and sample quality depend on the temperature [42]. Therefore, NOx measurement and prediction are the critical factors in diesel engines for clean operations.

Furthermore, the EPA and California Air Resource Board (CARB) confirmed that current control strategies are successfully achieving high-speed-load (Highway run) NOx control goals. However, for NOx abatement from tailpipes at low load and low speed conditions, a few more strategies are needed (Normal City runs). As a result, special attention is being paid to designing control strategies for low load-speed conditions [6]. Low load conditions, on the other hand, are low temperature operations with greater operating point volatility

(City run – normal traffic). These uncertainties are too much for the sensors listed above to manage. As a consequence, with controlled approaches, the need for prediction techniques arises.

1.2.2 Summary

Various environmental protection organizations around the world have updated their clean transportation strategies and emission thresholds over the last decade. Surveys on various technologies used to achieve these organizations' goals indicate that accurate cylinder states and emission prediction is the key to achieve these targets for the emission and performance control in diesel engines. Physics-based combustion models have been shown to be accurate methods for prediction and regulation of modern diesel engines when used in conjunction with various engine simulation techniques. These models are generic and can be integrated with the engine's ECU to monitor a variety of functions such as emissions, performance, and on-board diagnosis (OBD). The key take-aways from the background for engine development and emission control are:

Shorter engine development time: Engine and exhaust gas aftertreatment control algorithms can be created, tested, and optimized early in the engine development phase using a combustion model.

Limited required engine measurement data: Using a "virtual engine", the use of expensive (both in terms of time and money) engine data can be greatly restricted.

More precise engine control and calibration: The complexity and time needed for controller calibration are significantly reduced by using model-based control strategies.

Virtual Sensing: Over the last decade, the number of sensors for system monitoring and engine control has increased dramatically. These sensors are more expensive and more prone to failure. In this case, combustion models can save money by acting as "virtual engine", reducing the number of sensors needed.

1.3 Research Gap

Efforts have been taken in developing models for engine air-path, combustion, and emissions. However, a very few collaborative works to build generic, physics-based engine models that integrate the detailed emission models exist. Also, application of these model varies that constraints the model details and integration methods. In addition, these models require a high-volume data to train (tune) to validate against the applied applications. A model developed by Unver et. al emphasizes on air-path model that achieved 90 percent accuracy in estimating the in-cylinder parameters, but it does not include the detailed combustion model based on the heat release rates [43]. They used the regression model to predict the engine out NOx which is not generic in other application. Another work by Durjasaran et. al focused on a real-time air-path and combustion model integrated with the cycle-based NOx model prediction achieved 93 percent accuracy [39]. But this work did not take care of the crank-angle-based heat release rate model and it required a high-volume data points to tune the model. Therefore, need for such a detailed models that include both air-path as well as combustion model integrated with the emission formation model is identified.

With this background, objectives of this thesis are listed below in short and discussed in detail later in the subsequent chapters.

1.4 Thesis Objectives

This work aims to develop an integrated model that estimates engine out NOx using the extended Zeldovich mechanism for an engine equipped with EGR and VGT. To achieve this, a detailed combustion model using the rate of heat release rate and mass fraction burnt is developed that estimates the in-cylinder pressure and temperature traces at every crank angle degree (CAD). A chemical equilibrium solver is also developed to estimate the thermo-chemical compositions of fuel reactants and products that predicts the flame temperature. This combustion model is then integrated with the air-path model created by Wahlström, J et al [44] that depicts the application of interest for an engine considered equipped with EGR and VGT. Further, this integrated engine and emission model is tuned against the GT-power virtual engine data for steady state as well as dynamic points in order to reduce

the use of high-volume data. Which is then validated against world harmonized stationary cycle (WHSC) to account for the harmonization of vehicle development globally. Some of the key milestones to achieve the objectives are as follows:

1. Physics based mean value diesel engine model
   (a) Adoption of a MATLAB and Simulink based engine model equipped with EGR and VGT
   (b) Development of a CAD based rate of heat release (ROHR) model
   (c) Development of a Chemical Kinetics equilibrium solver to determine the adiabatic temperature
2. Engine out (EO) NOx model using the extended Zeldovich mechanism
3. Engine Tuning (parametric estimation) and Validation
   (a) Stationary and dynamic tuning for engine and emission model parameter estimation
   (b) Model validation against the GT-power virtual engine using world harmonized stationary cycle (WHSC)

2. DIESEL ENGINE MODELING

As previously discussed, mean value engine models depict the behavior of an engine that follows the physics and thermochemistry involved in the engine operation. Similar model was developed by Wahlström, J et al. that ensures the operation of a diesel engine equipped with EGR and VGT [44]. This model is used as a baseline model in this work as it is generic diesel engine model equipped with the EGR and VGT that replicates the benchmark Cummins 6.7-liter turbo diesel engine. And then it is used to calibrate and validate against a virtual GT-power model of the same. It is developed in the MATLAB and Simulink environment, and further validated against the results from the GT Suite's GT Power simulations. Further, a NOx function is developed based on the Rate of Heat Release (ROHR) through the diesel engine combustion that follows the Zeldovich Mechanism for predicting the cycle NOx. An overview of an engine model with the NOx predictor is given in Figure 2.1. The system is divided in to two subsystems viz. Engine and NOx predictor as shown below. Engine is model into sub-systems like Manifolds, Cylinder, EGR, and VGT. The details of these systems are discussed below.

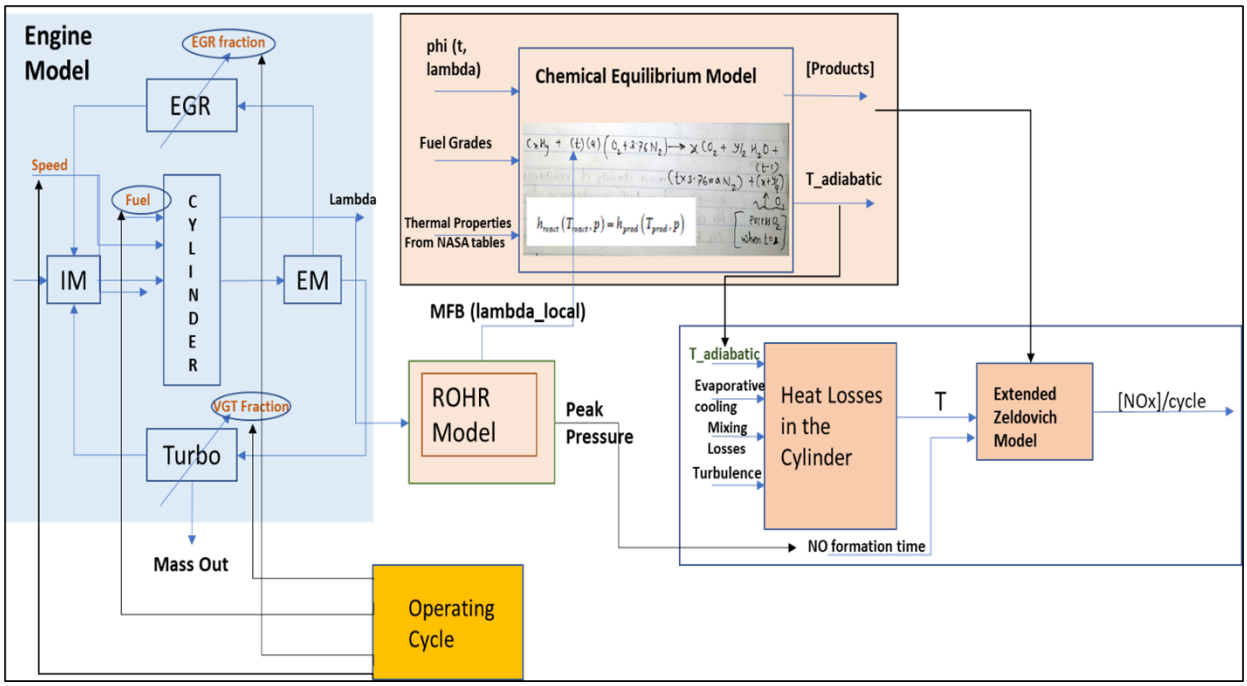

Figure 2.1. Integrated Engine Model with the NOx Predictor

2.1 Physics Based Engine Model

A physics based mean value engine model comprises of Air path and cylinder models that depict the mass exchange in the engine through subsystems such as EGR, VGT, manifolds and cylinder. There are five states that are required for the NOx predictor to calculate the cumulative NOx produced in each engine cycle (each revolution) as given in the equation 2.2. Considering the engine speed, n_{e} as an engine operating variable, the input to the model is (u_{egr}, u_{vgt}, u_{δ}) and it has five main states (p_{im}, p_{em}, T_{em}, w_{ei}, and λ_O) related to the engine. Therefore, the resultant model is represented in the form of function as,

$$\dot{\mathrm{x}} = f\left(x, u, n_{\mathrm{e}}\right) \tag{2.1}$$

Where x is a state vector,

$$x = \left(p_{\mathrm{im}}, p_{em}, T_{em}, w_{\mathrm{ei}}, \lambda_O\right)^T \tag{2.2}$$

And p_{im} and p_{em} are intake and exhaust manifold pressure. T_{em} is the exhaust manifold temperature. w_{ei} is the cylinder mass flow, and λ_O is the oxygen to fuel ratio in cylinder.

And u is an input control vector,

$$u = \left(u_{egr}, u_{vgt}, u_{\delta}\right)^T \tag{2.3}$$

Where u_{egr}, u_{vgt}, and u_{δ} are the EGR valve position, VGT actuator position, and Fuel injected, respectively. Ranges of u_{egr} and u_{vgt} are 0 to 100 percent for closed and open, respectively. Engine speed and fuel injected are the operating variables that are given as a part of the operating cycles from the tuning as well as validation cycles. Additionally, X_{Oim} and X_{Oem} are the oxygen mass fractions at intake and exhaust manifolds, w_{ei}, w_{eo}, w_{egr}, w_c are the masses to engine inlet, from engine outlet, from EGR, and compressor, respectively. Figure 2.2 shows the layout of an engine model as a continuous system of subsystems such as cylinder, EGR, VGT and manifolds and the respective inputs and outputs. Detailed modeling parameters and sub-models are discussed below.

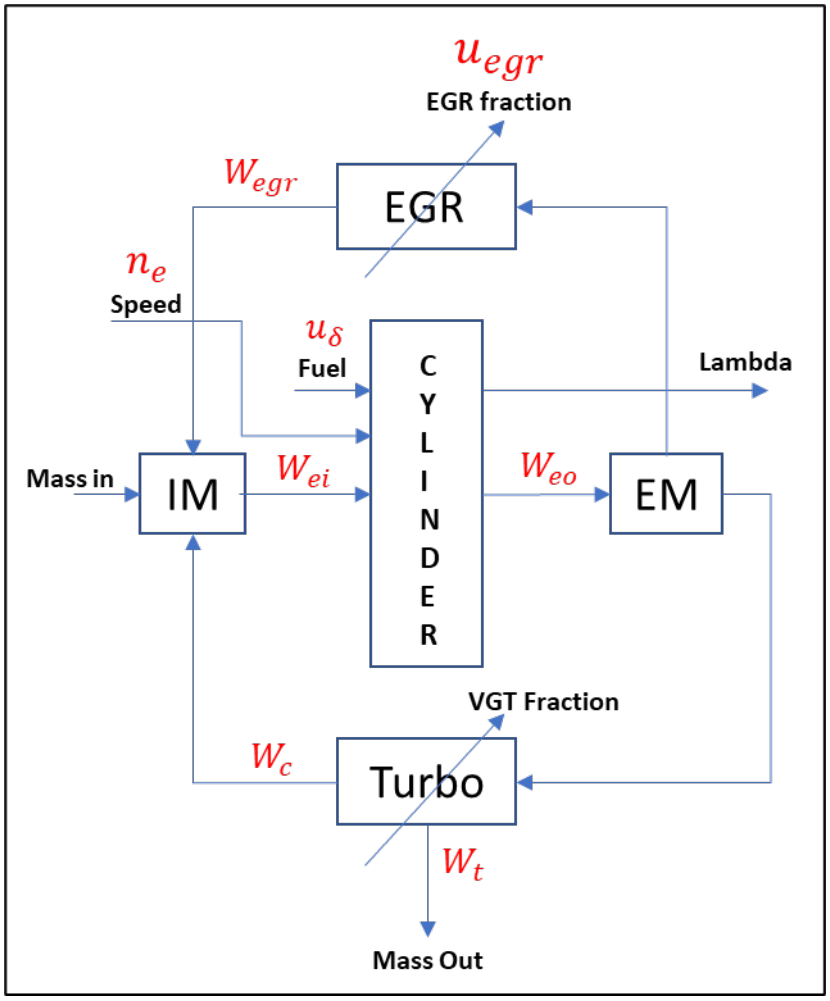

Figure 2.2. Engine Model with EGR and VGT involved - Mass Flow and Fractions from Each System

2.1.1 Engine Manifolds

Intake and exhaust manifold systems are modeled as two states that are pressure and oxygen mass fractions For an isothermal process, the temperature is constant or varies slowly, ideal gas law and conservation of mass principle is applied while modeling the manifolds for

the pressure and mass fractions. Therefore, the differential equations for the pressure in manifolds are given as [44]

$$\begin{aligned} \frac{d}{dt}p_{\mathrm{im}} &= \frac{R_a T_{\mathrm{im}}}{V_{\mathrm{im}}}\left(W_c + W_{egr} - W_{\mathrm{ei}}\right) \\ \frac{d}{dt}p_{\mathrm{em}} &= \frac{R_a T_{\mathrm{em}}}{V_{\mathrm{em}}}\left(W_{\mathrm{eo}} - W_t - W_{egr}\right) \end{aligned} \tag{2.4}$$

Where T_{im} and T_{em} are the intake and exhaust manifold temperatures, R_a and R_{e} are the ideal gas constants for air and exhaust gas, and V_{im} and V_{em} are the manifold volumes. w_{ei}, w_{eo}, w_{egr}, w_c, w_t are the masses to engine inlet, outlet, EGR, compressor and turbine, respectively. These masses are discussed in detailed later in the subsections. Further, to address the effect of oxygen mass from the EGR, oxygen mass fractions are modeled in the controlled volume. Oxygen fraction in the manifolds can be defined as ratio amount of oxygen to the total mass as follows [44],

$$X_{\mathrm{Oim}} = \frac{m_{\mathrm{Oim}}}{m_{\mathrm{totim}}}, X_{\mathrm{Oem}} = \frac{m_{\mathrm{Oem}}}{m_{\mathrm{totem}}} \tag{2.5}$$

Where m_{Oim} and m_{Oem} are the oxygen masses in intake and exhaust manifolds respectively, and m_{totim} and m_{totem} are the total masses in the intake and the exhaust manifolds. Similarly, using the mass conservation principle, the differential equations for the oxygen mass fractions are given as follow [44],

$$\frac{d}{dt}X_{\mathrm{Oim}} = \frac{R_a T_{\mathrm{im}}}{p_{\mathrm{im}} V_{\mathrm{im}}}\left(W_c\left(X_{Oc} - X_{\mathrm{Oim}}\right) + W_{\mathrm{egr}}\left(X_{\mathrm{oem}} - X_{\mathrm{oim}}\right)\right) \tag{2.6}$$

$$\frac{d}{dt}X_{\mathrm{Oem}} = \frac{R_{\mathrm{e}} T_{\mathrm{em}}}{p_{\mathrm{em}} V_{\mathrm{em}}}\left(W_{\mathrm{eo}}\left(X_{O\mathrm{e}} - X_{\mathrm{Oem}}\right)\right) \tag{2.7}$$

Where X_{Oc} and $X_{O\mathrm{e}}$ are the oxygen concentrations coming from compressor and engine cylinders. X_{Oc} is taken as 23.14 % as its only air that is coming from the compressor. Further the manifold volumes are tuning parameters for the model, and these are addressed later in the model tuning section 3.5.5.

2.1.2 Cylinder Model

Cylinder model consists of two sub-models, cylinder flow and cylinder temperature. The cylinder flow model describes the gas and fuel flows that enters the cylinder and leaves cylinder. Further it also computes the air-fuel (oxygen to fuel ratio in the cylinder from the in-cylinder oxygen concentrations and oxygen fractions from intake and exhaust manifolds. Temperature model depicts the thermodynamic cycle that calculates the cylinder temperature based on an iterative method that relates the behavior of a few thermodynamic properties that are explained in detailed later in the following sections. The zero-dimensional models are generally only able to predict the heat release rate. For emission formation prediction, at least two zones are required.

Cylinder Mass Flow

The cylinder mass flow w_{ei} from the intake manifold to the cylinder is modeled as follows [44],

$$w_{\mathrm{ei}} = \frac{\eta_{\mathrm{vol}}\, p_{\mathrm{im}}\, n_{\mathrm{e}} V_d}{120 R_a T_{\mathrm{im}}} \tag{2.8}$$

Which is modeled as a function of intake manifold pressure p_{im} and temperature T_{im}, engine speed n_{e}, displaced volume V_d and volumetric efficiency η_{vol} that is modeled as [44]

$$\eta_{vol} = c_{\mathrm{vol1}}\sqrt{p_{\mathrm{im}}} + \mathrm{c_{vol2}}\sqrt{n_{\mathrm{e}}} + \mathrm{c_{vol3}} \tag{2.9}$$

$c_{vol1,2and3}$ is a polynomial coefficient vector that is tuned during the model tuning and it is explained in the model tuning section 3.5.4.

The fuel mass flow W_f is the injected mass in grams per cycle to the cylinder is given as a function of the controlling input u_δ, engine speed and number of cylinders n_{cyl}

$$W_f = \frac{10^{-6}}{120} u_\delta n_{\mathrm{e}} n_{cyl} \tag{2.10}$$

Therefore, the mass flow out from the cylinder is given as

$$W_{eo} = W_f + W_{\mathrm{ei}} \tag{2.11}$$

Hence the oxygen to fuel ratio λ_O in the cylinder is given by,

$$\lambda_O = \frac{W_{eo} X_{Oim}}{W_f (O/F)_s} \tag{2.12}$$

Where $(O/F)_s$ is the stoichiometric ratio of the oxygen to fuel mass which is equivalent to the air-fuel ratio and that defines the performance and emission characteristics of an engine.

For the diesel engine combustion to be smoke free, $\lambda_O > 1$, and therefore the oxygen concentration out from the cylinder, which is equivalent to the unburnt oxygen mass fraction, is defined as [44]

$$X_{O\mathrm{e}} = \frac{W_{\mathrm{ei}} X_{Oim} - W_f (O/F)_s}{W_{eo}} \tag{2.13}$$

Cylinder flow parameters i.e., volumetric efficiency coefficients, $c_{vol1,2and3}$ are tuned using the stationary and dynamic measurements as described in the model tuning and optimization section 3.5.4.

Cylinder Temperature

The cylinder temperature is modeled according to the work by Skogtjärn, P et al. [45] that is based on the ideal-gas Seliger cycle, and it is given as [44]

$$T_{\mathrm{e}} = \eta_{SC} \Pi_{\mathrm{e}}^{\left(1-\frac{1}{\gamma_a}\right)} r_c^{1-\gamma_a} x_p^{\left(\frac{1}{\gamma_a}-1\right)} \times \left(q_{\mathrm{in}} \left(\frac{1 - x_{cv}}{c_{pa}} + \frac{x_{cv}}{c_{Va}} \right) + T_1 r_c^{\gamma_a - 1} \right) \tag{2.14}$$

Where, η_{SC} is a compensation factor for the non-ideal cycles, and x_{cv} is the ratio of fuel consumed during constant volume combustion process. Π_{e} is the pressure ratio between exhaust and intake manifold.

$$\Pi_{\mathrm{e}} = \frac{p_{em}}{p_{\mathrm{im}}} \tag{2.15}$$

The pressure ratio between the points 3 and 2 in a Seliger process as shown in Figure 2.3, is given by

$$x_p = \frac{p_3}{p_2} = 1 + \frac{q_{in} X_{cv}}{c_{Va} T_1 r_c^{\gamma_a - 1}} \tag{2.16}$$

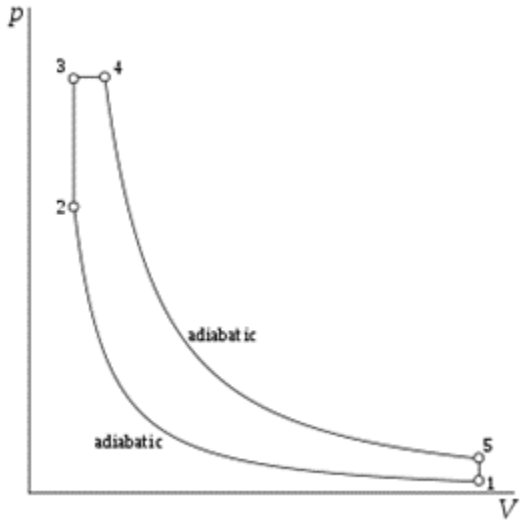

Figure 2.3. Ideal Seliger cycle PV diagram

The specific energy content of the charge is given by

$$q_{in} = \frac{W_f q_{HV}}{W_{\mathrm{ei}} + W_f} (1 - x_r) \tag{2.17}$$

Temperature at which intake valve closes after the intake stroke and mixing of the charge is

$$T_1 = x_r T_{\mathrm{e}} + (1 - x_r) T_{im} \tag{2.18}$$

Where residual gas fraction is given as

$$x_r = \frac{\Pi_{\mathrm{e}}^{1/\gamma_a} \mathbf{x}_p^{-1/\gamma_a}}{r_c x_v} \tag{2.19}$$

The volume ratio between point 3 (after combustion) and point 2 (before combustion) in a Seliger cycle

$$x_v = \frac{v_3}{v_2} = 1 + \frac{q_{\text{in}}\,(1 - x_{cv})}{c_{pa}\left[\left(\frac{q_{\text{in}} x_{cv}}{c_{Va}}\right) + T_1 r_c^{\gamma_a - 1}\right]} \tag{2.20}$$

Note that the equations above are nonlinear and depend on each other, the cylinder out temperature is calculated with the fixed-point iteration method during each sample time given to the model simulation.

Temperature Drops Across the Exhaust Pipe

To include the heat loss through the exhaust manifold and piping to get the accurate exhaust manifold temperature, the temperature drop model is given by Eriksson L et al. [46] and is given as

$$T_{em} = T_{amb} + (T_{\text{e}} - T_{amb}) \exp \frac{h_{tot} \pi d_{pipe} l_{\text{pipe}}\, n_{\text{pipe}}}{W_{\text{e}o} c_{\text{pe}}} \tag{2.21}$$

Where T_{amb} is the ambient temperature, h_{tot} the total heat transfer coefficient, l_{pipe} is pipe length, d_{pipe} the pipe diameter, and n_{pipe} the number of pipes. Tuning parameters and the coefficients are discussed in detail in the model tuning section 3.5.4.

Engine Torque

This work does not include the torque model as it is assumed that for fuel injected an optimal torque is produced and there is an optimal injection timing. Moreover, model states are not affected by the torque value as long it meets the optimal fuel injection. Therefore, the given model is also not tuned for the engine torque system.

2.1.3 Exhaust Gas Recirculation (EGR) Model

EGR is a technique to lower the cylinder temperatures to lower the NOx produced in the cylinder by re-circulating the exhaust mass back into the cylinder. The EGR mass flow is

modelled as a simple throttling model by applying the restrictions in the compressible flow. It is assumed that the flow is irreversible. This assumption avoids the complexity involved in the change in mass and temperatures in case of reversed flow. However, p_{em} is always higher than the p_{im} for the engine operating cases taken and cycle generated for this study. Therefore, there is no reversed flow in the system. The mass flow through the EGR valve restriction is given as [44]

$$W_{egr} = \frac{A_{\mathrm{egr}} p_{em} \psi_{egr}}{\sqrt{T_{em} R_{\mathrm{e}}}} \tag{2.22}$$

Where ψ_{egr} is modeled as a parabolic function of pressure ratio in EGR Π_{egr} as [44]

$$\psi_{egr} = 1 - \left(\frac{1 - \Pi_{\mathrm{egr}}}{1 - \Pi_{\mathrm{egropt}}} - 1 \right)^2 \tag{2.23}$$

With the assumptions that the flow is choked, and no back flow can occur, pressure ratio Π_{egr} is given as [44]

$$\Pi_{\mathrm{egr}} = \begin{cases} \Pi_{\mathrm{egropt}} & \text{if} \quad \frac{p_{im}}{p_{em}} < \Pi_{\mathrm{egropt}} \\ \frac{p_{im}}{p_{em}} & \text{if} \quad \Pi_{\mathrm{egropt}} \leq \frac{p_{im}}{p_{em}} \leq 1 \\ 1 & \text{if} \quad 1 < \frac{p_{im}}{p_{em}} \end{cases} \tag{2.24}$$

For a compressible flow Π_{egropt} is

$$\Pi_{\mathrm{egropt}} = \left(\frac{2}{\gamma_{\mathrm{e}} + 1} \right)^{\frac{\gamma_{\mathrm{e}}}{\gamma_{\mathrm{e}} - 1}} \tag{2.25}$$

Further effective area A_{egr} is modelled as a polynomial function of a EGR valve position and its dynamics $\tilde{u}_{egr}$ [44] .

$$A_{egr} = A_{egrmax} f_{egr} \left(\tilde{u}_{egr} \right) \tag{2.26}$$

Function f_{egr} and A_{egrmax} are tuned with the described method in section 3.5.3.

2.1.4 Turbocharger

Turbo charger model includes three models namely turbine mass model, compressor mass model, and turbo Inertia model.

Turbine Mass Model

Turbine mass flow is modelled using the choke function to correct the density change in the mass flow and is given as [44]

$$\frac{W_t\sqrt{T_{em}R_{\mathrm{e}}}}{p_{em}} = A_{vgtmax} f_{\Pi_{\mathrm{t}}}\left(\Pi_{\mathrm{t}}\right) f_{vgt}\left(\tilde{u}_{vgt}\right) \tag{2.27}$$

Where, A_{vgtmax} is the maximum area in the turbine that gas flows through. In addition, turbine flow W_t is modelled as a chocking function of pressure ratio $f_{\Pi_t}(\Pi_t)$ and VGT actuator position $f_{vgt}\left(\tilde{u}_{vgt}\right)$. And it is given as [44]

$$f_{\Pi_{\mathrm{t}}}\left(\Pi_{\mathrm{t}}\right) = \sqrt{1-\Pi_{\mathrm{t}}^{K_t}} \tag{2.28}$$

And,

$$f_{vgt}\left(\tilde{u}_{vgt}\right) = c_{f2} + c_{f1}\sqrt{\max\left(0, 1-\left(\frac{\tilde{u}_{vgt}-c_{vgt2}}{c_{vgt1}}\right)^2\right)} \tag{2.29}$$

Parameters in the choking function f_{Π_t} and the effective area function f_{vgt} are tuned according to the methods shown in the model tuning and optimizing chapter.

Compressor Mass Model

Compressor mass flow is modelled using two variables namely energy transfer coefficient ψ_c and volumetric flow coefficient ϕ_c as [44]

$$\psi_c = \frac{2c_{pa}T_{amb}\left(\Pi_c^{1-\frac{1}{\gamma_a}}-1\right)}{R_c^2\omega_t^2} \tag{2.30}$$

ψ_c is the ratio of isentropic kinetic energy of gas at given pressure ratio Π_c to the kinetic energy of a turbine blade tip with the compressor blade radius R_c [44].

$$\phi_c = \frac{W_c/\rho_{amb}}{\pi R_c^3 \omega_t} = \frac{R_a T_{amb}}{p_{amb} \pi R_c^3 \omega_t} W_c \tag{2.31}$$

ϕ_c is the ratio of volume flow rate coming into the compressor to the volume swept by the compressor blades for the air of density ρ_{amb} at ambient temperature.

ϕ_c and ψ_c are given relation according to Wahlström, J et al. [44], and they represent the axes an ellipse and they can be modelled as the polynomial functions of each other. Polynomial coefficient vectors for the same are described in the model tuning and optimization chapter that follows the following equation [44] for minimizing the objective as following cost and with the parameters as $c_{\psi_{1,2}}$ vectors and $c_{\phi_{1,2}}$ for the tuning sessions described in the section 3.5.1.

$$\phi_c = \sqrt{\max\left(0, \frac{1 - c_{\psi_1}\left(\psi_c - c_{\psi_2}\right)^2}{c_{\phi_1}}\right)} + c_{\phi 2} \tag{2.32}$$

Turbocharger Inertia Model

According to Newton's second law, for the turbo speed ω_t citewahlstrom2011modelling

$$\frac{d}{dt}\omega_t = \frac{P_t \eta_m - P_c}{J_t \omega_t} \tag{2.33}$$

Where, J_t is the turbo inertia, P_t is the turbine power delivered with the η_m mechanical efficiency, and P_c is the power required to drive the compressor.

2.2 Diesel Engine Combustion and Emissions Model

Diesel combustion is a heterogeneous chemical process during which the liquid fuel consisting of hundreds of hydrocarbon species interacts with gaseous in-cylinder charge (air) leading to heat release and emission formation. These thermal reactions are influenced by several parameters such as engine geometry, state of the charge mixing with fuel, and

residuals from combustion. Based on this combustion principle, engine manufacturers have developed a few technologies such as Variable Valve Technology (VVT), Electronics Fuel Injection Systems, Turbochargers, Superchargers, EGR, and After Treatment Systems. These techniques aim for optimal fuel consumption and emission reduction in both the tailpipe and the cylinder causing engine control to be a complex task. As a result, developers have a new task: the need to understand this complex phenomenon. Combustion models are valuable tools to aid in the understanding of the combustion process and have led to new technological insights that have yielded better fuel efficiency and reduced emissions.

A detailed crank angle degree (CAD) based diesel combustion model is developed in this work that depicts the behavior of the engine combustion chamber and the thermochemical phenomena involved during each engine power stroke (engine cycle). This model is divided into three sub models as

1. Rate of Heat Release (ROHR) model
2. Chemical Equilibrium Solver
3. NOx Predictor - Zeldovich Mechanism to predict the engine out (EO) NOx

Figure 2.4 represents the primary blocks involved in Diesel Engine Combustion Model and NOx prediction.

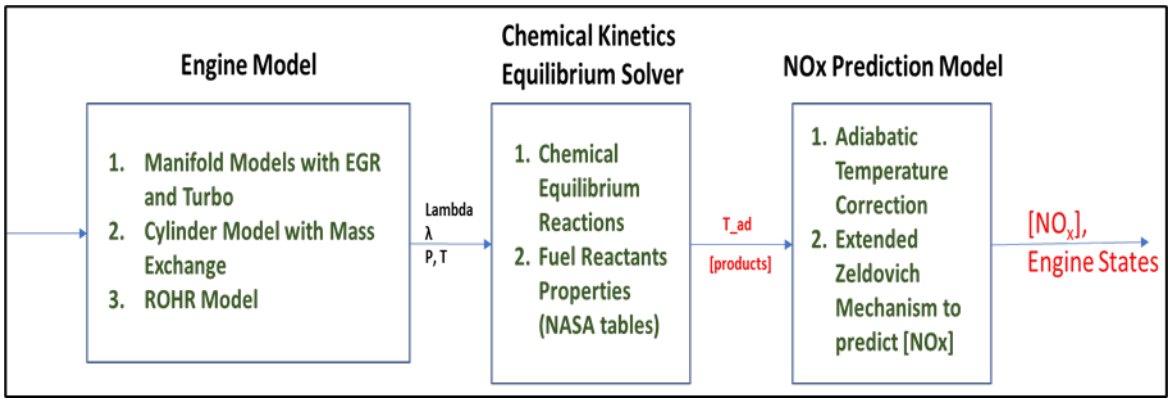

Figure 2.4. Integrated Engine Model Overview

Physics based engine model generates engine states such as Mass flows, Pressures and Temperature at manifolds and in cylinder that are required to calculate the heat release rates

for each CAD of engine cycle. These states are provided to the chemical equilibrium solver that predicts the adiabatic temperature by using the standard fuel reactants properties. Equilibrium model also estimates the concentration of the different species (hydrocarbons and other flue gases) formed after the combustion. Further NOx is predicted from these chemical species and cylinder states that are estimated from the Engine, ROHR, and Chemical equilibrium model. A brief flow of the algorithm is shown in the Figure 2.5 that depicts the engine cycle and CAD based estimations done in this work. Details of these models are discussed in the upcoming sub-section 2.2.1.

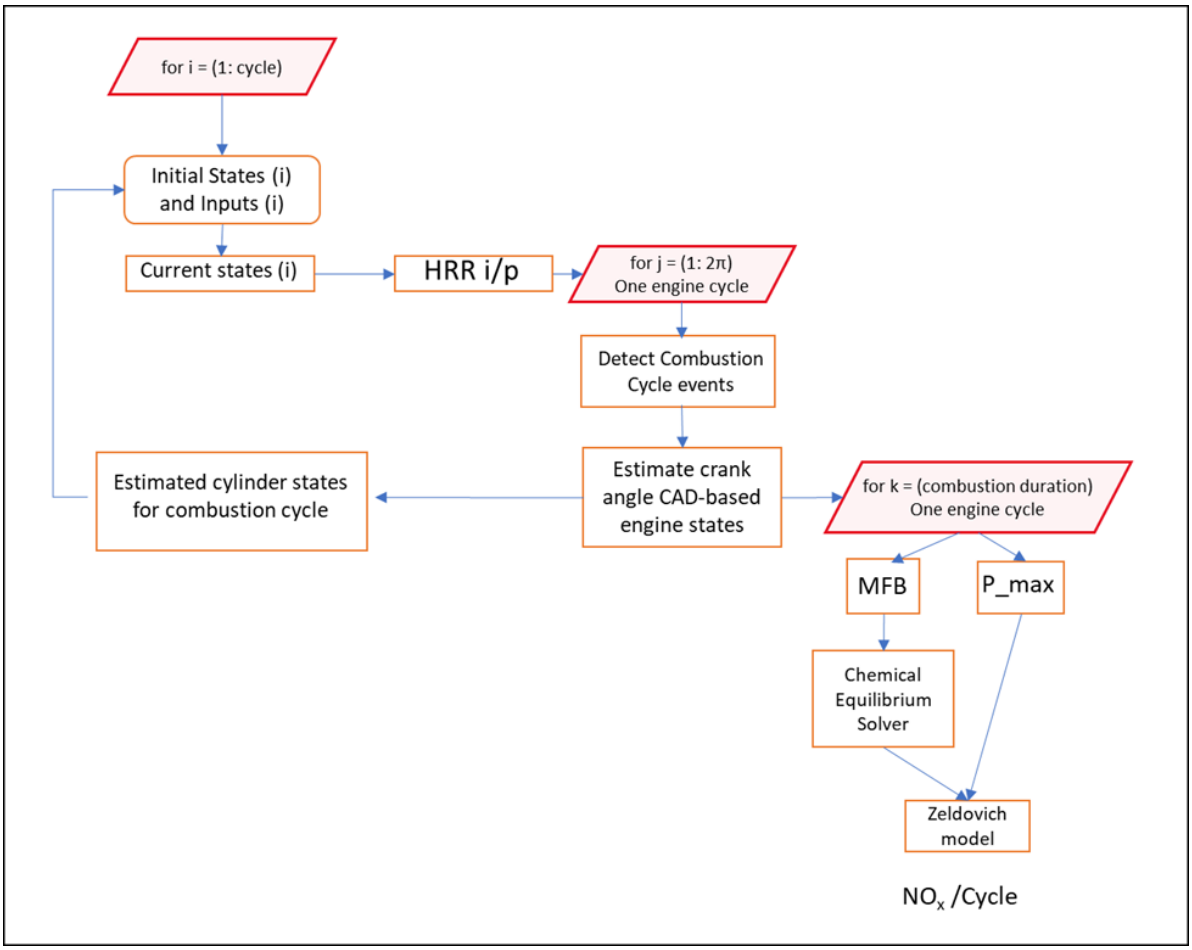

Figure 2.5. Algorithm for Complete Cycle States Estimation

2.2.1 Rate of Heat Release Model

Engine Emission models are validated using "measured" heat release rate profiles, i.e., as derived from measured in-cylinder pressure curves. Trivially, these measured profiles contain all information regarding the influence of the applied engine operating variables on the fuel burning rate and subsequent emission formation. This work focuses on developing HRR model with respect to CAD to get the detailed traces of in-cylinder parameters to achieve the maximum resolution of estimation. Heat release rates depend on the fuel injection rate and composition of the charge air entering the cylinder. Also, speed and torque requirements decide the fuel injection rates and related timings like start of injection (SOI), end of injection (EOI), and followed by the ignition delay calculated from the ignition delay correlation which is not in the scope of this work. Air charge entering the cylinder decides the air-fuel ratios for the current cycle. After the actuated EGR and VGT, composition of the charge entering the cylinder changes thus changing the local air-fuel ratio. Injection duration and air-fuel ratio are required to calculate the ignition delay. That decides the start of combustion (SOC) and then the combustion duration decides the combustion rate from the mass burnt fractions. Cylinder pressure and temperature are then estimated based on the heat release rate using the ideal gas laws. Figure 2.6 shows a block diagram of inputs and outputs for an HRR model. Fuel and air masses or lambda (air-fuel ratio) decide the mass burnt fractions and heat released after combustion. Expansion caused by heat released determines the pressure inside the cylinder. Cylinder pressure and temperatures are required for predicting emissions that are associated with the reaction rates at respective temperature and pressure. In Figure 2.6, green curve indicates the motoring curve that is plotted when there is no combustion involved in engine cranking. Red curve indicates the combustion curve after the combustion phenomenon. Added heat due to combustion in presented by a red curve after the ignition i.e. after the combustion event that shows the peak in added heat.

Heat Release Rate (HRR) modeling requires the modeling of engine motoring curve based on the thermodynamic ideal cycle. Change in volume is modelled with respect to CAD and pressure is estimated based on ideal gas laws. A few relations for engine geometry to estimate the volume and pressure curves are discussed below.

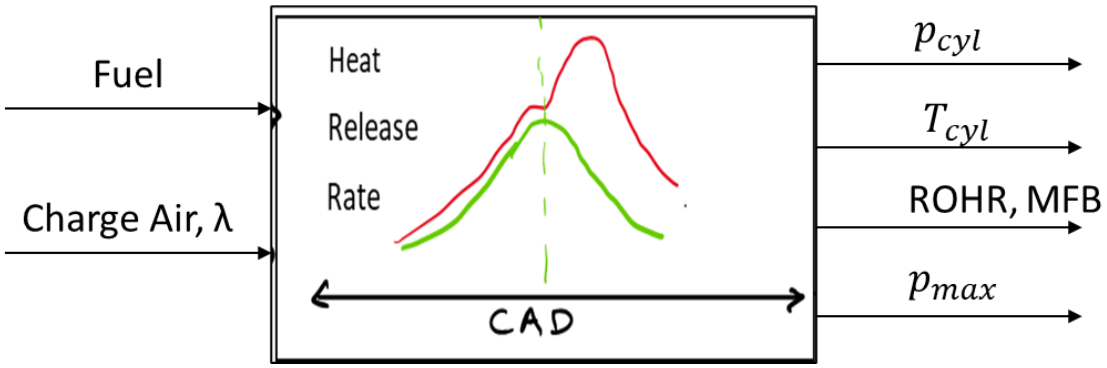

Figure 2.6. HRR Model Block

Engine Geometry

The cylinder volume and piston speed are determined by basic geometric analysis of the engine component, which is summarized here for as follows and given by Figure 2.7. The piston position relative to top dead center (TDC) is given by,

$$z = l + a - s \tag{2.34}$$

where, l is the length of piston connecting rod and a is the crank radius (half stroke) and s piston stroke with respect to the crank angle is determined as follows,

$$s = a\cos\theta + \sqrt{l^2 - a^2\sin^2\theta} \tag{2.35}$$

where, θ is crank angle position. Piston position is a function of crank angle θ,

$$z(\theta) = l + a(1 - \cos\theta) - \sqrt{l^2 - a^2\sin^2\theta} \tag{2.36}$$

the clearance volume, V_c of the engine is define as the combustion chamber volume with the piston position at top dead center (TDC). Thus, engine volume as a function of piston position is,

$$V(\theta) = V_c + \frac{\pi B^2 z(\theta)}{4} \tag{2.37}$$

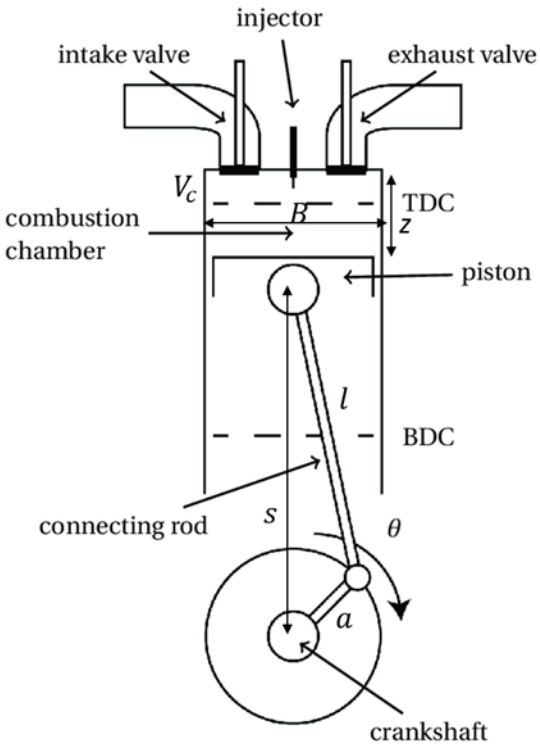

Figure 2.7. Engine Cylinder Geometry

Where B is the cylinder bore.

Additionally, volumetric efficiency of a cylinder is determined by the model tuning for the different measurements as discussed in the cylinder mass model and tuning section 3.5.4. Resultant volume of incoming mass in the cylinder is then calculated for the further estimations.

Engine Thermodynamic Cycle

A conventional automotive 4 stroke engine cycle consists of four distinct strokes, each determined by one half engine revolution. The first stroke is the intake stroke, where fresh air and fuel are drawn into the engine together or separately depending on the type of injection system. This leads to the second, or compression, stroke, where the fuel-air mixture is brought to a combustible state useful for converting the chemical fuel energy into useful work. At the end of the compression stroke, the mixture is ignited, and the combustion defines the beginning of the expansion stroke. It is this stroke that accounts for work output

of the engine. At the end of the expansion stroke, the hot gases are expelled from the engine during the exhaust stroke in preparation for a fresh charge of air and fuel in the subsequent intake stroke, thus completing the cycle. The complete cycle therefore encompasses two full revolutions of the crankshaft. The conversion of chemical energy into useful mechanical work occurs during the combustion and expansion phase of the cycle and is given by,

$$W = \int_{-2\pi}^{2\pi} P(\theta) dV(\theta) \tag{2.38}$$

Ideal Gas Cycle for Determining the Motoring Curve of Engine

The combustion in engine follows the ideal gas law in general. Pressure was modeled as a function of the angle of the crank, which ran for 720 degrees per cycle or two revolutions because the crank completes two rotations per cycle. The valve timing, engine geometry, engine speed and inlet pressure were entered in the model. The individual processes of the engine cycle, intake, compression, combustion, expansion, and blowdown/exhaust are discussed below in order of occurrence. In cylinder pressures and volumes are modeled with respect to crank angle by following the ideal gas laws as follow,

$$P_{\text{motor}} = \left[\frac{V\left(\theta_{\text{ref}}\right)}{V(\theta)}\right]^{k} \times P\left(\theta_{\text{ref}}\right) \tag{2.39}$$

Where, P_{motor} is the motoring pressure with respect to the crank angle (CAD), $V(\theta_{ref})$ is the reference volume at initial reference CAD, $V(\theta)$ is the volume at CAD, $P(\theta_{ref})$ is the initial reference pressure (atm pressure here with turbo boost) and k is the adiabatic constant equal to 1.33. Further Temperatures can be found out using ideal Gas law,

$$PV = mRT \tag{2.40}$$

Figure 2.8 to 2.11 show the motoring and combustion curves for pressure and temperature with respect to CAD for 0 to 2π for two cases as follow. These plots are just to illustrate the model working taken for the 800rpm speed.

- **Case 1:** Start of injection (SOI) = 0, End of injection (EOI) = 5 and Combustion duration = 8
- **Case 2:** Start of injection (SOI) = -20, End of injection (EOI) = 5 and Combustion duration = 30

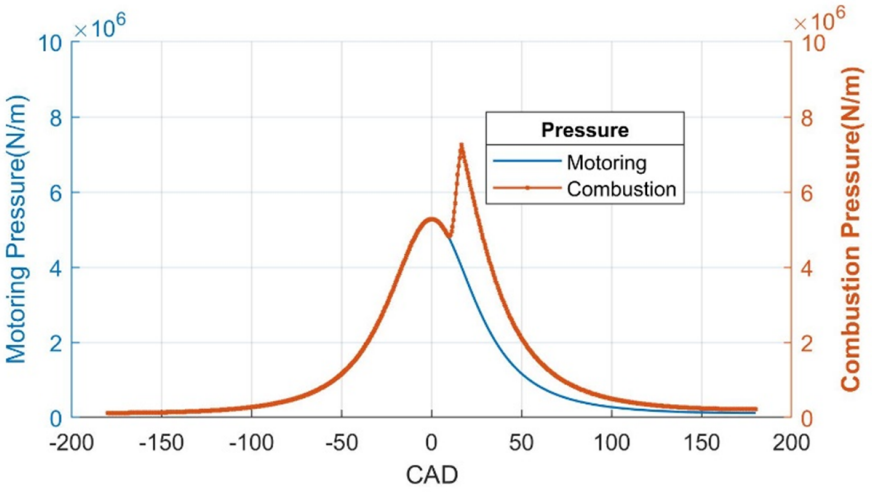

Figure 2.8. Pressure v/s CAD results: Case 1

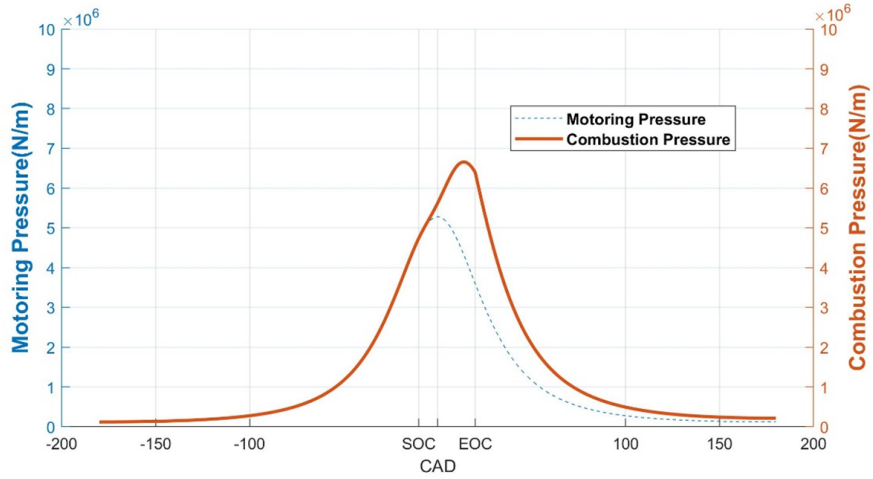

Figure 2.9. Pressure v/s CAD results: Case 2

Primary validation of the motoring and the combustion pressure/temperatures are done with changing the engine events such as start of injection (SOI), end of injection (EOI), and

injection duration. Significant shifts in the peak pressure and temperatures are observed before the model is integrated with the main engine model for the stationary and transient cycles. These peaks are due to the heat added after the combustion from start of combustion (SOC) to end of combustion (EOC).

In-cylinder Pressure: From the predicted heat release rate profile, the in-cylinder pressure curve can be reconstructed. From this signal several important variables for combustion control can be determined such as the indicated specific fuel consumption, maximum pressure rise during combustion and maximum in-cylinder pressure.

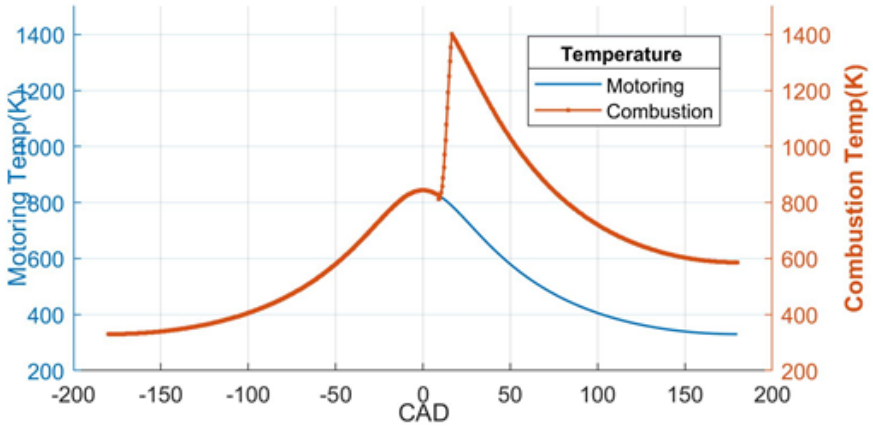

Figure 2.10. Temperature v/s CAD results: Case 1

In-cylinder Temperature: The in-cylinder averaged temperature can be derived when the heat release rate is known. This is an important variable to determine thermal loading. Furthermore, the exhaust gas temperature, which is an important variable in exhaust gas aftertreatment control, can be computed using this temperature.

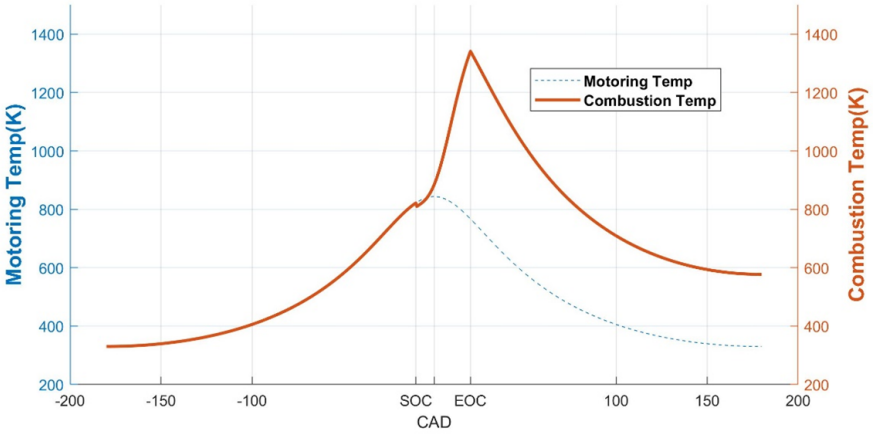

Figure 2.11. Temperature v/s CAD results: Case 2

Mass Fraction Burnt – Application of Wiebe Function

Many previous works on estimating the emissions are based on the Mass Fractions burnt during the ignition duration. Similar approach is used in this work to estimate the mass fraction burned as a function of engine position using the Wiebe function [18]. The Wiebe function is expressed as:

$$MFB, x_b = \left\{ 1 - \mathrm{e}^{\left(-a\left(\frac{\theta-\theta_{SOC}}{\Delta\theta}\right)\right)^{m+1}} \right\} \tag{2.41}$$

Where, a and m are the correlation constants taken to be constant here, and θ, θ_{SOC}, and $\Delta theta$ are current CAD, CAD at SOC and combustion duration, respectively. The Wiebe function curve has a characteristic S-shaped curve that is demonstrated for this study in

Figure 2.12. It is commonly used to characterize the combustion process. Ignition delay is calculated from the Watsons et al. [17] correlation that is given by as follows,

$$\tau_{ig} = A\phi^{-k} p_{EOI}^{-n} e^{\frac{E_a}{RT_{EOI}}} \tag{2.42}$$

Where, A, k,n are constants and E_a is an activation energy. The mass fraction burned profile grows from zero, where zero mass fraction burn indicates the start of combustion, and then tends exponentially to one indicating the end of combustion. The difference between those two ends is known as the duration of combustion. In the other words, it is a duration between start of combustion and end of combustion. NOx in diesel engine predominantly occurs in between the SOC and EOC, which is 10% of mass burnt (CA10) to 90% of mass burnt (CA90). According to the experimental data for various engines, the duration between CA10 and CA90 is roughly around 30 CAD [39]. Thus, combustion duration of 30degrees is considered for the study to estimate the MFB and ultimately NOx formation duration.

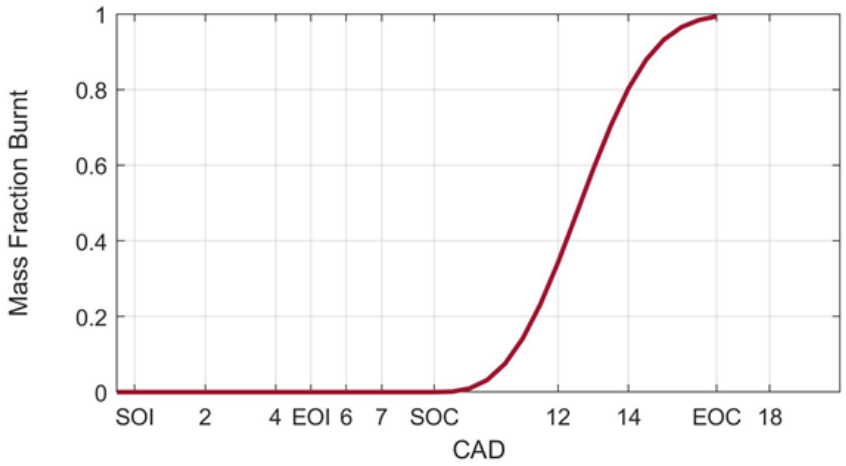

Figure 2.12. Mass Fraction and Combustion Events, SOI, EOI, SOC and EOC

CHRR (Cumulative Heat Release Rate)

The first law of thermodynamics applied to the combustion chamber is now applied for the heat release rates,

$$dQ_{hr} = dU + dQ_{ht} + dW \tag{2.43}$$

To calculate the pressure at exhaust ports and respective temperatures to predict the EO emissions, we need to consider the first law of thermodynamics. Cumulative heat release rates with respect to crank angle CA is modeled to provide the exhaust gas temperature as follows,

$$\frac{dQ}{d\theta} = \frac{dU}{d\theta} + P\left(\frac{dV}{d\theta}\right) = \frac{\gamma}{(\gamma-1)P(\theta)\left(\frac{dV}{d\theta}\right)} + \frac{1}{(\gamma-1)V(\theta)\left(\frac{dP}{d\theta}\right)} \tag{2.44}$$

To calculate the heat release Q, we need to consider the mass burned fraction MFB (x_b) obtained from the equation 2.41 and Q is given as

$$Q = x_b \times m_f \times q_{LHV} \tag{2.45}$$

Where m_f is fuel mass at that CAD which is calculated from the optimized air-fuel ratio based on the outputs from cylinder and mass exchange model discussed before. HRR traces are shown in Figure 2.13 from start of combustion (SOC) to End of combustion (EOC). MFB from this model decides the concentration of the reactants having both fuel and air masses used in chemical equilibrium solver that are discussed further. Pressure peak from this model gives the data estimates for the emission formation duration. Figure 2.14 shows the HRR model algorithm. The cylinder events and parameters follow ideal gas laws for the suction, compression, and expansion. And it follows the combustion cycles for the combustion stroke i.e., it is associated with the heat released from the mass of fuel burnt at corresponding crank angle degree (CAD).

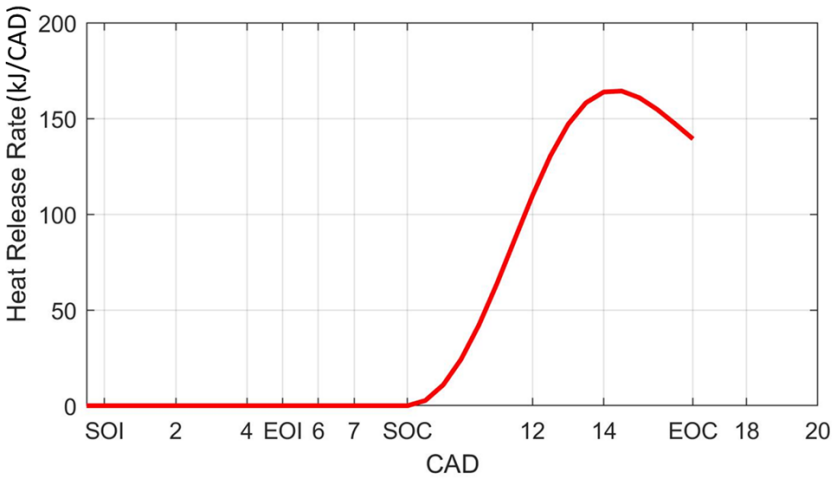

Figure 2.13. HRR and Combustion Events

2.2.2 Chemical Kinetics Equilibrium Solver

For ideal diesel combustion, reactants (fuel and air) and products are balanced in the equilibrium state converting all reactants into to the products undergoing a complete combustion as shown in the following equation 2.46.

$$\begin{aligned} &C_x H_y + (t)(a)\,(O_2 + 3.76N_2) \\ &\qquad \rightarrow xCO_2 + \frac{y}{2}H_2O + (t \times 3.76 \times N_2) + (t-1)\left(x + \frac{y}{a}\right)O_2 \end{aligned} \tag{2.46}$$

When fuel $C_x\ H_y$ reacts with the air mixture at stoichiometric proportions, products are formed in such way that they maintain the chemical equilibrium. Products formed in above reaction depends on the fraction 't' which defines the local air-fuel ratios and mass burnt fractions received from the HRR model. According to the first thermodynamics law, total enthalpy of the products and reactants as follows,

$$h_{\text{reat}}\ (T_{\text{react}}\ , P) = h_{\text{prod}}\ (T_{\text{prod}}\ , P) \tag{2.47}$$

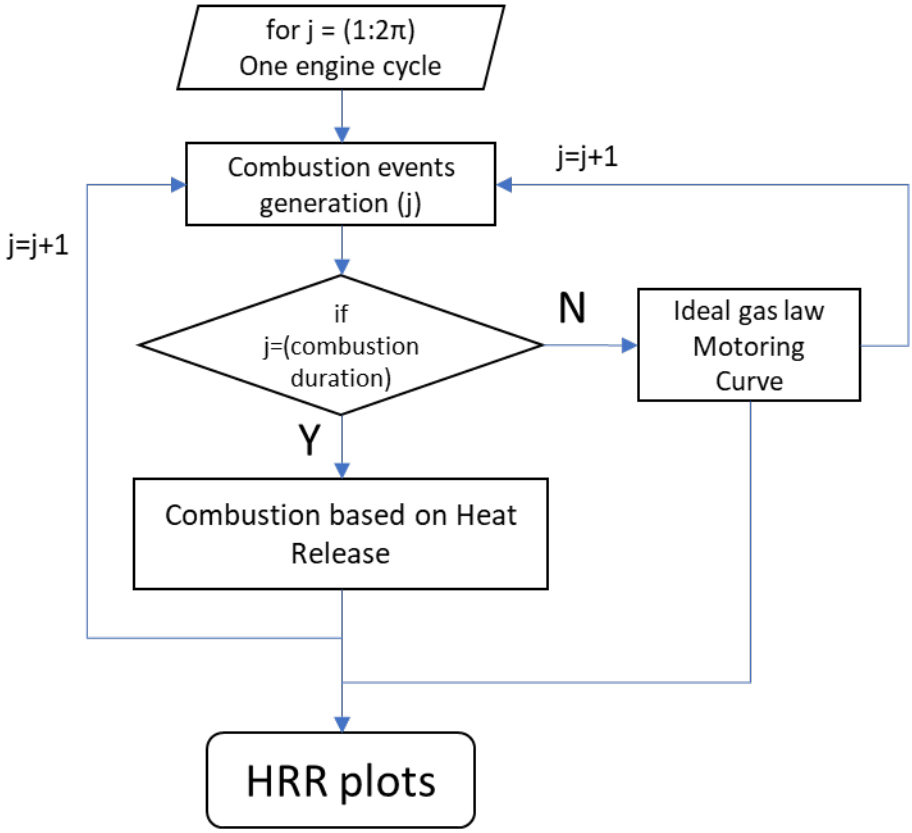

Figure 2.14. HRR Model Algorithm

For this adiabatic constant pressure and constant volume process gives an adiabatic temperature required for Zeldovich mechanism as mentioned in section 2.2.3. Enthalpy of formation for reactants and products are taken from JANAF and NASA tables. Newton Rapson iterative method is used to calculate the adiabatic temperature, T_{ad} by minimizing the enthalpy difference between products and reactants, refer Figure 2.15. Concentration of the products formed are also required for emission calculation.

This model is evaluated at each crank angle CAD for each mass burnt fraction and local air-fuel ratios that are estimated from an HRR model.

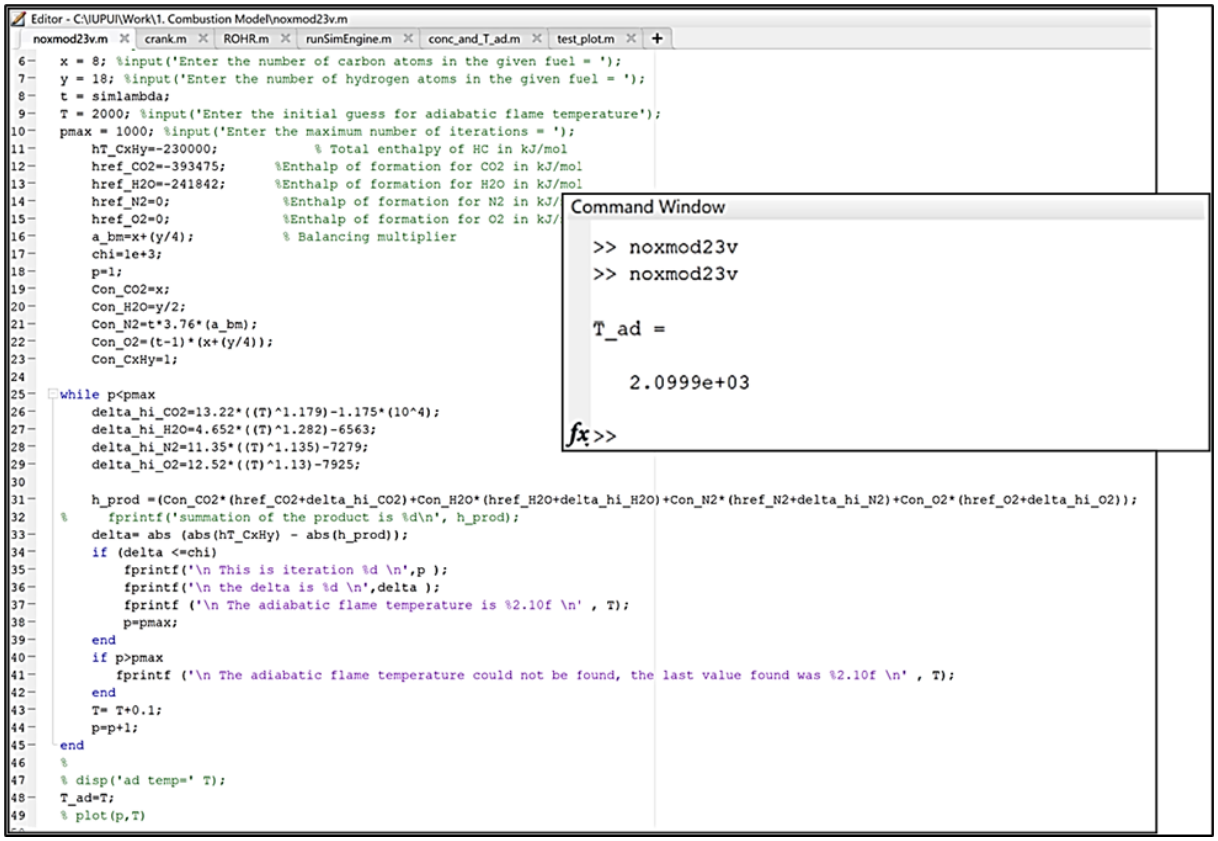

Figure 2.15. Chemical Kinetic Equilibrium Solver

2.2.3 NOx Prediction Model

This work focuses on predicting the NOx based on Zeldovich Mechanism [31]. Kinetics of NOx formation involves series of reactions that are predominantly of oxidation of N2 to NOx. There are two types of NOx, first are NO (Nitric Oxides) and NO2 (Nitrogen Oxides). This NOx depends on the engine operating condition. But NO is predominantly observed for the normal engine operations as compared to NO2 that are results of light load conditions.

Moreover, NO is formed mainly at the flame front where the temperature of the gas is higher than 2000K in presence of oxygen and nitrogen molecules [47]. This is termed as a thermal NOx as shown in Figure 2.16 [6]. This work will only focus on predicting the NO (Nitric Oxides) emissions. Also, the effect of multipoint injection strategy on NO formation is ignored. The amount recirculated masses from the EGR are high enough to neglect the

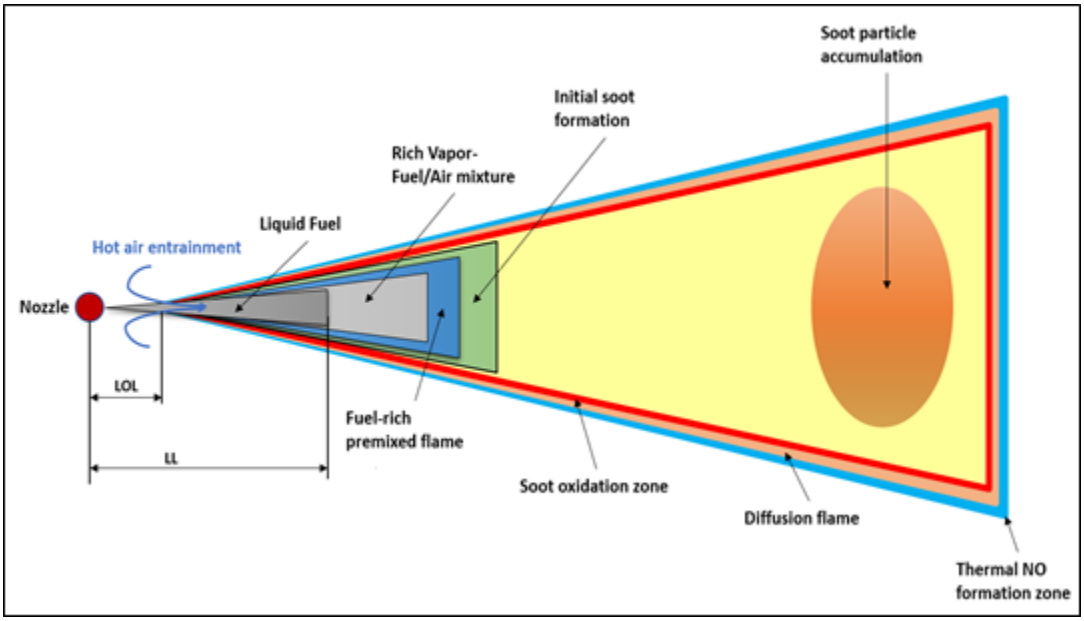

Figure 2.16. NOx Formation at Flame Front in the Flame Propagation

effect of the residuals in the cylinder. Figure 2.17 shows the NO formation model with the parameters involved from other models.

Zeldovich Mechanism involves following series of chemical reactions,

$$\begin{aligned} O + N_2 &= NO + N \\ N + O_2 &= NO + O \\ N + OH &= NO + H \end{aligned} \tag{2.48}$$

Formation of the NO in above reactions depends on initial rates of the reactions that are solely driven by the temperature to initiate the same. Adiabatic temperature from the chemical equilibrium model along with the concentrations of O2 and N2 involved in the reactants.

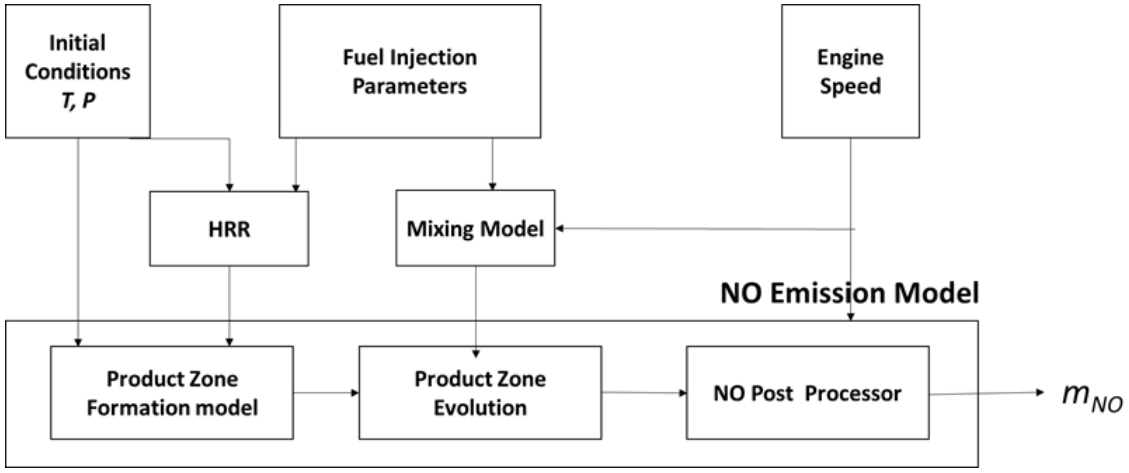

Figure 2.17. NO Formation Model Blocks

According to Zeldovich mechanism, rate of NO formation is given by following expression [48].

$$\frac{d[NO]}{dt} = \frac{6 \times 10^{16}}{T^{\frac{1}{2}}} \times \mathrm{e}^{\left(\frac{-69090}{T}\right)} \times [O_2]_{\mathrm{e}}^{1/2} [N_2]_{\mathrm{e}} \, mol/cm^3 s \tag{2.49}$$

$[O_2]_{\mathrm{e}}$ and $[N_2]_{\mathrm{e}}$ are taken from the chemical equilibrium model and the mass burnt fraction from HRR model for the respective concentrations with respect to CAD. T is the adiabatic temperature in kelvin. Characteristics time for the NO formation process is given by [48],

$$\zeta_{NO} = \frac{8 \times 10^{-16} \times T \times \mathrm{e}^{\frac{58300}{T}}}{\sqrt{P_{peak}}} s \tag{2.50}$$

P_{peak} is taken from the HRR model as p_{max}. Generally, ζ_{NO} is assumed to be same as combustion duration.

NO formation reaction zone volume is required to calculate the total NO formed during the cycle [49]. It depends on mass burnt and number of moles of products involved in the formation reaction. Reaction zone volume, $V_{b,\mathrm{i}}$ is given by,

$$V_{b,\mathrm{i}} = m_{b,\mathrm{i}} \times \frac{R}{\text{Total number of moles} \times \text{Total molecular weights}} \times \frac{T_{\mathrm{i}}}{P_{\mathrm{i}}} \tag{2.51}$$

Where, $m_{b,\mathrm{i}}$ is burnt stoichiometry mass based on local equivalence fuel-air ratio, ϕ_{Local} is given by,

$$\phi_{\mathrm{Local}} = C_1 \cdot \phi_{\mathrm{mean}} + (1 - C_1)\, \phi_{\max NO} \tag{2.52}$$

where $C1$ is a calibration constant determined from the engine design ($0 \leq C1 \leq 1$) and appropriate values of C1 are 0.23 for the heavy-duty engine and 0.31 for the light-duty engine. ϕ_{mean} and ϕ_{maxNO} are mean equivalence ratio and NO formation zone equivalence ratio derived from mass burnt fraction and reaction products moles, respectively. Thus, total NO formed in one combustion cycle is given by,

$$NO_{\mathrm{cycle,\ i}} = V_{b,\mathrm{i}} \int_{SOC}^{EOC} \frac{d[NO]}{dt} d(CAD) \tag{2.53}$$

Figure 2.18 shows NO formation rate with respect to mass burnt fraction (MFB) and CAD. It depicts that peak NO formation rate is observed at peak cylinder pressure and it is proportional to the mass burnt fraction.

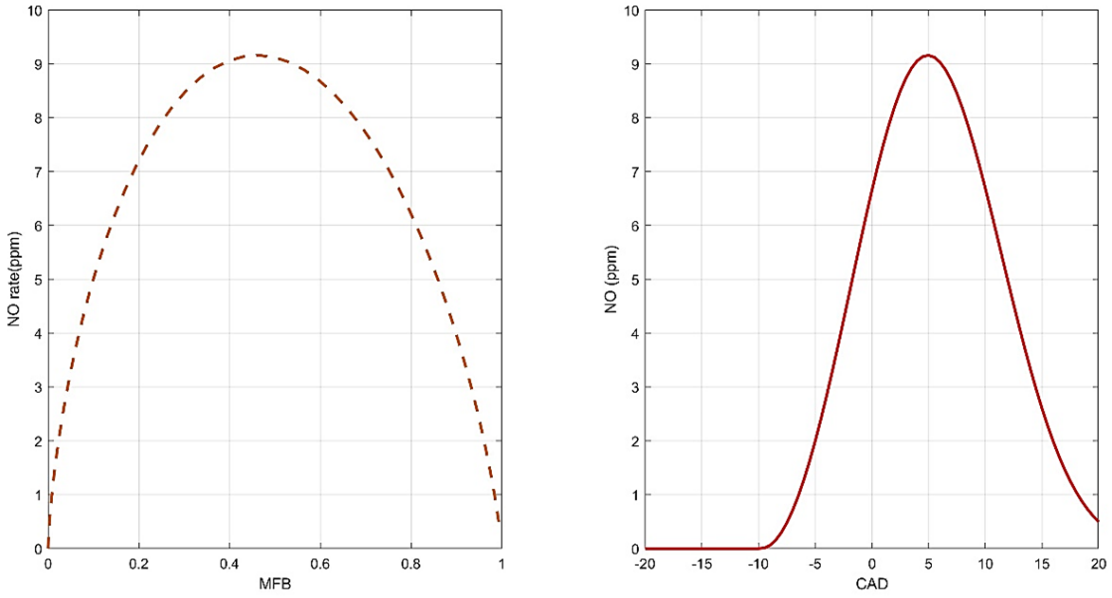

Figure 2.18. NOx Formation Rate w.r.t. MFB and CAD for One Cycle

Adiabatic temperature correction for the losses due to radiation and dissociation

The initial combustion product temperature is determined using a chemical equilibrium solver based on minimizing Gibbs free energy, considering the effect of dissociation. Figure 2.19 [50] graphically illustrates how this temperature is corrected for the presence of certain phenomena:

1. Fuel evaporation absorbs heat from the environment, resulting in evaporative cooling. The flame temperature is corrected for this by using the latent heat of evaporation in the computation of the adiabatic flame temperature.

2. Soot radiation contributes to some of the heat transfer through the wall. The flame temperature is corrected using the radiative energy transferred during the crank angle of zone formation.

3. Turbulence induces flame straining, which is a form of turbulence. Physical time scales associated with the flow affect chemical time scales at high levels of turbulence.

A simplified approach to calculate the temperature loss is given by Andersson et al. [28] that considers the heat loss through radiation only as,

$$\Delta T_{rad} = \frac{C_{rad} \left(T_{ad}\right)^4}{c_p} \tag{2.54}$$

Where δT_{rad} is local temperature drop due to radiation, C_{rad} is a constant to be tuned, T_{ad} is adiabatic temperature compensated for the dissociation, and c_p is specific heat at constant pressure. No temperature losses than the radiation losses from the burned zone are consider for the simplicity. Results of the NO for the tuning and validation are discussed in section 3.6.

2.3 Summary

A physics-based model is adopted from Wahlström, J et al. [44] to model the diesel engine equipped with EGR and VGT. Dynamic equations of all subsystems involved in

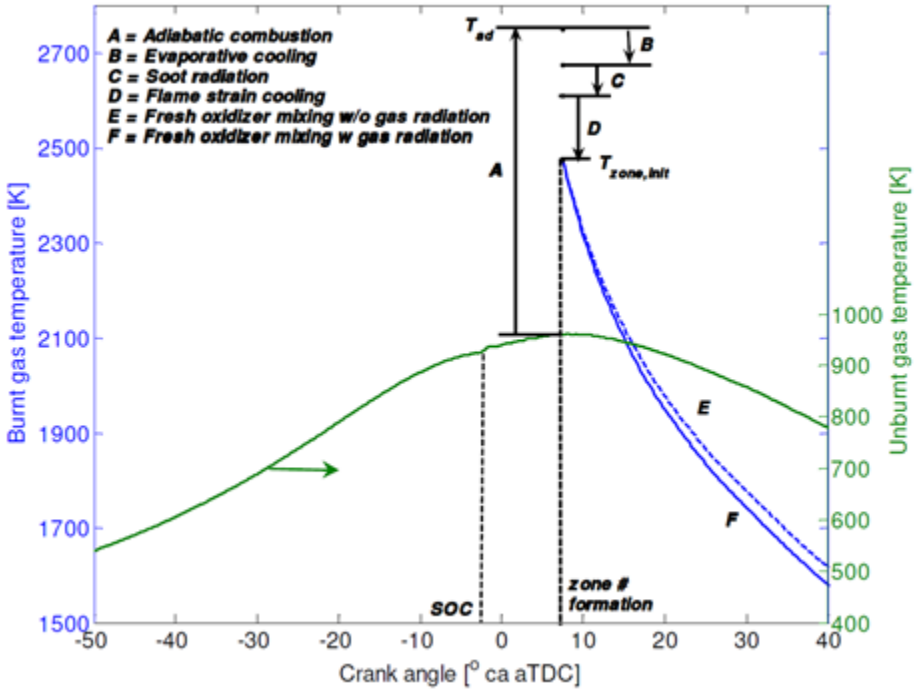

Figure 2.19. Graphical Overview - Adiabatic Temperature and Subsequent Evolution

the model are formulated considering the conservation of mass practice. According to the model, unknown parameters are modeled in terms of polynomial functions that need to be tuned using least square methods as discussed in chapter 3. Extended combustion model that estimates the rate of heat release rates based on the cylinder parameters is derived and implemented to predict the EO NOx. The ROHR and NOx models are developed as a function of CAD with the resolution of 0.5 CAD. Motoring and combustion parameters for the model are formulated using the ideal gas laws and then ROHR is using the mass burnt fractions assuming the combustion duration of CA10 to CA90 to target the thermal NOx only. NOx model is derived from the extended Zeldovich mechanism. Adiabatic temperature correction is added by considering the radiative heat losses during the mixing and NOx formation. Reaction zone volume for the formation of NOx is added to estimate the masses of reactants and product in chemical equilibrium solver that helps determining the accurate concentrations involved during the NOx formation. Next chapter discusses the integration

of the NOx model with the engine model along with testing and tuning of both engine and combustion model followed by the validation for the proposed cycle against GT-power data.

3. MODEL INTEGRATION, TESTING, TUNING AND VALIDATION

A mean value model developed in MATLAB and Simulink for a Diesel Engine equipped with EGR and VGT is adopted from the Erikson et. al. work and further modified for the application of interest for this work. This model is tuned for the applied engine parameters using the MATLAB parameter estimation tool for different cases and tests as discussed in upcoming sections. Model tuning and validation is done against the data from virtual model developed in the GT-power. Development of the GT-power model is not in the scope of interest, but the test requirements needed to run the GT model are designed in this work to acquire the best possible data that depicts the actual engine test data. The Simulink model is then integrated with the emission model to predict the cycle-based emission (NOx in this work) to achieve the objective of this work. Details of the application, virtual test requirements and preparations are discussed in the following sections.

3.1 Application of Interest

This work focuses on the light duty commercial diesel engine that has both on and off-road applications. Cummins 6.7L turbo diesel engine equipped with EGR and Turbocharger is considered for the benchmarking and testing. A similar engine is available at the IUPUI facility, and all the physical measurements have been taken for the model development.

Table 3.1. Engine Data - Cummins 6.7 L Turbo Diesel

Engine Design	Inline 6 Cylinder DI Diesel
Bore	4.21” (106.9 mm)
Stroke	4.88” (124 mm)
Displacement	6.7 Liters
Compression ratio	17.3:1
Firing order	1-5-3-6-2-4
Horsepower	350-385 at 2800-3013 rpm
Torque	610-930 lb/ft at 1500-1700 rpm

Figure 3.1. Cummins 6.7L Turbo Diesel Engine

To study the engine performance characteristics, a performance sheet is referred from the manufacturer catalogue. The performance sheet is utilized for the further development in deriving the operating points for both tuning and validation cycles that are discussed in this chapter. Figure 3.1 shows the engine considered for the benchmarking study [51]. Engine specifications and data is provided in the Table 3.1 [51].

3.2 Model Integration in MATLAB and Simulink

A mean value model developed in the MATLAB and Simulink that depicts the continuous operation of an engine cycle including the effects of EGR and VGT. The engine model is then integrated with the NOx function block developed to predict the engine out NOx. A various arrangement such as sample time and simulation environment to configure the model for the tests have been done to produce the data that can be compared with the experimental data and its sample rates/size. Input for the models is derived in the form of signals generated in the signal generator block in the Simulink. These signals are developed based on the test

cases and cycles discussed in the Cycle Generation heading below. Additionally, a parameter file is generated to tune the model parameters separately using the parameter estimation tool in Simulink. These parameters are masked in the sub-models as tunable parameters that are required to tune individual systems as well as in full model tuning. An integrated full engine model with the NOx model is given along with the complete test setup require to run the co-simulations in Figure 3.2 below. Signal generator in the system is providing the required inputs the system that generates the required data that is used as a virtual channel (sensor) to perform the further estimations. Figure 3.3 shows the NOx function integrated with the model parameters from the cylinder. In this work, engine model is cycle based, which means it generates only one data value for one engine cycle. But the NOx model generates 720 data points for one engine cycle that helps estimating the in-cylinder parameters in details based on the CAD. Therefore, the complexity and simulation time increases when the NOx model is integrated and tested for the same.

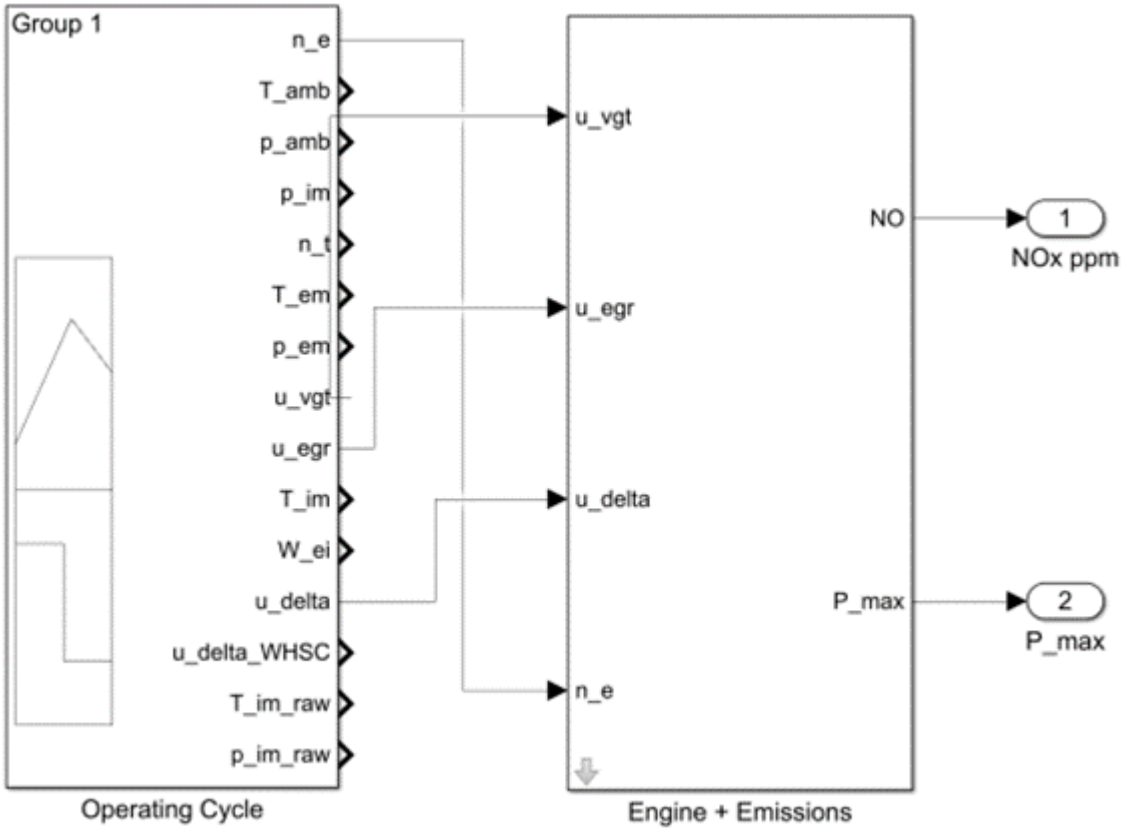

Figure 3.2. Complete Simulink Model Setup

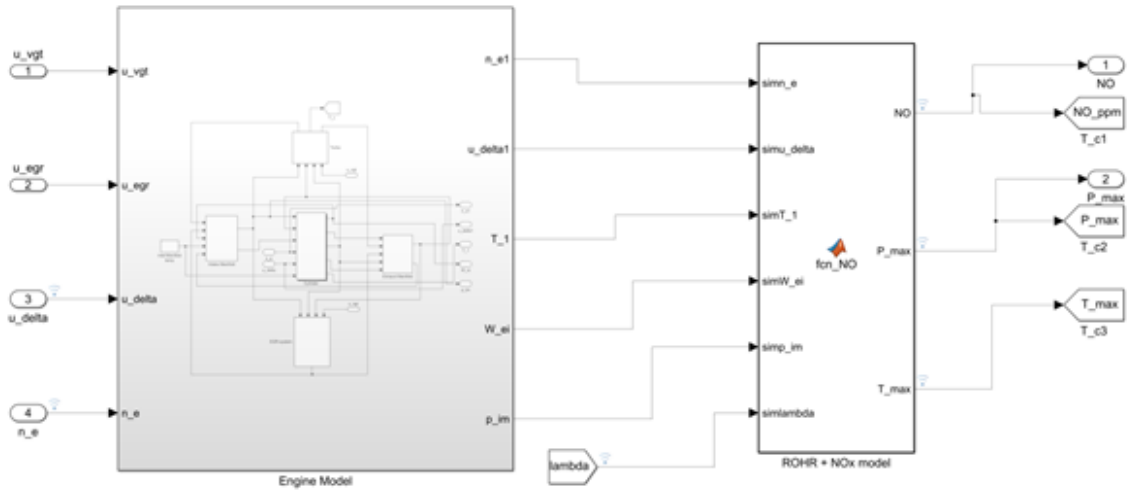

Figure 3.3. Integrated Model with the NOx Function

Thus, the model workflow follows from the engine model to NOx model that simulates an actual engine as if its running through a cycle at a given speed and load. To summarize, NOx function developed in this work is integrated in the engine model such that it adheres to the continuity in the mass flow from engine intake to exhaust as it does in the actual engine operation. Note that, after all the efforts made in this work to make the model as accurate as possible, but certain model properties such as solver and time step restricts the model to be as real as it should be. For this work, fixed time step solvers are used to avoid the validation complexities as the data from GT model is based on the fixed time steps.

3.3 GT-power Reference Model and Data

Development of the GT-power model is not under the scope of this work but providing the detail test requirements is. Required test plans and cases have been provided to the colleague who has modeled the same engine in GT-suite using GT-power toolbox and libraries [52]. Figure 3.4 shows a 6-cylinder diesel engine model developed for the application of the interest. Time based data was collected from the simulations ran on the GT-power for different cases in MATLAB and excel files that are used in the tuning and validation. Additionally, data smoothening techniques and signal filters are implemented to produce the feasible datasets

required in the tuning and validation. Details of these techniques are elaborated in the engine tuning and calibration section for each sub-systems and models later in this chapter.

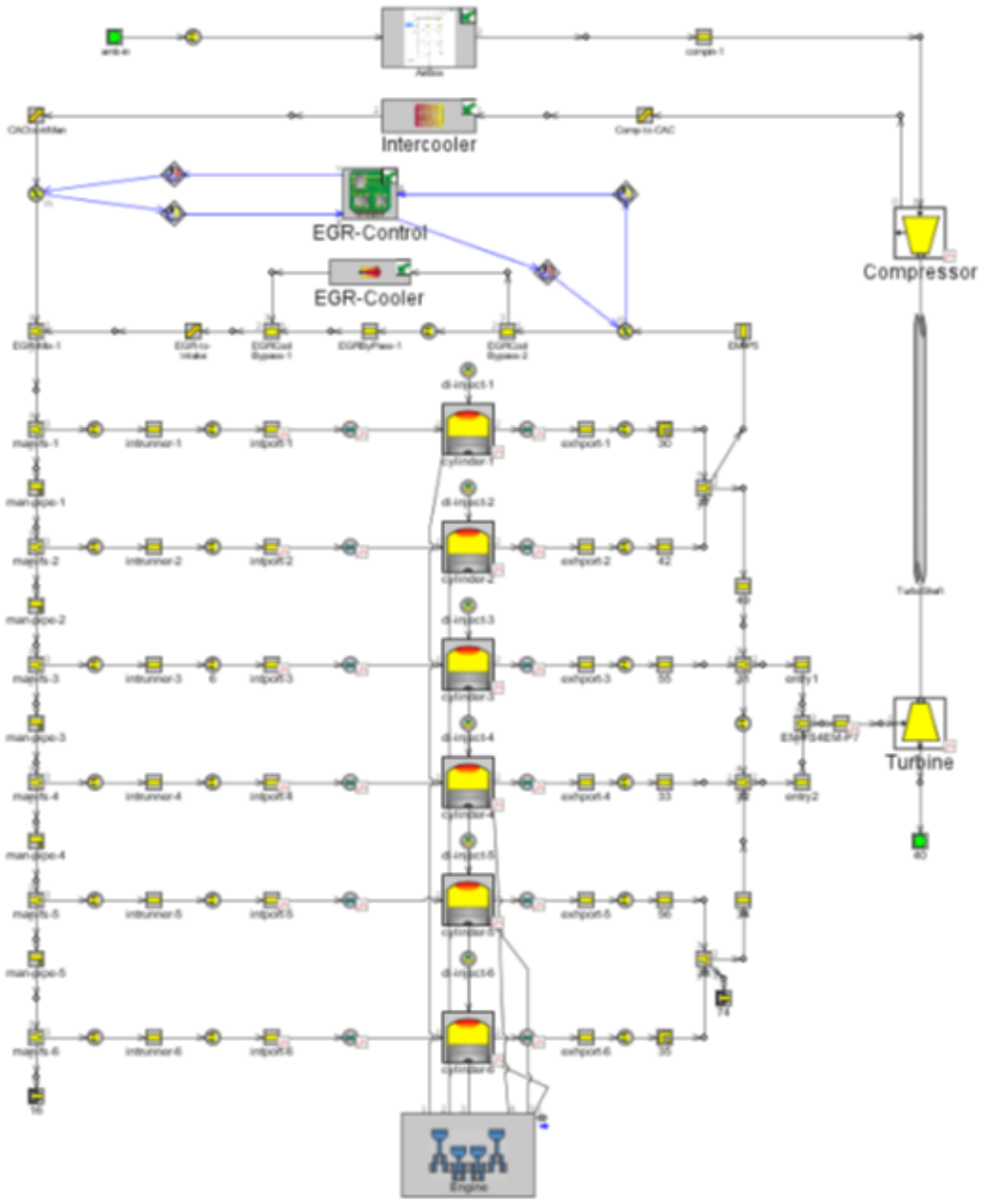

Figure 3.4. GT-power Engine Model for Validation

3.4 Testing Cycle Generation and Design of Experiments (DOE)

Guidelines to choose the engine operation testing points depends on the performance curves provided by the manufacturers for different applications. Performance curves for the Cummins 6.7L turbo diesel engine is taken from the manufacturers catalogue available on the official website. Based on the same, two types of tuning methods are derived that cover the engine operating ranges for low load-speed, high load-speed and rated maximum torque at a given speed. To validate the model for the stationary and transient cycles, a globally recognized cycle – World Harmonized Cycle/s is adopted. The details of the tuning points and the derived cycles are discussed in the following sections.

3.4.1 Stationary and Dynamic Tuning Points for Engine Tuning

Model tuning and parameter estimation are the vital phases of this work. Optimal points from the data sheet released by the manufacturer are taken to tune the model for it physical and empirical parameter that are not possible to measure physically. To capture both steady state and dynamic behaviors of the engine, model parameters are tuned for both steady state and dynamic operations.

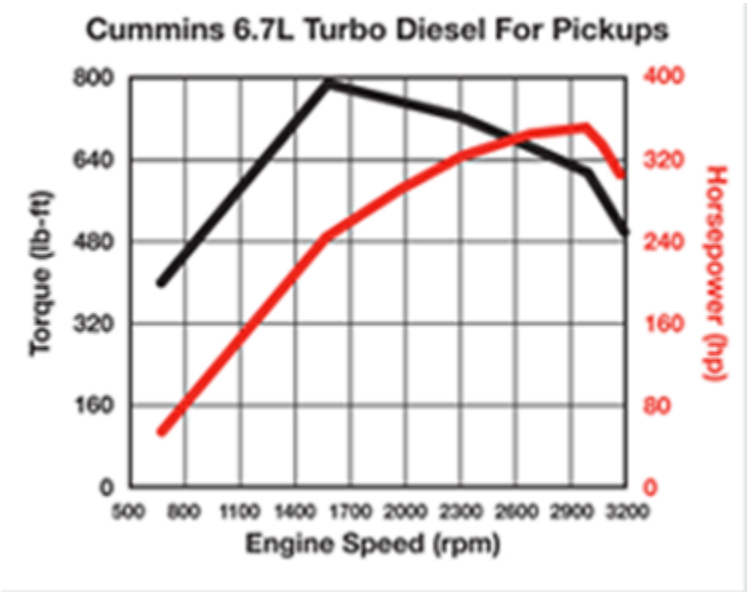

Figure 3.5. Cummins 6.7L Turbo Diesel Engine Torque and Speed Curve

Figure 3.5 shows the torque and power curve for the engine operating range [53]. It indicates the optimal operating ranges for the given engine, which means that the engine cannot operate beyond these profiles for given speed and load. With this background, a steady state simulation plan is derived for three speeds – 800 rpm, 1400 rpm and 2300 rpm for 10 seconds each and constant EGR and VGT input of 50%. These cases are given to the GT-power simulation and data was acquired for the comparison.

Note that, GT-power model has the time delays in the systems while generating the simulation data. These time delays are given the GT-power model to make the model as real as possible. For example, if a sample data is taken for intake and exhaust manifold pressures at a same time, then the exhaust manifold pressure data is taken soon by a fraction of microseconds that depends on the engine speed. Therefore, different sample rates are adopted for the data collection in the GT-power to overcome these delayed or advanced samples that takes care of the measurement errors. These sample times are calculated such that the engine measurements are divided in to the four-time fractions in one cycle. For instance, if engine is running at 800 rpm then 37.5ms sample time covers all subsystem measurements twice in one engine rotation. However, this was applied for the steady state measurements and then a sample rate of 10ms is adopted for further dynamic points and validation cycles and then the data was smoothened and filtered as per the channel need.

Further, to cover the step changes in the speed and load, three operating points are chosen with the ramp for each change in the operating point. A dynamic tuning profile is shown in the Figure 3.6. It is developed based on the same stationary points but for the dynamic step changes from one operating point to another one. This profile is used to tune the parameters that capture the change in speed and load condition. Positions of the EGR and VGT actuators are kept constant for avoiding complexity involved in the actuator dynamics. A constant sample time of 20ms is adopted to record the data from GT-power model.

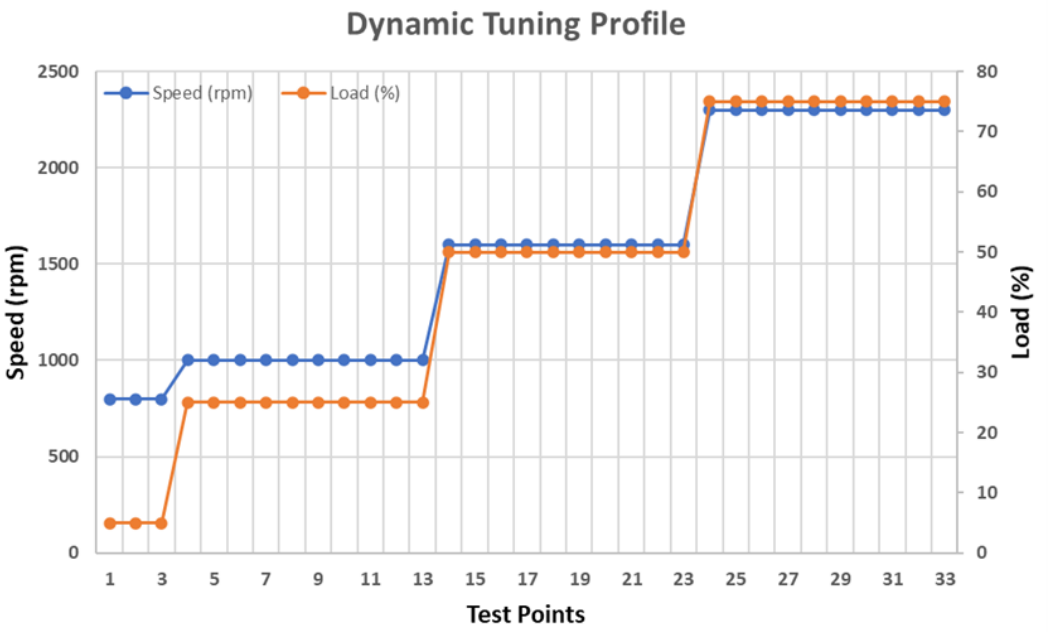

Figure 3.6. Dynamic Three Point Tuning Profile

3.4.2 World Harmonized Cycles for Validation

Worldwide, different vehicle emission testing cycles are used that are developed by the national commissions that govern the legislative regulations for on/off-highway pollutions. In USA, Federal Test Procedure (FTP72) and FTP75 are used along with a few supplemental tests depending on the application of interest. Similarly, European Steady State Cycle (ESC) and Transient Cycle (ETC) are used, whereas other regional cycles in Japan and China are also adopted locally. However, an effort is being made by United Nations Economic Commission for Europe (UN ECE) World Forum for application of the standard test cycle across the world that will lead to cost reductions in the engine development [54]. A framework of this effort is developed in UN ECE World Forum for the Harmonization of Vehicle Regulations (WP.29) in Geneva. These procedures include two cycles: A ramped World Harmonized Steady State Cycle (WHSC) and World Harmonized Transient Cycle for medium and heavy-duty vehicles. The procedure represents the driving conditions in European Union, USA, and Japan. This work focuses on adopting a ramped WHSC cycle for the

validation purpose. Transient validation is not included in this scope as vehicle simulator or experimental setup is not available to conduct the procedure and hence the required data.

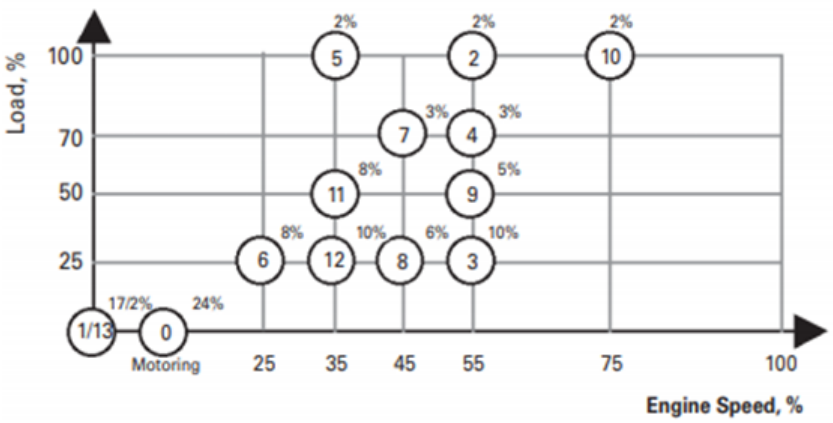

Figure 3.7. WHSC Normalized Operating Points

WHSC is a steady state test cycle with the 13 operating points under the engine map. A ramp is also included after every point. Emissions are continuously sampled in this cycle. Whereas other cycles have cold and hot start zones followed by the stability zones where the emissions are not sampled. Length of each operating point is measured by the weighing factor. Figure 3.7 shows the normalized map of the operating points for both engine speed and load [54]. Weighing factors are superscripted on each point that defines the length of that operation. Meaning 13 operating points are taken for the different load conditions that covers the low, high, and critical rated load conditions. Weights are given according to the application of these loads accordingly. Following the same procedure for WHSC cycle, a validation cycle is generated for the application interest where the speed and load are normalized from the minimum to maximum. Figure 3.8 shows the generated profile for the cycle used in this work. Based on the guidelines, cycle has a length of 1695 seconds. But ramps are not included to validate the sudden steps. Generated cycle data with the weighted the lengths is shown in the Table 3.2.

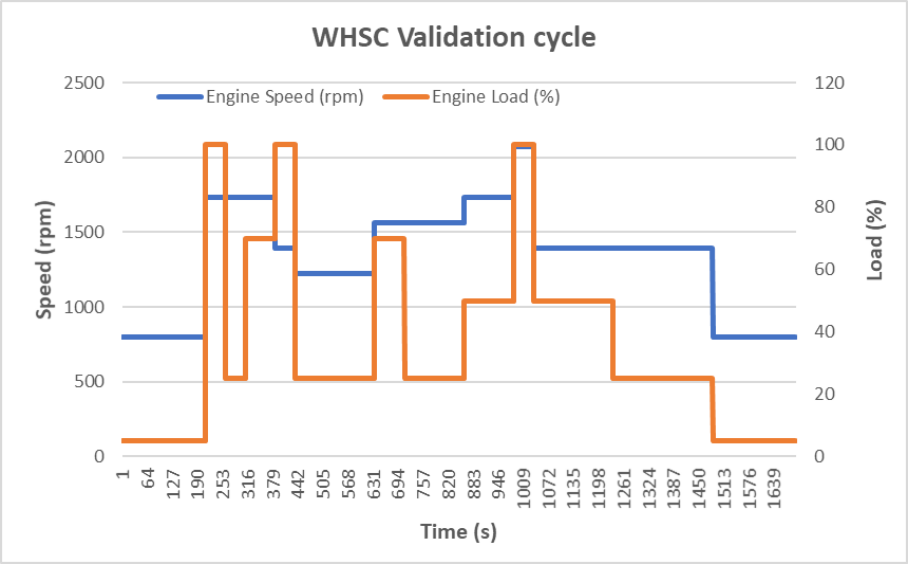

Figure 3.8. Generated WHSC Cycle for Validation

Normalization of the load and speed is done by taking the minimum and maximum operation points taken from the performance data extracted from the manufacturers catalogue.Normalization of the load and speed is done by taking the minimum and maximum operation points taken from the performance data extracted from the manufacturers catalogue. And these normalized points then divided in to the same range of minimum and maximum rated load and speed which are then calculated as percent load and speed. This profile was provided to the GT-power simulation input and data is taken for the sample rate of 20ms for the validation purpose. A detail tuning and validation for subsystems and full model is discussed in the next section.

Table 3.2. Weighted Validation Points for the WHSC

Mode Point	**Time**	**Normalized Speed %**	**Normalized Load %**
0	0	motoring	motoring
1	210	0	0
2	260	55	100
3	310	55	25
4	385	55	70
5	435	35	100
6	635	25	25
7	710	45	70
8	860	45	25
9	985	55	50
10	1035	75	100
11	1235	35	50
12	1485	35	25
13	1695	0	0

3.5 Engine Tuning and Parameter Estimation

Engine Tuning (calibration) and parameter estimation is done by deriving an optimization problem to minimize the squared error between measured (GT-power data) and simulated data. This cost problem (minimizing the error between measured and simulated data) is then optimized to estimate the unknown parameters in the physics-based dynamic system equations that are used while modeling the system. This process is called as parameter estimation, it is done for both stationary and dynamic tuning points that are derived for the application of estimation. Considering the total number of parameters and the cost of function evaluation, tuning is done for both sub-models and full model. It is necessary to tune both sub-models and full integrated model to eliminate the errors caused in sub-systems and full model or in combination of both. Tuning experiments are conducted in MATLAB and Simulink – Parameter Estimator Tool. A virtual experiment is created that allows the preprocessing of the experimental data can be done that helps filtering and smoothening the data. Unknown parameters can be defined from the local or global workspace and then updated automatically after the tuning. Also, parameter trajectories are also obtained to evaluate the feasibility of the optimization problem. Both gradient and non-gradient based methods with different solvers are available in the solver configuration options. Both gradient and non-gradient based methods are used in this work depending on the system complexity and number of objectives. However, multi-objective optimization is not supported in the non-gradient method. But It is done by the Non-linear least square optimization technique. Mean Absolute Relative Error (MARE) is calculated to validate the models against the experiments as it does not consider the effect of the outliers. System under consideration is too dynamic to expect such outliers because of the various channels and their effects involved. MARE is given as,

$$MARE\% = \text{Mean}\left|\left(\frac{\text{measured (i)} - \text{simulated(i)}}{\text{measured(i)}}\right)\right| \times 100 \tag{3.1}$$

A detail discussion regarding sub-model and full model tuning is given in the following sections.

3.5.1 Compressor Tuning

Compressor flow is an important variable in the engine air-path model as it decides the fresh air flow entering the intake manifolds. Thus, compressor efficiency, temperature, and power need to be modelled accurately. Compressor tuning session is divided into three variables tuning namely efficiency, temperature, and mass flow.

Compressor Efficiency

Compressor efficiency depends on the compressor pressure ratio Π_c which is a ratio of intake manifold pressure and ambient pressure as [44],

$$\Pi_c = \frac{p_{im}}{p_{amb}} \tag{3.2}$$

And compressor efficiency η_c is given by,

$$\eta_c = \frac{P_{c,S}}{P_c} = \frac{T_{amb}\left(\Pi_c^{1-\frac{1}{\gamma_a}} - 1\right)}{T_c - T_{amb}} \tag{3.3}$$

Where, P_c is compressor power and $P_{c,s}$ compressor power in the isentropic process given by

$$P_{c,s} = W_c c_{pa} T_{amb}\left(\Pi_c^{1-\frac{1}{\gamma_a}} - 1\right) \tag{3.4}$$

Where W_c is compressor mass flow, c_{pa} is specific heat capacity at constant pressure Therefore, compressor power P_c is

$$P_c = \frac{P_{c,s}}{\eta_c} = \frac{W_c c_{pa} T_{amb}}{\eta_c}\left(\Pi_c^{1-\frac{1}{\gamma_a}} - 1\right) \tag{3.5}$$

To tune the efficiency, it is model in terms of ellipsoid function as given in the reference [13], and the ellipse is given by

$$\eta_c = \eta_{cmax} - x^T Q_c x \tag{3.6}$$

Where, X is a vector given by

$$\mathcal{X} = \begin{bmatrix} W_c - W_{\mathrm{cop}\,t} \\ \boldsymbol{\pi}_c - \boldsymbol{\pi}_{copt} \end{bmatrix} \tag{3.7}$$

Where, $\boldsymbol{\pi}_c$ is a non-linear transformation of Π_c such that,

$$\boldsymbol{\pi}_c = (\Pi_c - 1)^{c_\pi} \tag{3.8}$$

And Q_c is a semidefinite, positive, and symmetric matrix of the parameters a_1, a_2, and a_3 as,

$$Q_c = \begin{bmatrix} a_1 & a_3 \\ a_3 & a_2 \end{bmatrix} \tag{3.9}$$

Compressor efficiency is measured from the GT-power data as $\eta_{c,meas}$ and η_c is tuned against the same with minimizing the $(\eta_{c,meas} - \eta_c)^2$ with setup as follows,

Inputs - p_{im}, p_{amb}, W_c

Output - η_c

Tuning Parameters - η_{cmax}, W_{copt}, $\boldsymbol{\pi}_{copt}$, c_π, $Q_c(a_1, a_2, a_3)$

Minimization problem - $(\eta_{c,meas} - \eta_c)^2$

This minimization problem is solved using the least square method by using the MATLAB & Simulink's parameter estimation tool. Figure 3.9 shows the model plot vs measured plot for the dynamic tuning points before tuning the parameters. In the mentioned plot, the trend is followed by the simulated output from the developed model till second dynamic step when compared to the measured result. However, error in the numerical values of both signals is visible along with a missed traced at the third dynamic step. A tolerance of 0.001 is given for the function evaluation for the optimizer and model is tuned for the dynamic points. Figure 3.10 shows the comparison of output for the tuned model against the measured output on the left-hand side whereas parameter tuning convergence graph on the right. Convergence of tuning parameters η_{cmax}, W_{copt}, $\boldsymbol{\pi}_{copt}$, c_π, $Q_c(a_1, a_2, a_3)$ was achieved in 32 iterations by least squared method to produce desired values. As a result of these parameters, the simulated

output follows the trend throughout the three dynamic cycles while achieving mean absolute relative error of (MARE) 1.7% and the maximum MARE of 2.05%. Maximum error is caused due to the initial peak observed in the simulated value for first operating points.

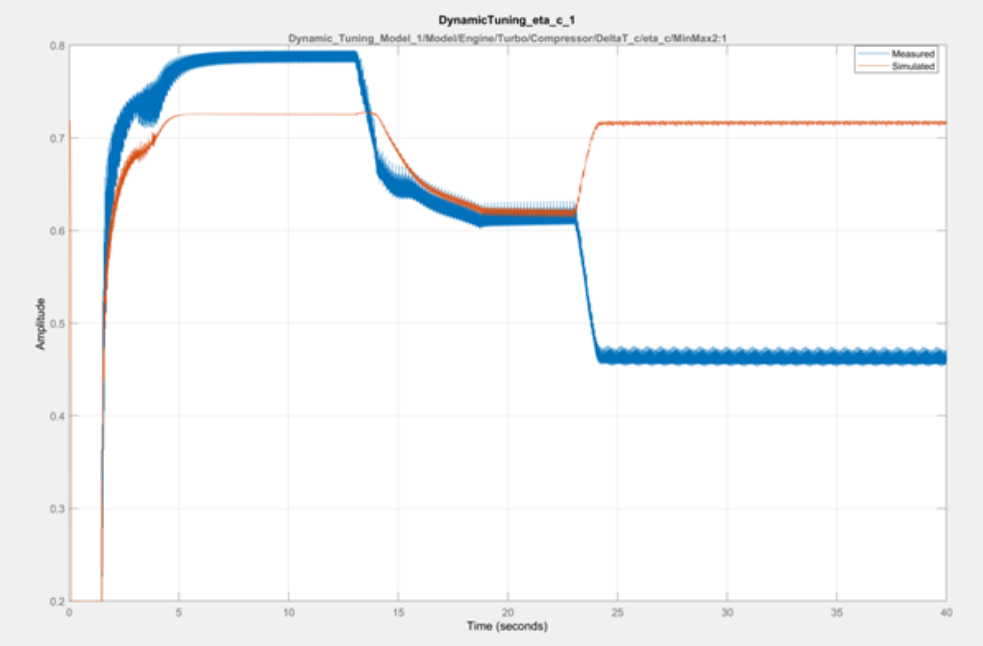

Figure 3.9. Model v/s Measured Plot for the Compressor Efficiency before Tuning

Further the model is validated against the WHSC cycle and MARE of 2.72% with maximum MARE of 19.38% is observed for the region of operation by eliminating the first peak as shown in the Figure 3.11.

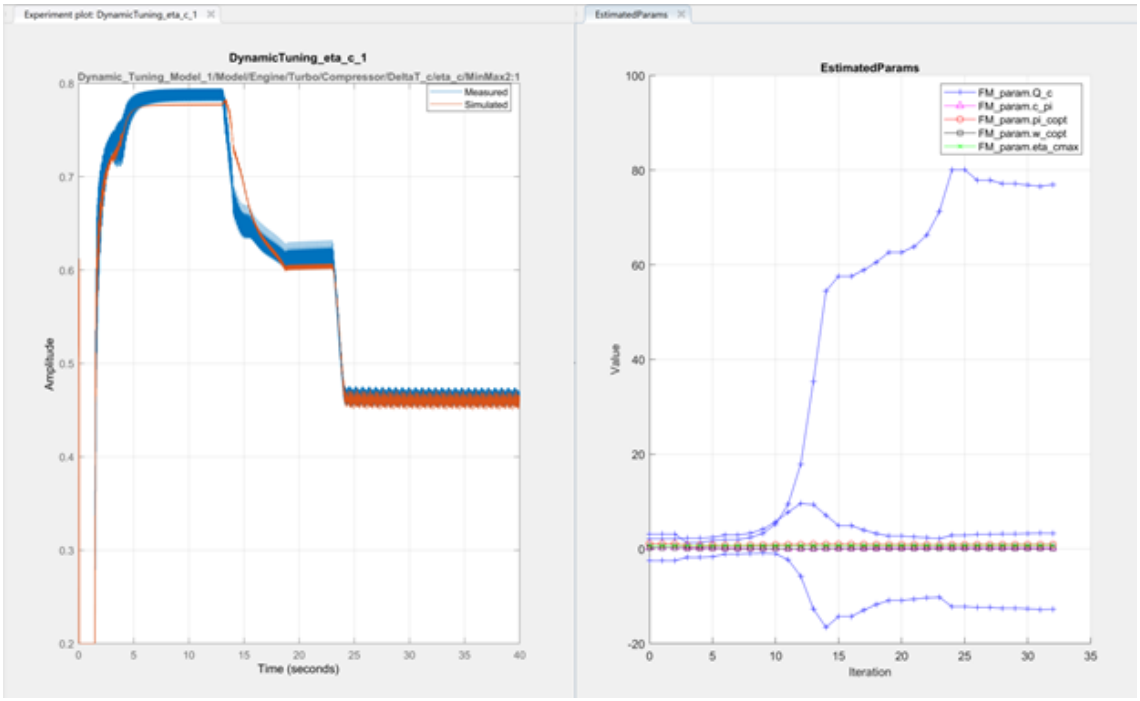

Figure 3.10. Dynamic Tuning Results for the Compressor Efficiency

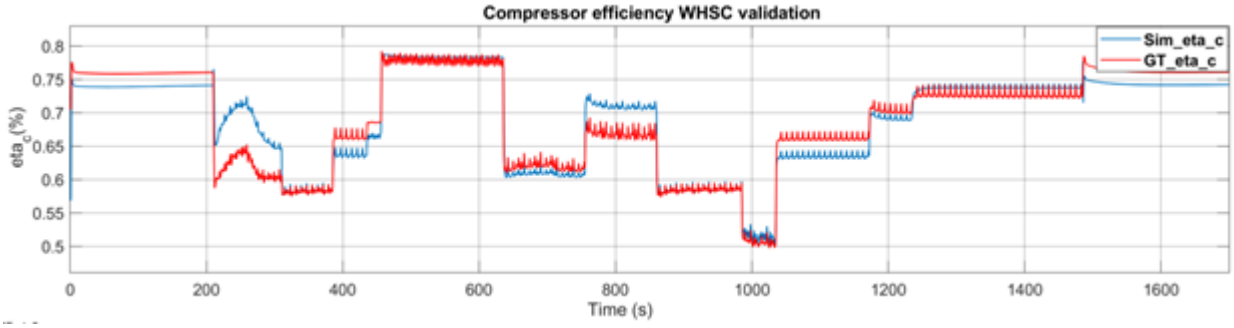

Figure 3.11. WHSC Validation for the Sub-model Compressor Efficiency

Compressor Temperature

Validity of the compressor efficiency can be also proved by validating the compressor outlet temperature. Figure 3.12 shows the compressor temperature validation for the WHSC cycle. Mean absolute relative error (MARE) of 0.7% is achieved with the maximum MARE of 8.27% for temperature validation.

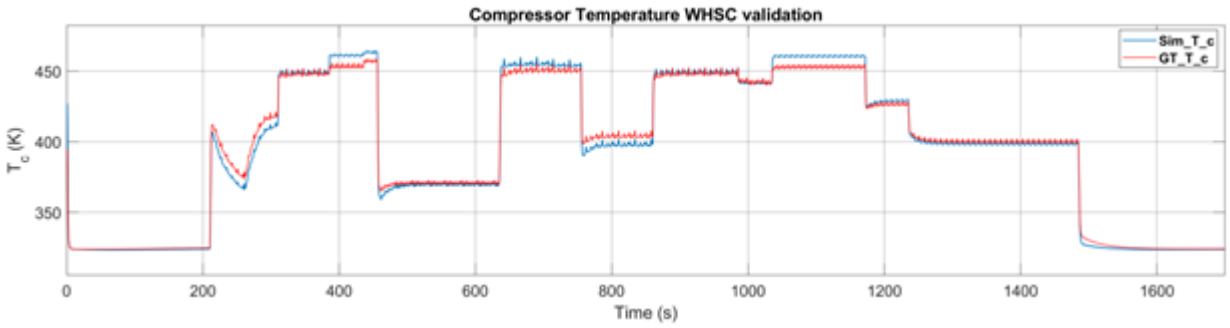

Figure 3.12. WHSC Validation - Compressor Outlet Temperature Sub-model

Compressor Flow

According to the equation 2.32, Tuning parameters for the compressor mass flow model are the coefficients of polynomial function ϕ_c and ψ_c are modelled in the form of ellipse [13]. The relation between them is given by

$$c_{\psi 1}\left(\omega_t\right)\left(\psi_c - c_{\psi 2}\right)^2 + c_{\phi 1}\left(\omega_t\right)\left(\phi_c - c_{\phi 2}\right)^2 = 1 \tag{3.10}$$

Where c_{ψ_1} and c_{ϕ_1} are function of turbine speed ω_t. They are modelled as polynomial functions as,

$$\begin{aligned} c_{\psi 1}\left(\omega_t\right) &= c_{\omega\psi 1}\omega_t^2 + c_{\omega\psi 2}\omega_t + c_{\omega\psi 2} \\ c_{\phi 1}\left(\omega_t\right) &= c_{\omega\phi 1}\omega_t^2 + c_{\omega\phi 2}\omega_t + c_{\omega\phi 2} \end{aligned} \tag{3.11}$$

Thus, tuning setup for the compressor mass flow is taken as,

Inputs - p_{im}, p_{amb}, T_{amb}, ω_t

Output - W_c

Tuning Parameters - c_{ψ_2}, c_{ϕ_2}, $c_{\omega\psi 1,2,3}$, $c_{\omega\phi 1,2,3}$, R_c

Minimization problem - $(W_{c,meas} - W_c)^2$

Parameter estimator tool from MATLAB & Simulink is used to tune the compressor mass flow for both steady state and dynamic tuning using the least square method. Figure 3.13 shows the steady state tuning for 800 rpm case with the parameter trajectory. In the mentioned plot, comparison between compressor flow from simulated and measured output

for a steady state condition is given on the left and estimated parameters on the right. It is seen that estimation process is converged in 4 iterations to achieve the given tolerance for error between measured and simulated output. Tuning parameters are tuned for the constraints given by the equation 3.10 and 3.11. Estimated parameters c_{ψ_2}, c_{ϕ_2}, $c_{\omega\psi 1,2,3}$ vector, $c_{\omega\phi 1,2,3}$ vector, R_c trajectory is given in the right till the convergence.

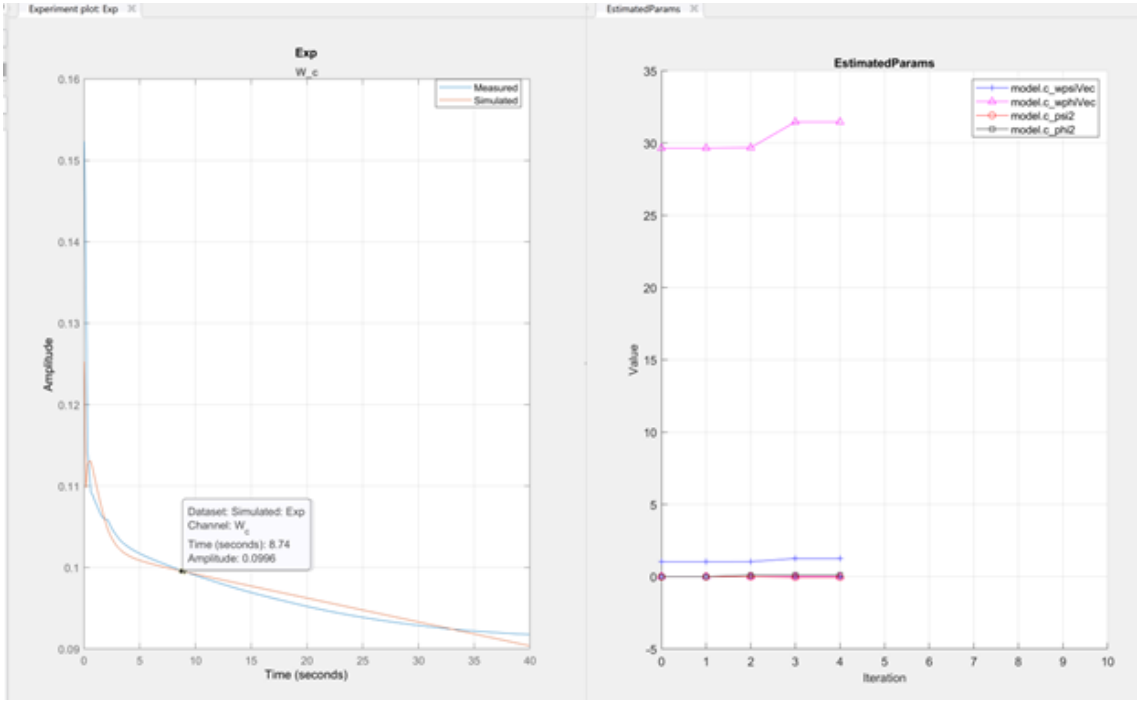

Figure 3.13. Steady State Tuning - Compressor Flow

Further, the compressor mass flow is tuned for the dynamic points to capture the effect of step changes, and MARE of 3.67% is observed with the max value of 49.63% due to the initial peak. Figure 3.14 shows measured and simulated data for a dynamic tuning profile with the estimated parameters trajectory on the right. It is seen that the simulated output follows the trend in step changes while maintaining the given tolerance. However, a few drifts been seen after the third step, that under the constrained error limits. Whereas on the right side, of the plot parameter c_{ψ_2} explored its lower and higher bounds to converge finally within 50 iterations.

Figure 3.15 shows the WHSC validation for the compressor mass flow. WHSC cycle validation MARE is 2.11% with 44.81% max MARE due to first 10 seconds of peak signals.

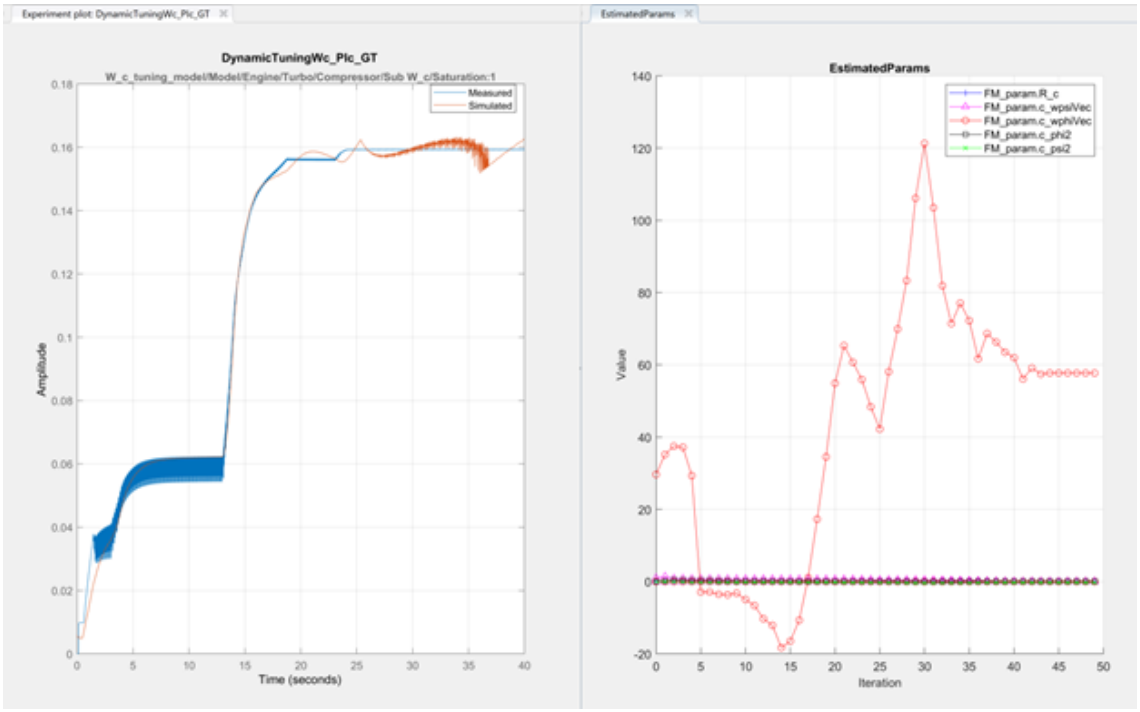

Figure 3.14. Dynamic Tuning - Compressor Mass Flow

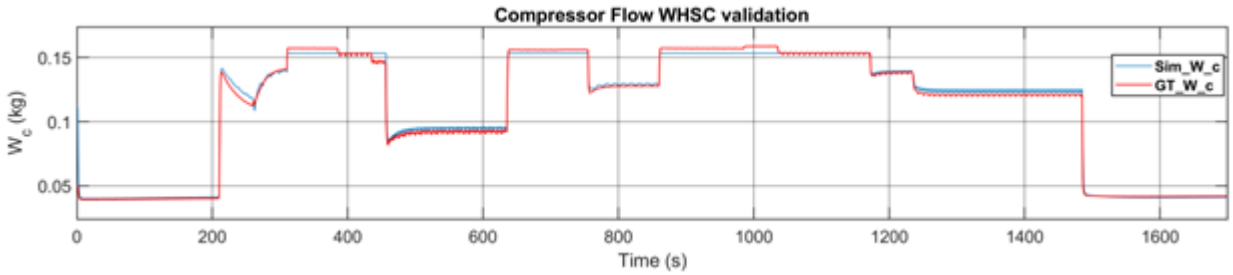

Figure 3.15. WHSC Validation – Compressor Mass Flow Sub-model

It is seen that the simulated output traced the measured output withing the range of accuracy mentioned above.

3.5.2 Turbine Flow Tuning

Turbine flow is tuned by tuning the three turbine variables namely turbine mass flow, turbine power, and turbine inertia. Dynamic equations from equation 2.27 to equation 2.29 are used to formulate the minimization problem, and the parameters are tuned using the least square method in the MATLAB and Simulink parameter estimator tool.

Turbine Flow

Turbine flow given by the equation 2.27 has choking function f_{Π_t}, effective area function f_{vgt} that are needed to be tuned. Choking function has a tuning parameter K_t which is an exponent of turbine pressure ratio Π_t as given in equation 2.28. Further Effective area function is modelled in the form of ellipse as [44],

$$\left[\frac{f_{vgt}\left(\tilde{u}_{vgt}\right) - c_{f2}}{c_{f1}}\right]^2 + \left[\frac{\tilde{u}_{vgt} - c_{vgt2}}{c_{vgt1}}\right]^2 = 1 \tag{3.12}$$

Thus, the parameters in the ellipse function are also needed to tune by solving the equation 3.12. Measured Output $W_{t,meas}$ is calculated from the GT-power data as $W_{t,meas)} = W_c + W_f$. Where, W_c and W_f are the compressor and fuel masses from the measured data. Therefore, an optimization problem is formulated as,

Inputs - p_{em}, p_{amb}, T_{em} and u_{vgt}

Output - W_t

Tuning Parameters -K_t, c_{f1}, c_{f2}, c_{vgt1}, c_{vgt2}, A_{vgtmax}, R_t, $\eta_{ltm,max}$

Minimization problem - $(W_{t,meas} - W_t)^2$

Figure 3.16 shows steady state tuning for full turbine model that includes compressor flow, compressor temperature and turbine flow. It is seen that the measured and simulated output follows the trend for steady state data.

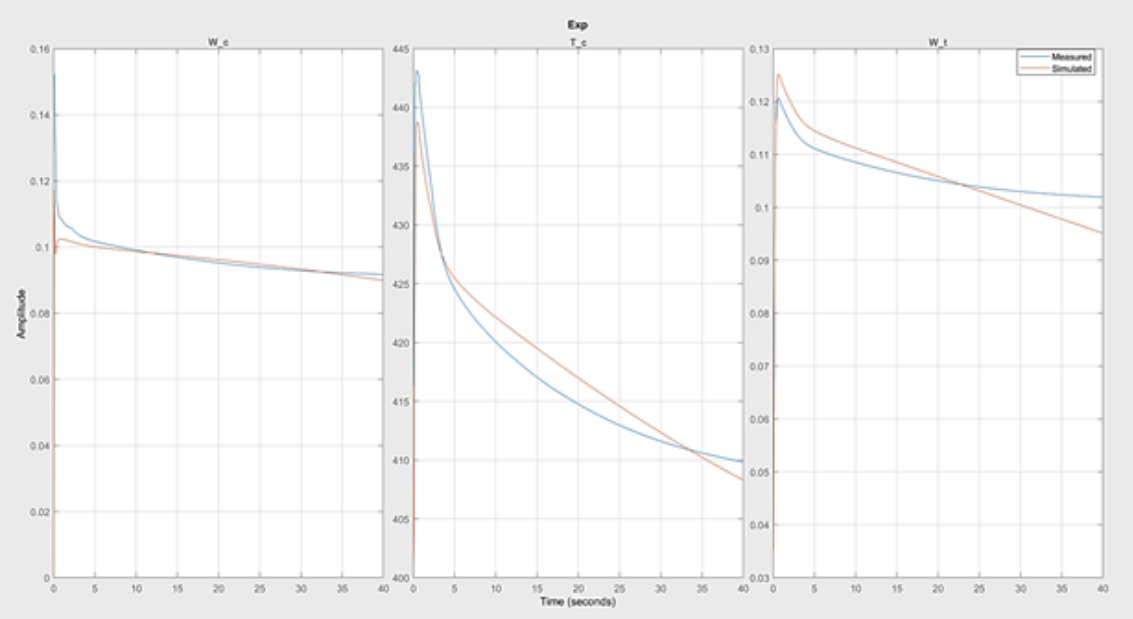

Figure 3.16. Full Turbo Steady State Tuning

Further, the model is tuned for dynamic tuning points and an MARE of 9.23% is noted with a few peaks in the measurement. It is seen that the parameters estimated did not explored from the values that are estimated in the steady state estimation as it is seen to converged to the desired values of parameters. Dynamic tuning session and WHSC validation are shown in Figure 3.17 and Figure 3.18. An MARE of 7.68% is noted in the WHSC validation. However, some noise is observed in simulated output which is acceptable.

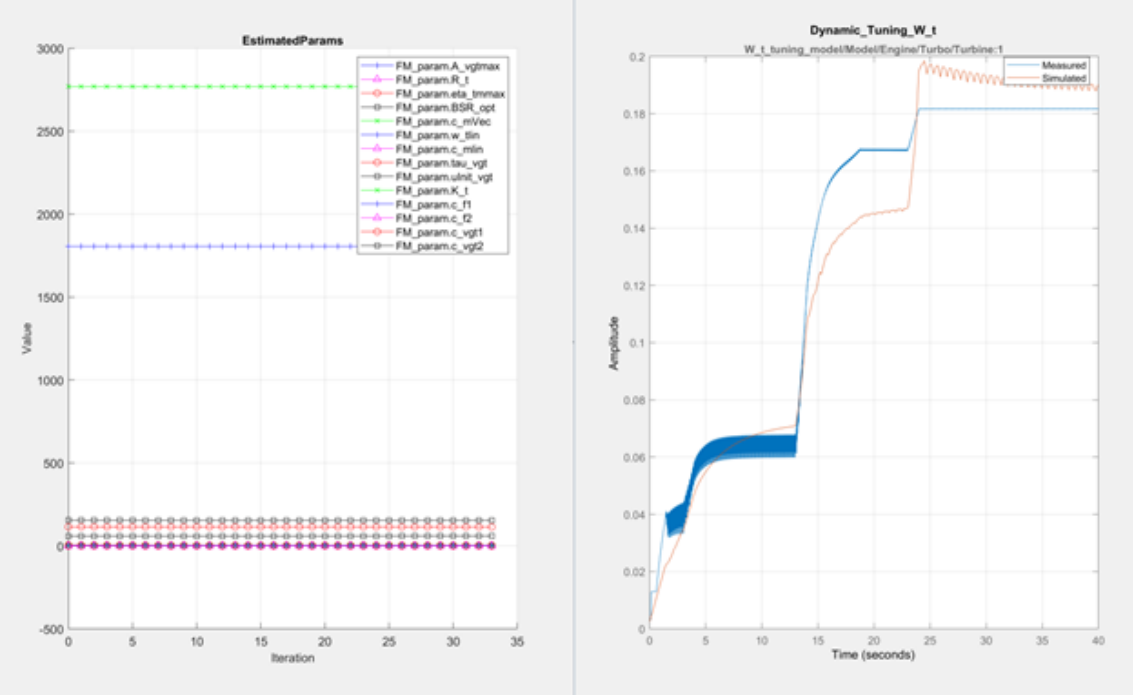

Figure 3.17. Dynamic Tuning Turbine Flow

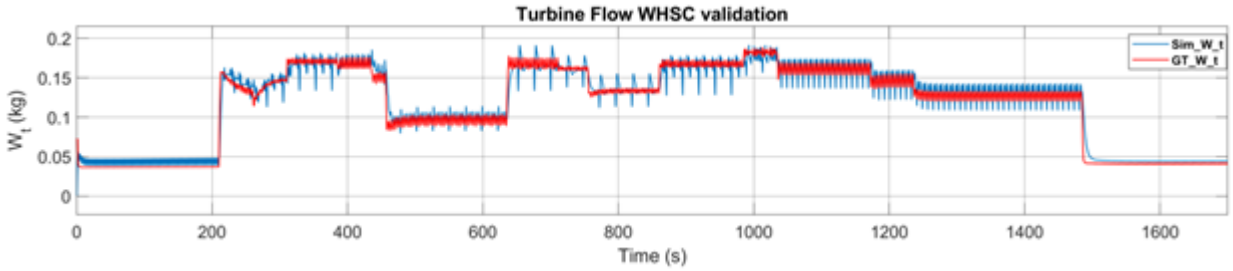

Figure 3.18. WHSC Validation - Turbine Mass Flow

Turbine Power

Validating the turbine power is another way to validate the turbine efficiency. It was difficult to tune the turbine efficiency for this work as the turbine maps are not available for the application of interest.

Turbine efficiency is given by [44]

$$\eta_t = \frac{P_t}{P_{t,s}} = \frac{T_{em} - T_t}{T_{em}\left(1 - \Pi_t^{1-\frac{1}{\gamma_e}}\right)} \tag{3.13}$$

Where, Π_t is the pressure ratio between ambient and exhaust manifold, P_t and $P_{t,s}$ are the turbine power and isentropic turbine power, T_t is turbine outlet temperature.
At steady state $P_{t,s}$ is equivalent to P_c, therefore another efficiency is obtained as η_{tm} such that.

$$P_t\eta_m = \eta_{tm}P_{t,s} = \eta_{tm}W_t c_{pe}T_{em}\left(1-\Pi_t^{1-\frac{1}{\gamma_e}}\right) \tag{3.14}$$

η_{tm} depends on the blade speed ratio (BSR) as

$$\eta_{tm} = \eta_{tm,\max} - c_m\left(BSR - BSR_{opt}\right)^2 \tag{3.15}$$

BSR is the ratio of turbine blade speed to the turbine speed at which gas expands isentropically at given pressure ratio.

$$BSR = \frac{R_t\omega_t}{\sqrt{2c_{pe}T_{em}\left(1-\Pi_t^{1-\frac{1}{\gamma_e}}\right)}} \tag{3.16}$$

Where, R_t is turbine blade radius and c_m is the parameter in the parabolic function that is modelled to take care the mechanical losses, it is modelled as a function of turbine speed as

$$c_m = c_{m1}\left[\max\left(0, \omega_t - c_{m2}\right)\right]^{c_{m3}} \tag{3.17}$$

Thus c_{m1}, c_{m2}, and c_{m3} are tuning parameter for this local least square problem that are added in the model parameter for the minimization define as

Inputs - p_{em}, p_{amb}, T_{em} and u_{vgt}

Output -P_t

Tuning Parameters - c_{m1}, c_{m2}, c_{m3}, $c_{mintial}$, $\omega_{tinitial}$, R_t, $\eta_{tm,max}$

Minimization problem - $(P_{t,meas} - P_t)^2$

Turbine speed is simulated from the GT-model that has unexpected noise and uncertainties because of the tuning parameters. First order low pass filter of frequency 0.1 Hz is applied to the GT-data for dynamic tuning and validation. Figure 2.19 shows the measured

and preprocessed signal after the filter is applied to smoothen the output data before the parameter estimation that does not compromise the estimation capabilities using least-squares.

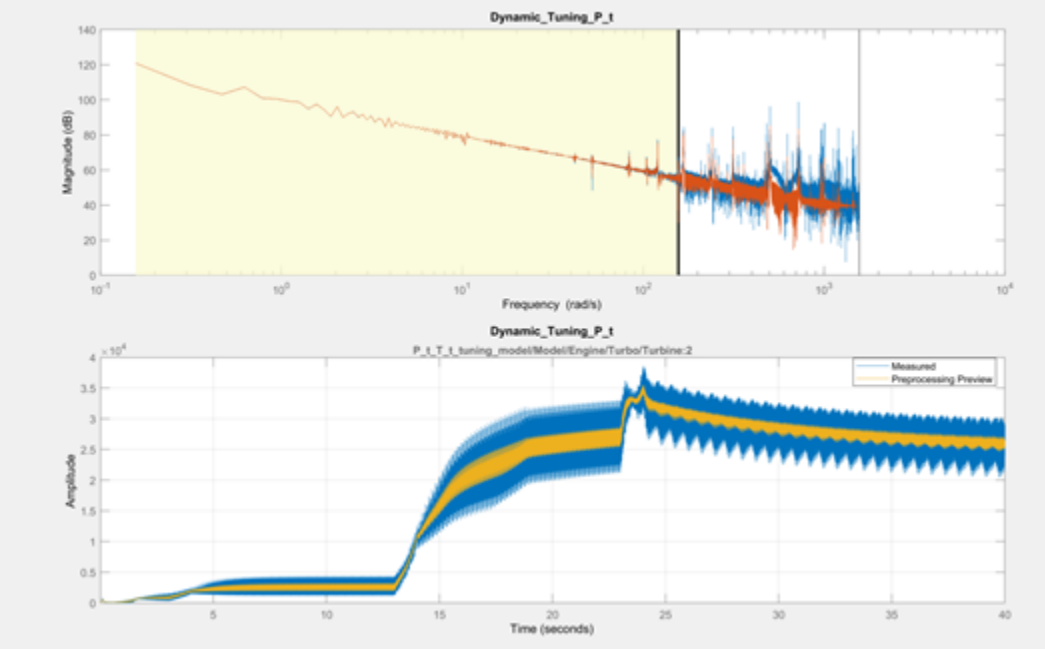

Figure 3.19. Filtered Turbine Power Profile from GT-power

With the setup discussed above, Dynamic and WHSC validation MARE of 5.05% and 13.6% are noted because of the uncertainty in the turbine speed. The turbine speed is tuned by tuning the turbine inertia, but model did not converge to the solution. Tuning and the validation sessions are shown in Figure 3.20 and Figure 3.21. It is seen from the Figure 3.20 that the dynamic profile for the simulated turbine power has adapted the step changes on the right and parameters trajectory for the explored values while converging in 25 iterations. Also, it is noted that the validation output for the simulated power traces the reference value from the GT-power measurement. However, a deviation is noted for few places as shown in Figure 3.21. This is due to the turbine speed estimated from the GT-power which has overshoots at the corresponding samples. Turbine speed is calculated in GT-power uses different solver than the solver used in the MATLAB and Simulink model used in this model. Also, these deviations are observed at the 100% load condition where turbine speed overshoots drastically beyond a practical value. Therefore a saturation for turbine rotational speed is applied to limit the value till 10000 rad/s.

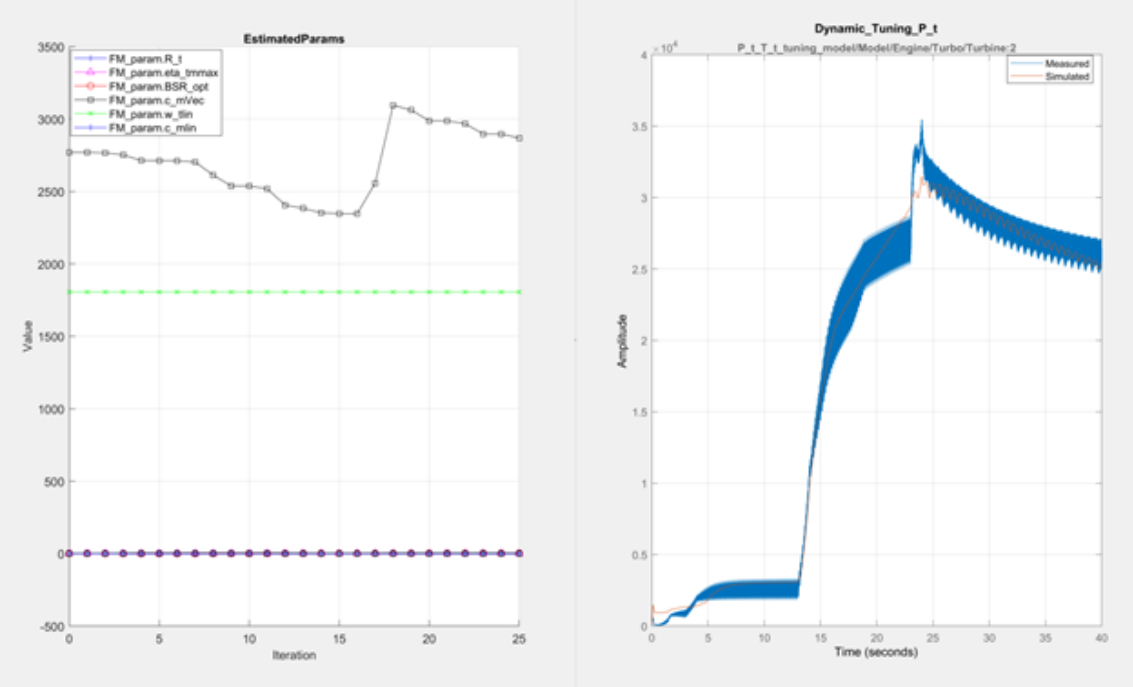

Figure 3.20. Dynamic Tuning- Turbine Power

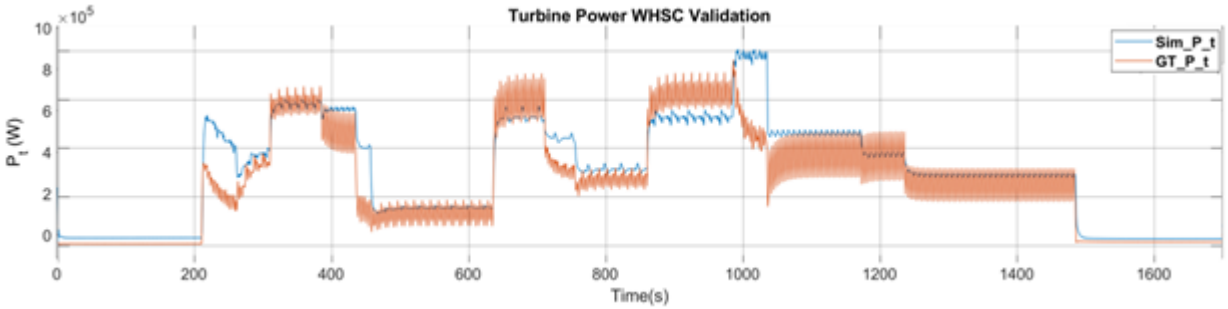

Figure 3.21. WHSC Validation - Turbine Power

Turbine Inertia

Turbine Inertia, J_t from the equation 2.33 is tuned using the full turbo model as the turbine speed model could not be tuned with GT-power data because of the noisy measurements.

Inputs - p_{em}, p_{im}, p_{amb}, T_{em}, T_{amb} and u_{vgt}

Outputs - ω_t, W_t, W_c, P_t, T_c

Tuning Parameters – J_t, $\omega_{tinitial}$

Minimization Problem – Squared difference of all measured and simulated outputs mentioned above.

GT-power data is filtered with the first order filter (LPF) with the frequency of 0.1Hz as shown in Figure 3.22. Dynamic tuning for the turbine inertia is attempted, but it could not converge to the solution as shown in the Figure 3.23. Thus, a theoretical value of turbine inertia is adopted from the GT-power for the given turbocharger setup. And turbocharger variables are validated as mentioned above in the respective sections.

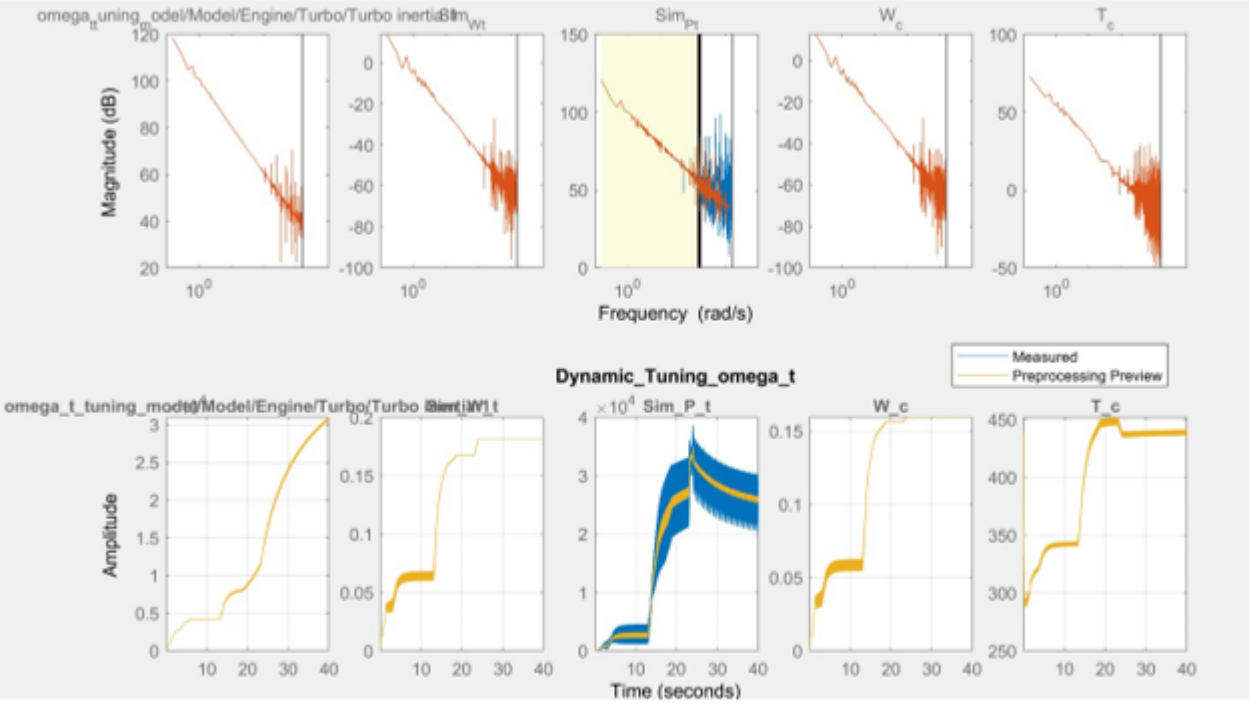

Figure 3.22. Filtered Measurements for Turbo Inertia Tuning

Moreover, as discussed above in the previous section, turbine speed is not validated against the WHSC cycle as it has impractical values at 100% and it does not support the tuning method as shown above in 3.23.

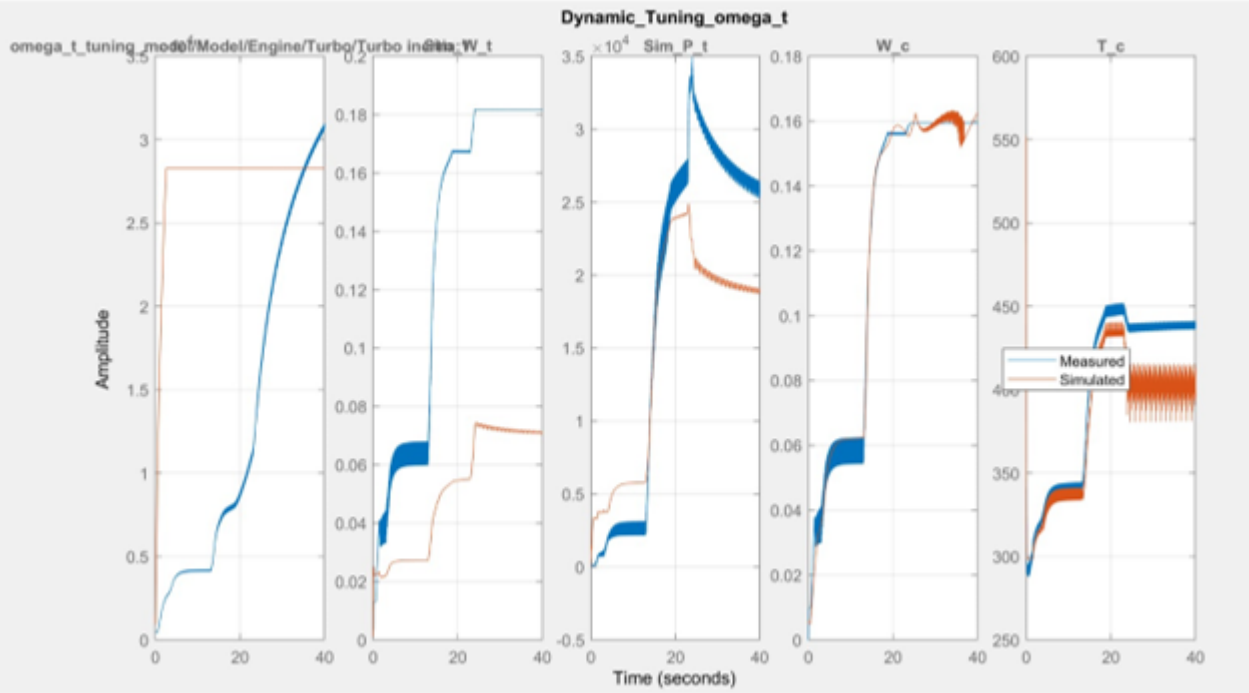

Figure 3.23. Dynamic Tuning - Turbine Inertia

3.5.3 EGR model Tuning

EGR Flow

In this study measured EGR mass flow is taken as a calculated channel from the cylinder and compressor mass flow as $W_{egr,meas} = W_{\mathrm{ei},calc} - W_{c,meas}$. W_{ei} is calculated as mentioned in the cylinder mass flow section. As discussed earlier in the section 2.1.3, EGR mass flow is a function of tunable parameters f_{egr} and A_{egrmax} that defines the EGR valve effective area. The effective are function f_{egr} is modelled in the form of polynomial as [44]

$$f_{egr}\left(\tilde{u}_{egr}\right) = \begin{cases} c_{egr1}\tilde{u}_{egr}^2 + c_{egr2}\tilde{u}_{egr} + c_{egr3} & \text{if } \tilde{u}_{egr} \leq -\frac{c_{egr2}}{2c_{egr1}} \\ c_{egr3} - \frac{c_{egr2}^2}{4c_{egr1}} & \text{if } \tilde{u}_{egr} > -\frac{c_{egr2}}{2c_{egr1}} \end{cases} \tag{3.18}$$

Where $\tilde{u}_{egr}$ EGR actuator dynamics. $c_{egr}vector(1,2,3)$ is tuning parameter for the polynomial given above. Therefore, the experimental setup for this tuning session is as

Inputs - p_{em}, p_{im}, T_{em}, u_{egr}

Output- - W_{egr}

Tuning Parameters - c_{egr1}, c_{egr2}, c_{egr3}, A_{egrmax}, $u_{initial,egr}$, Π_{egropt}

Minimization Problem- $(W_{egr,meas} - W_{egr})^2$

Figure 3.24 shows steady state tuning for 800 rpm where the actuator dynamics with actuation delays are not considered. Parameter trajectory is given in the right shows the Π_{egropt} tends to go to 1 meaning, that has changed significantly from the theoretical value from the equation 2.25 increasing the accuracy. It is seen in right hand side of the indicated plot that the parameters are converged in 34 iteration to achieved the tuning tolerance.

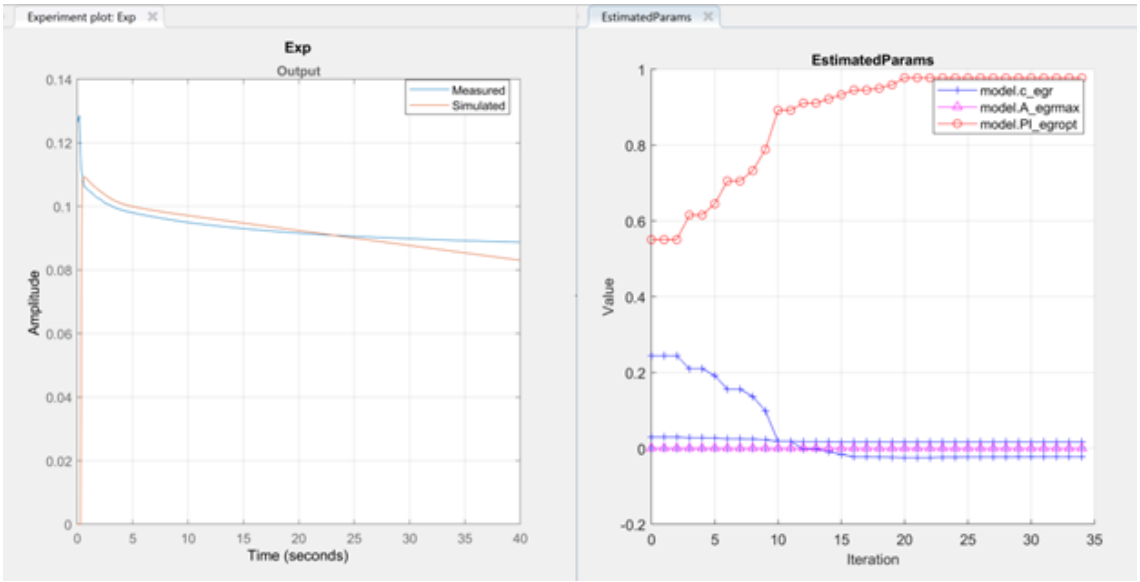

Figure 3.24. Steady State Tuning - EGR Mass Flow

Actuator dynamic parameters are added for the dynamic tuning that considers the EGR valve actuation. The parameters are actuator delay and actuator gain as shown in the Figure 3.25 in the estimated parameters trajectories. With the previous tuned model for steady state and addition of actuator dynamics, dynamic tuning converged within 4 iteration giving mean absolute relative error (MARE) of 16.35% with a maximum MARE 50.05% for WHSC. It is seen due to the first and last few seconds of the cycle shown in Figure 3.26 for the WHSC.

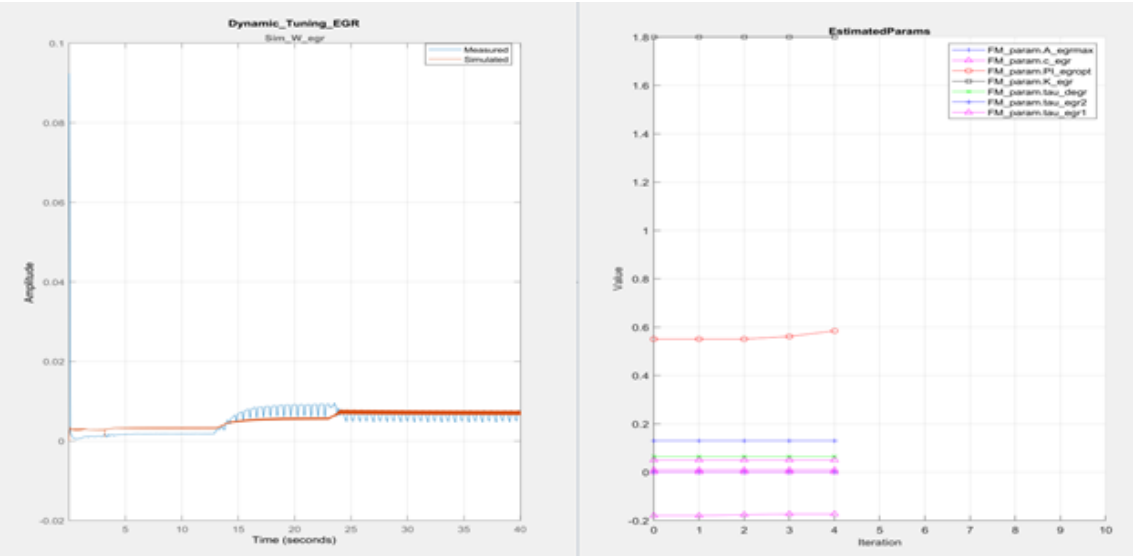

Figure 3.25. Dynamic Tuning - EGR Mass Flow

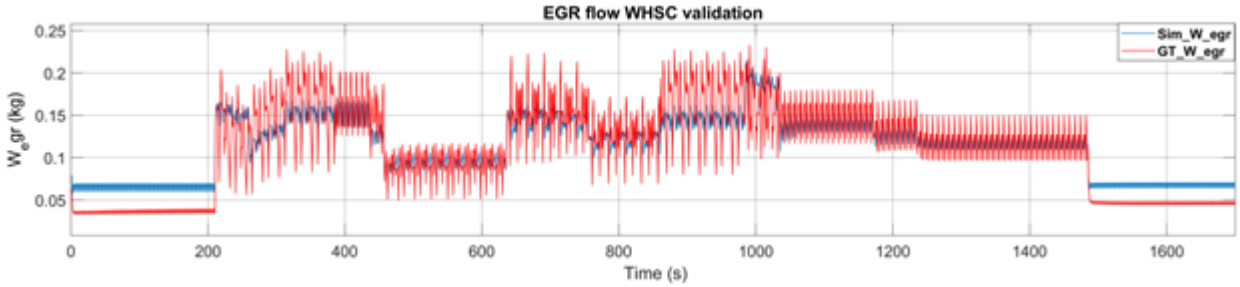

Figure 3.26. WHSC Validation - EGR Flow

3.5.4 Cylinder Tuning

Cylinder tuning is done for two variables namely cylinder mass flow and cylinder out temperature. Torque model in not needed to be tuned as it is not used for any of the application of interest, and it does not affect the full system model.

Cylinder Flow

Cylinder mass flow is the mass coming inside the cylinder that is coming from the compressor and EGR mixed. Thus, it is calculated from the measurement as

$$W_{\text{ei},meas} = \frac{W_{c,meas}}{1 - x_{egr}} \tag{3.19}$$

Where, x_{egr} is EGR fraction given by

$$x_{egr} = \frac{W_{egr}}{W_c + W_{egr}} \tag{3.20}$$

and $W_{c,meas}$ is the measured compressor flow from the GT-power data. Cylinder flow depends on the volumetric efficiency of the cylinder as modelled in equation 2.8. It is assumed that volumetric efficiency of the cylinder is constant for the given application and cycle. Volumetric efficiency is parametrized in the form of a polynomial given by equation 2.9. Thus, coefficients of the polynomial are the parameters for the estimation session as,

Inputs - p_{im}, T_{im},n_{e}

Output - W_{ei}

Tuning Parameters - $c_{vol,vector}$ - $c_{vol1}, c_{vol2}, c_{vol3}$

Minimization Problem – $(W_{\text{ei},meas} - W_{\text{ei}})^2$

Figure 3.27, Figure 3.28, and Figure 3.29 show the steady state tuning, dynamic tuning, and WHSC validation for the cylinder flow. It is seen from the Figure 3.27 and Figure 3.28 that the parameters on the right-hand side converged in one iteration as this estimation problem has only one vector to estimate. It is also noted that every system before the cylinder flow that is compressor and EGR flow is tuned before tuning the cylinder flow. Therefore, there is a less cumulative error in the continuous system. Thus, mean absolute relative error (MARE) of 5.4% and 6.86% are recorded for the dynamic tuning and WHSC validation, respectively. However, maximum MARE of 42.41% was recorded because of the noise in intake manifold data from the GT-power for dynamic tuning. It is validated for the WHSC maximum MARE of 11.1%.

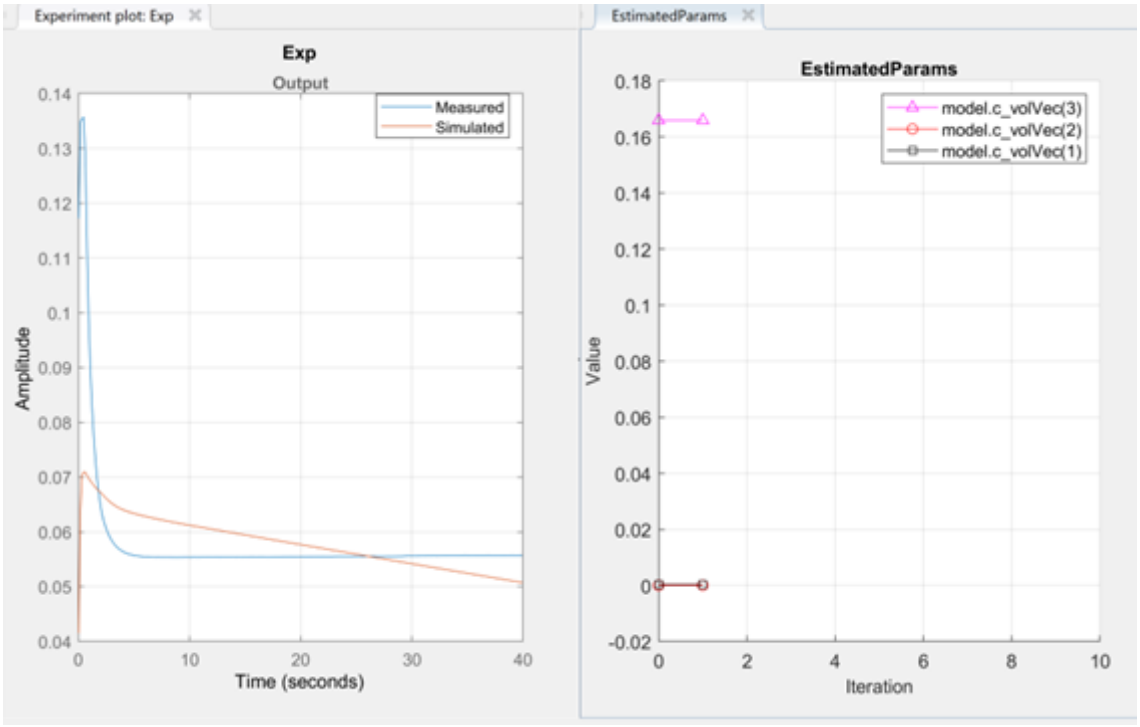

Figure 3.27. Steady State Tuning - Cylinder Flow

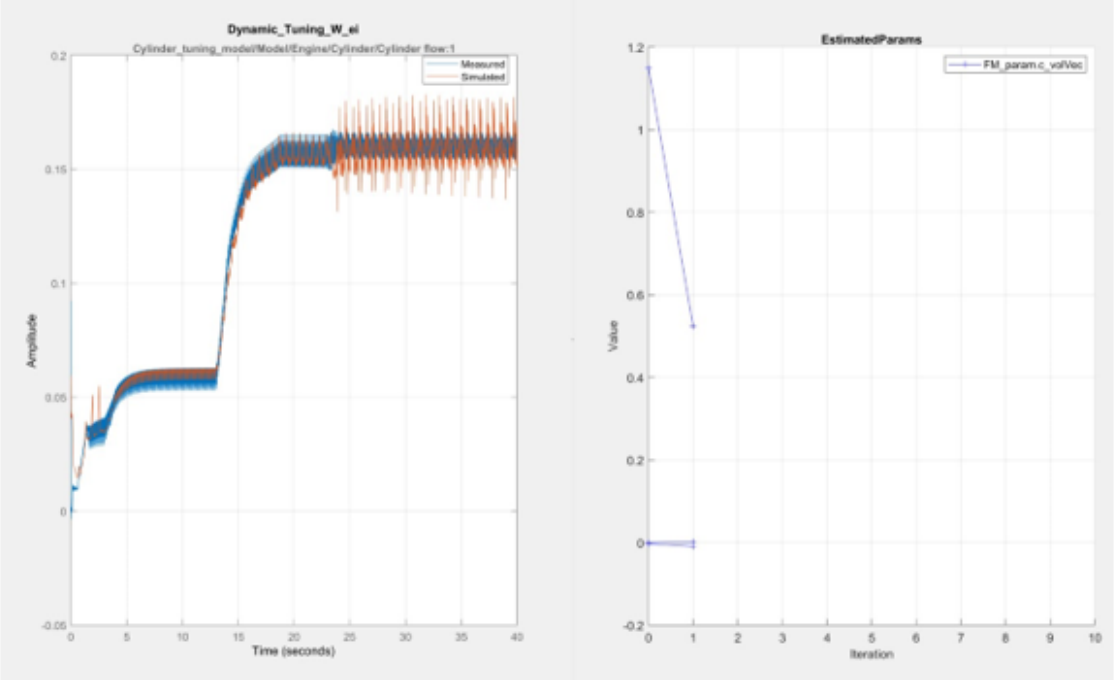

Figure 3.28. Dynamic Tuning - Cylinder Flow

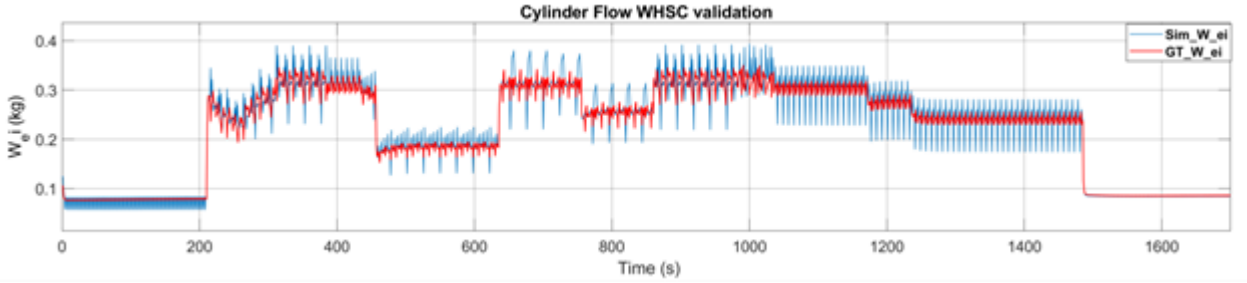

Figure 3.29. WHSC Validation - Cylinder Flow

Cylinder Out Temperature

Cylinder temperature and exhaust manifold temperatures are modelled as given in the equation 2.14 to 2.21. Parameters from the Seliger Cycle are tuned along with the heat transfer parameters from the pipe to the ambient. Steady state parameter estimation is done separately for the cylinder temperature and exhaust temperature. But dynamic tuning is done in combined cylinder and exhaust manifold to account the heat loss through the pipe. The minimization problem is given as

Inputs - p_{im}, T_{im}, T_{amb}, p_{em}, W_f, W_{ei}

Output - T_{em}, T_{e}

Tuning Parameters - h_{tot}, d_{pipe}, l_{pipe}, x_{cv}, η_{SC}

Minimization Problem – $(T_{em,meas} - T_{em})^2$

As cylinder temperature is calculated with the iterative process, a first order filter is used for the dynamic tuning. Figure 3.31 and Figure 3.31 show the steady state tuning session for cylinder temperature and exhaust temperature, respectively. It is seen that the initial temperature parameter for the engine temperature as shown in Figure 3.30 has shown higher value of 2600K within 4 iteration to converge the estimation. Further, steady state estimation for the exhaust manifold temperature is done by taking care of the heat loss through the pipes by tuning the heat transfer coefficient. It is seen that heat transfer coefficient has converged to the value of around 7000 W/m^2K in 5 iterations.

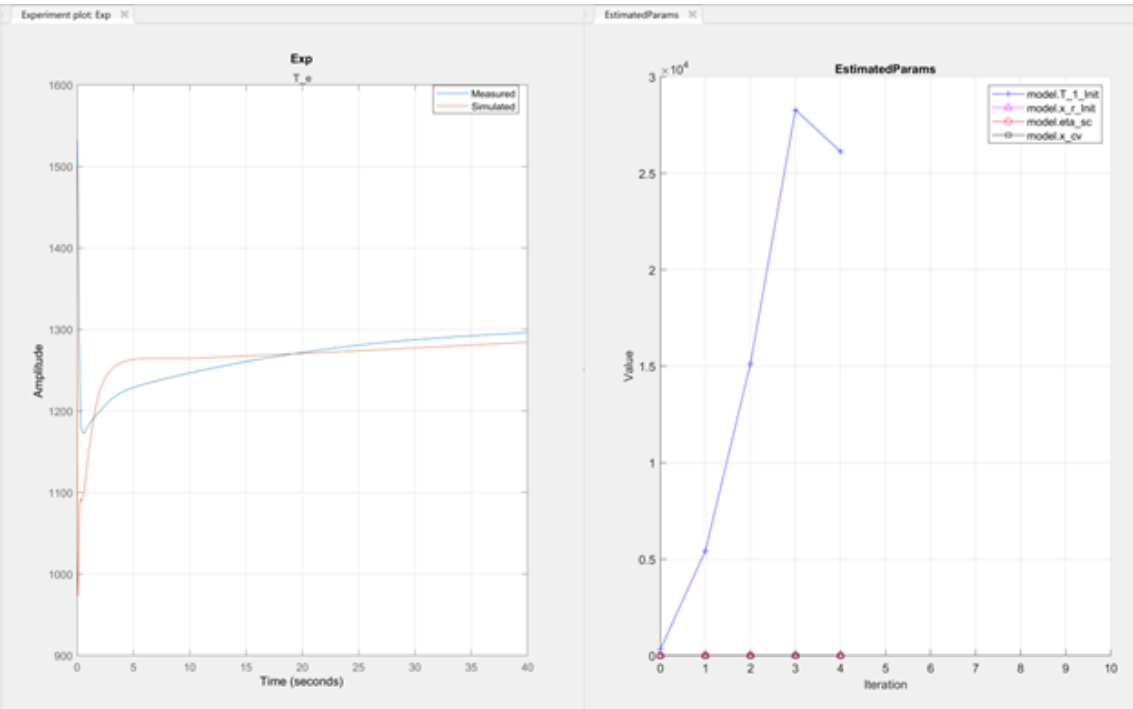

Figure 3.30. Steady State Tuning - Cylinder Temperature

Figure 3.32 and Figure 3.33 show dynamic tuning session and WHSC validation results. In the dynamic tuning, it is seen that the heat transfer coefficient has converged to a value around 5000 W/m^2K considering the step changes. However, a change in trend is noted after the 23rd second of dynamic tuning. Mean absolute relative error (MARE) for WHSC

validation is 15.29%. Although dynamic tuning error is maximum, the profile follows the step changes from 2nd and 3rd steps as shown in Figure 3.32. Thus, WHSC validation follows accurate reference tracking for certain regions of the cycle. Similarly, as discussed in the turbine power section, it is seen that the trend is opposite in Figure 3.33, where the load is 100 percent and has introduced the maximum error due to turbine speed estimation from the GT-power.

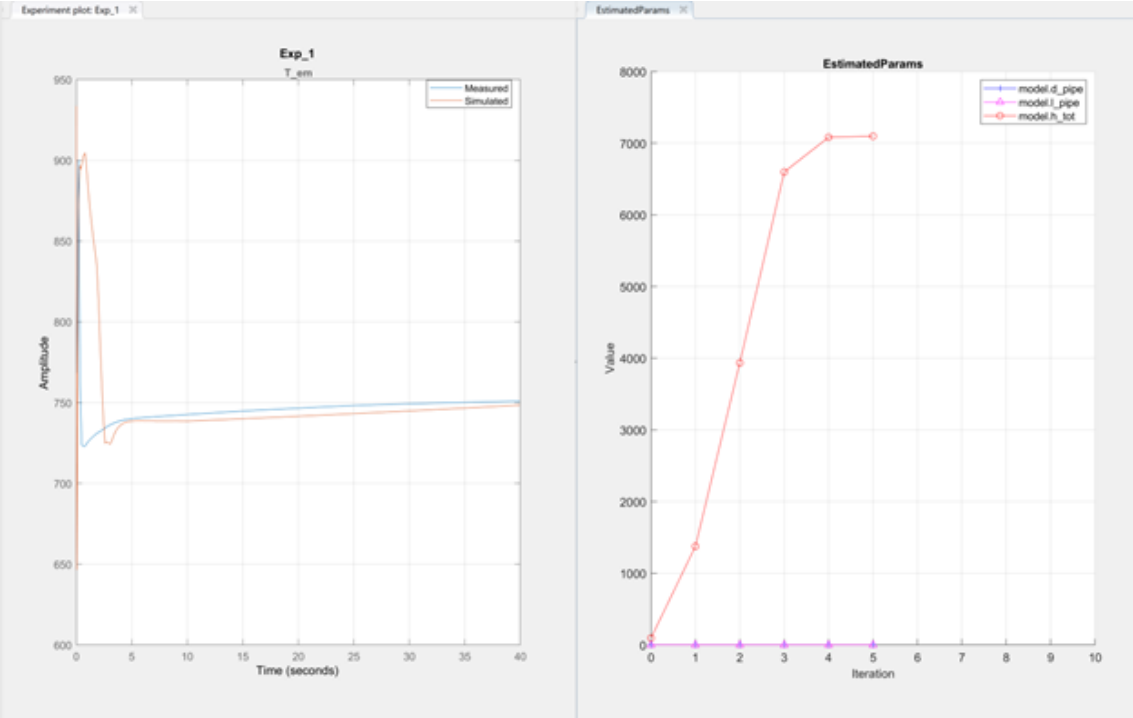

Figure 3.31. Steady State Tuning - Exhaust Temperature

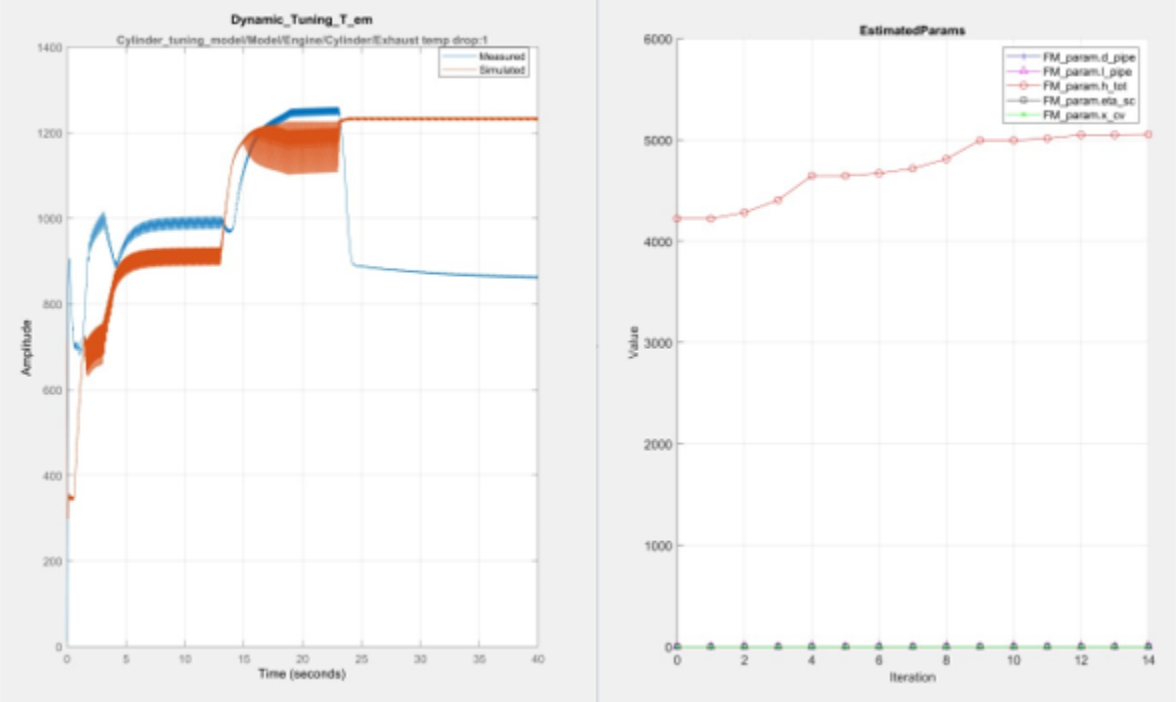

Figure 3.32. Dynamic Tuning - Exhaust Manifold Temperature

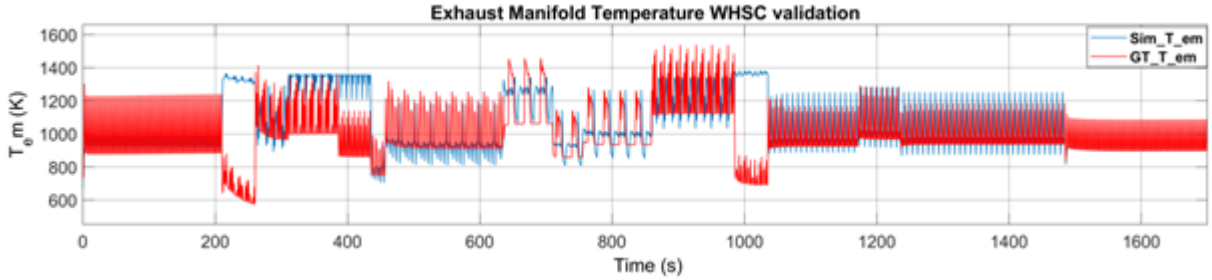

Figure 3.33. WHSC Validation - Exhaust Manifold Temperature

3.5.5 Full Model and Manifold Tuning

Complete model is a continuous Simulink model created using the sub-models mentioned above. Inputs and outputs of these sub-models are considered as input and output for the full model. Till now all the parameters in the model are tuned except manifold volumes. Intake and exhaust manifold pressures are the important channels that are needed to validate from this final model tuning as mentioned in equations 2.4. Thus, all the estimated parameters are used in this estimation as the constant values. Finally, model inputs such as speed and load

profile, injected fuel, EGR and VGT inputs, and ambient conditions such as temperature and pressure are given to the model. Thus, formulation of this multi-objective minimization problem is given as,

Inputs – n_e, u_δ (fuel injected), p_{amb}, T_{amb}, u_{egr}, u_{vgt}

Outputs - p_{im}, p_{em}, T_{em}, T_c, W_c, W_t, W_{ei}, W_{egr}, P_c, P_t

Tuning Parameters - V_{im} and V_{em}

Model results before tuning and after tuning are given in the Figure 3.34 and Figure 3.35. It is seen that intake and exhaust manifold pressures were tuned but found local minimum. However, there is no effect on the compressor flow, whereas turbine flow and the temperatures at compressor and exhaust manifolds are also affected by these new volumes. Note that, the effect of turbine speed estimation is affecting these model output. Thus, direct measured turbine speed is taken as an input to the model by neglecting the calculated model turbine speed. And model is again tuned for the parameters using WHSC cycle.

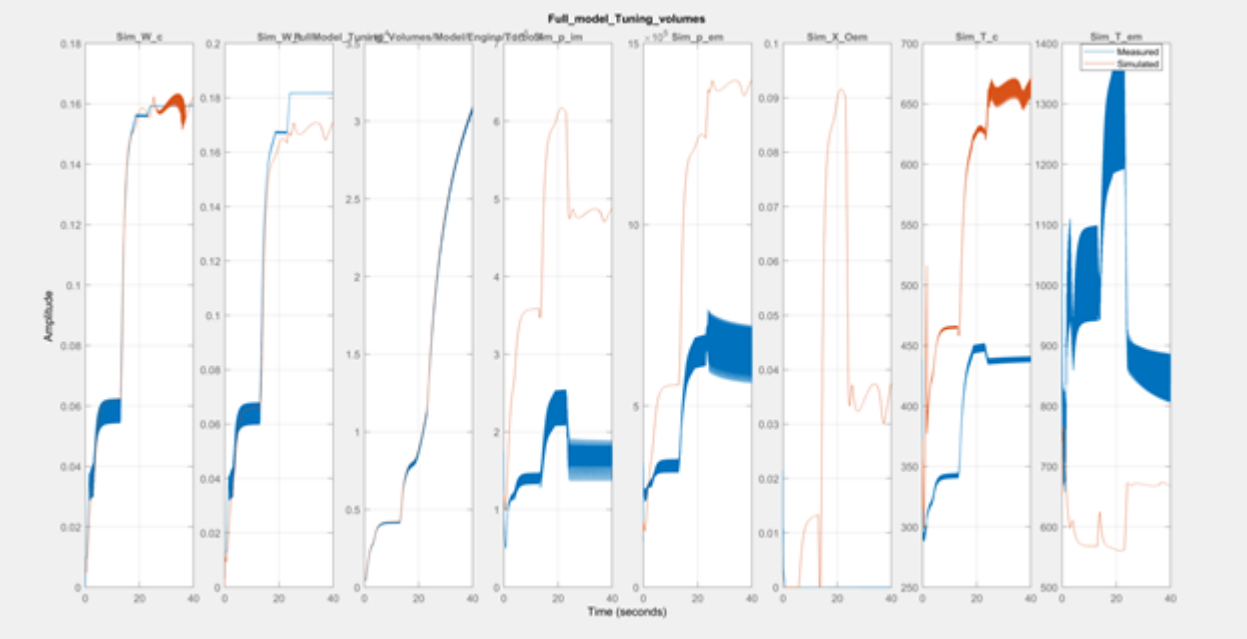

Figure 3.34. Full Model Results before Tuning

To address this issue of validation, model is tuned for the WHSC cycle itself to estimate the volumes. Model setup for input and outputs is kept same, but transient outputs are filtered by using the first order low pass filter allowing 0.1Hz signals only to smooth the intake

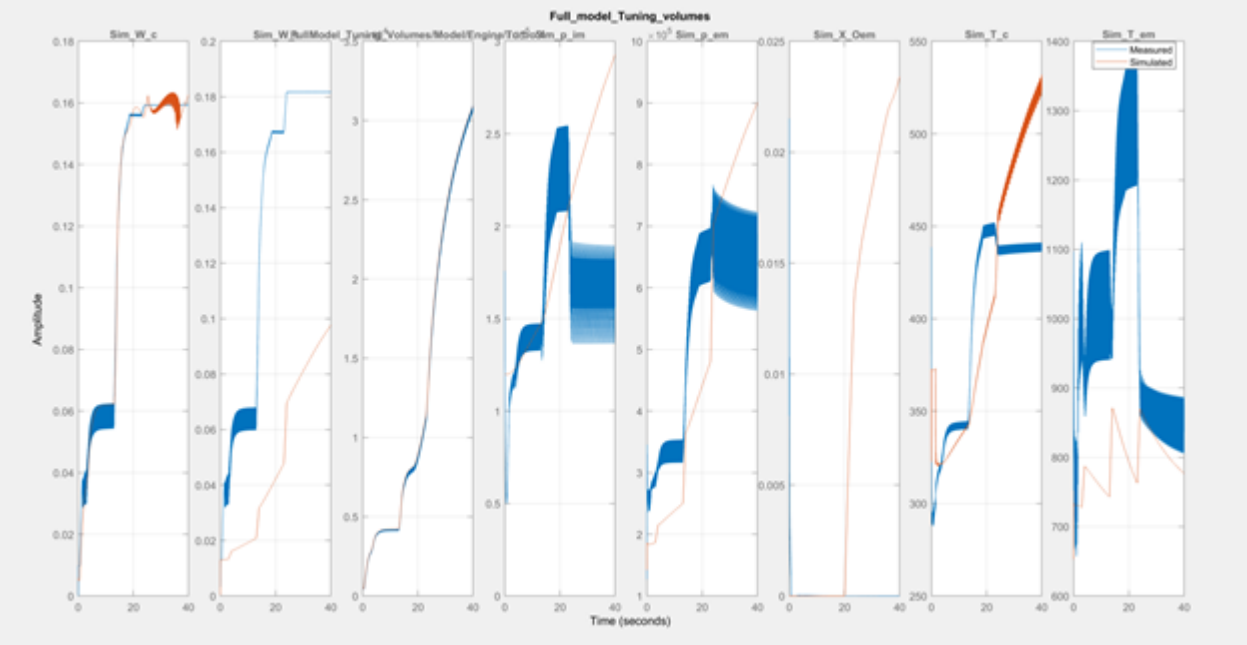

Figure 3.35. Full Model Results after Tuning

manifold pressure and exhaust manifold pressure and temperature. It is seen from the tuning results that the intake and exhaust manifold temperature are not tracing the reference after the 23rd second i.e. third step indicating that the effect of errors in exhaust manifold temperature, turbine flow and power has carried forward to accumulate here. However, the model is fully tuned till this end except the volumes, and it adds an advantage of exploring the accepted bounds for the intake and exhaust manifold volumes. Intake manifold volume cannot be lesser than the cylinder volume (accepted physics indicating the concept of volumetric efficiency, refer equation 2.8. Thus, lowed bound is fixed for the further estimation. Similarly, exhaust manifold volume should be less than the cylinder volume considering the account of burned volume to produce the work. Thus, fixing the upper bound for the exhaust manifold volume. Further tuning is done with the above-mentioned session setup. It is observed that the simulated outputs follow the trend for the steps, but there is an offset that needed to be taken care by adding the offset gains that are tuned again for the same estimation setup. Model outputs for intake and exhaust manifold pressures are validated with the MARE of 8.33% and 9.67% respectively as shown in Figure 3.36 and Figure 3.37. It is seen that the simulated output for the pressures trace the reference GT-power outputs

with a few initial errors due to integral windup in the Simulink model. In addition, turbine speed peaks are also seemed to affect the intake pressure estimation at 100 percent load condition durations as shown in mentioned figure below.

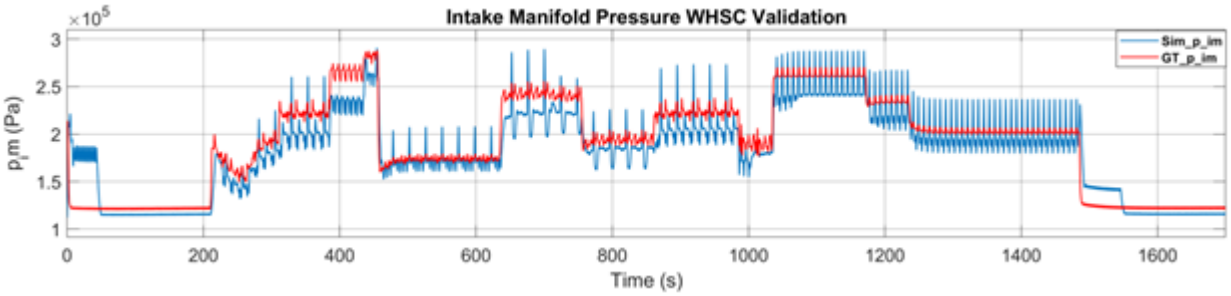

Figure 3.36. Intake Manifold Pressure WHSC Validation- Full Model

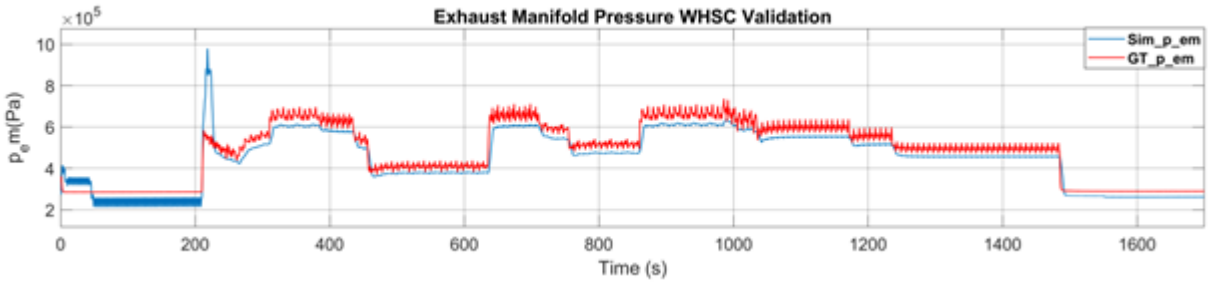

Figure 3.37. Exhaust Manifold Pressure WHSC Validation- Full Model

3.6 Full Model Validation

Manifold volumes are tuned according to the previous section that leads to the estimation of the required variables such as pressure and mass flows in and out to the cylinder. It is seen from the Figure 3.38 to Figure 3.44, that mass flows from the compressor and EGR, to cylinder are validated using the full integrated continuous model and error are given in the Table 3.3. Exhaust manifold temperature is also validated as it was for the individual system models. However, there are a few validation errors of more than 50 percent for turbine mass flow and power. These errors are due to the turbine speed estimation as mentioned in the turbine inertia model errors caused due to dynamic behavior of the turbine inertia model

for the step changes as discussed in previous section for the 100 percent load. Also, turbine inertia is tuned using the GT-power turbine speed data which has unexpected overshoots for the step changes.

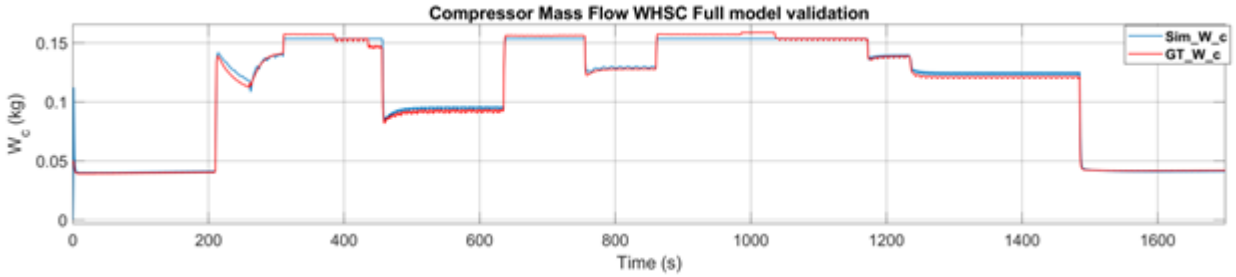

Figure 3.38. Compressor Flow WHSC Validation - Full Model

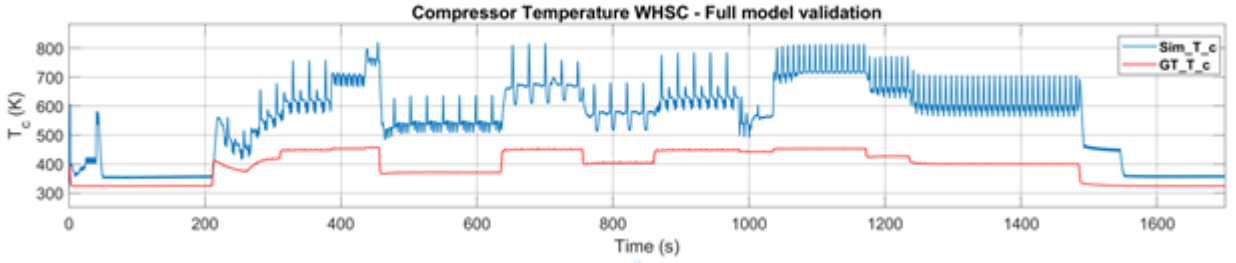

Figure 3.39. Compressor Temperature WHSC Validation - Full Model

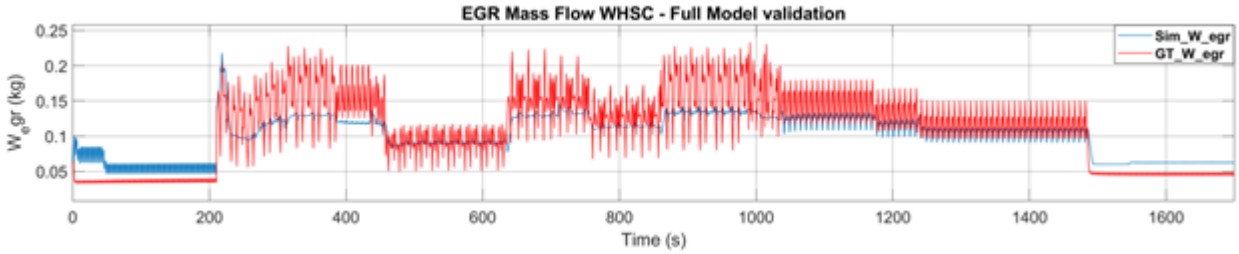

Figure 3.40. EGR Flow WHSC Validation - Full Model

From the validations results above, it is seen that the variables such as compressor flow, cylinder flow, EGR flow, exhaust manifold temperature and pressure, and intake manifold pressure show MARE of 2.07, 8.67, 25.43, 15.41, 9.67, and 8.33 percent errors, respectively. It indicates that there are -0.04, 1.81, 9.08, 0.12 percent increased errors in Compressor,

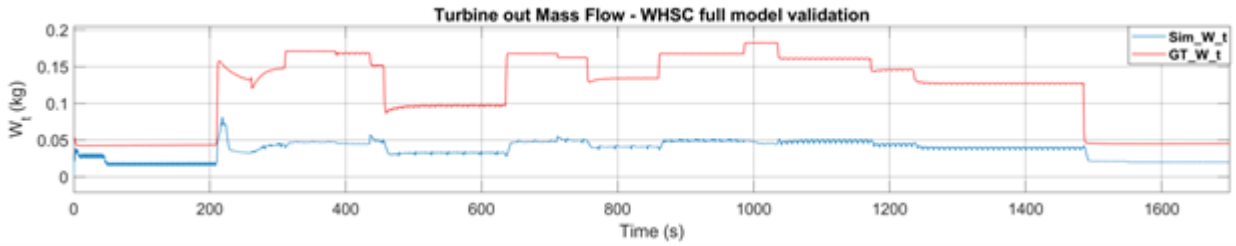

Figure 3.41. Turbine Out Flow WHSC Validation - Full Model

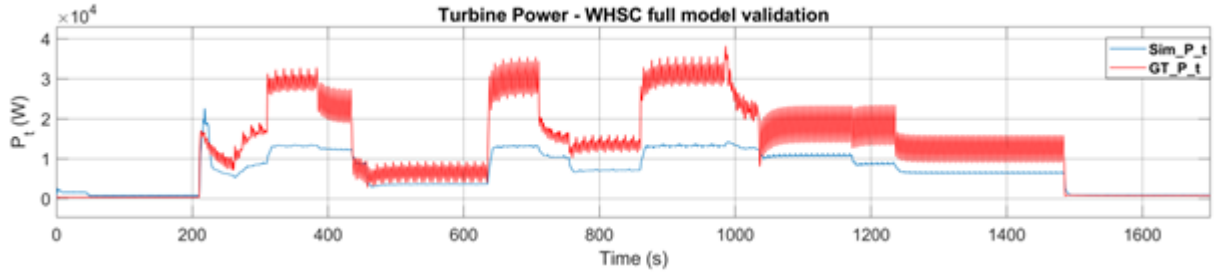

Figure 3.42. Turbine Power WHSC Validation - Full Model

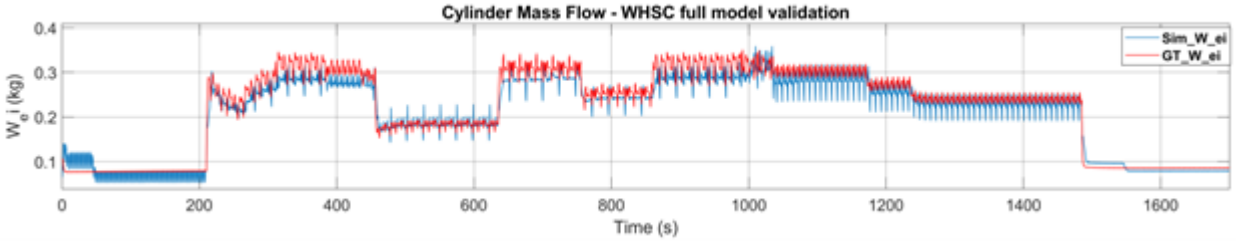

Figure 3.43. Cylinder Mass Flow WHSC Validation - Full Model

cylinder, EGR flow, and exhaust manifold temperature respectively as compared to the individual model validations. Whereas significant deviation in validation errors observed in turbine flow and power due to discussed reasons at 100 percent load as given in Table 3.3.

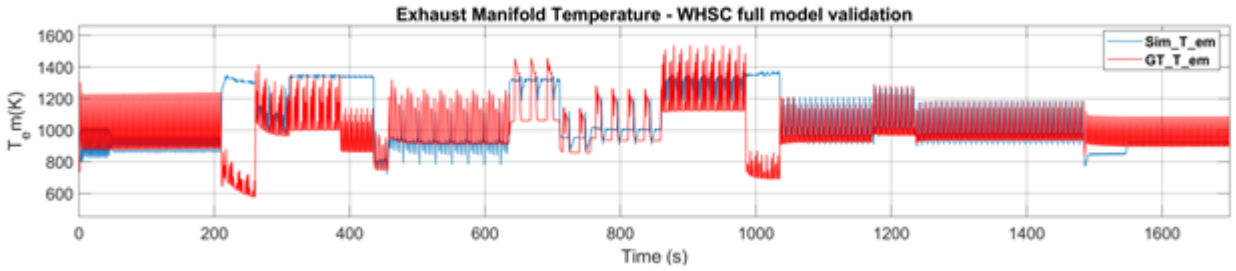

Figure 3.44. Exhaust Manifold Temperature WHSC Validation - Full Model

Table 3.3. Validation Mean Absolute Relative Errors for Individual and Full Model

Variable	Individual Model	Full Model
W_c	2.11	2.07
W_t	7.68	65
P_t	13.6	59.08
W_{egr}	16.35	25.43
W_{ei}	6.86	8.67
T_{em}	15.29	15.41
P_{im}	–	8.33
P_{em}	–	9.67

Although the errors are more that 50 percent in turbine variables as seen above, but accuracy of the desired variables for the NOx model such as mass and temperature entering and leaving the cylinder is more than 88.4 percent in average. Thus, estimated states are then used for the NOx model tuning and validation as given in the section 3.7.

3.7 NOx Model Validation

As discussed in section 2.2.3, NOx is a function of adiabatic temperature, oxygen-to-fuel ratio (lambda). Further accurate prediction of temperature depends on the heat loss due to radiation, dissociation, and turbulence while mass exchange and mixing in cylinder. A radiative temperature drop function in included to correct the adiabatic temperature and tuned for the radiative constant C_{rad} as given in equation 2.54. Figure 3.45 shows the estimation of C_{rad} for the same. It is seen that adiabatic temperature depends on the chemical equilibrium solver which is an iterative method of estimating temperature based

on the enthalpy taken from standard enthalpy data and fuel composition. First order filter was applied to take care of the noise from the measure data for NOx. Estimated radiative constant is too low, that corrected the temperature in the estimation.

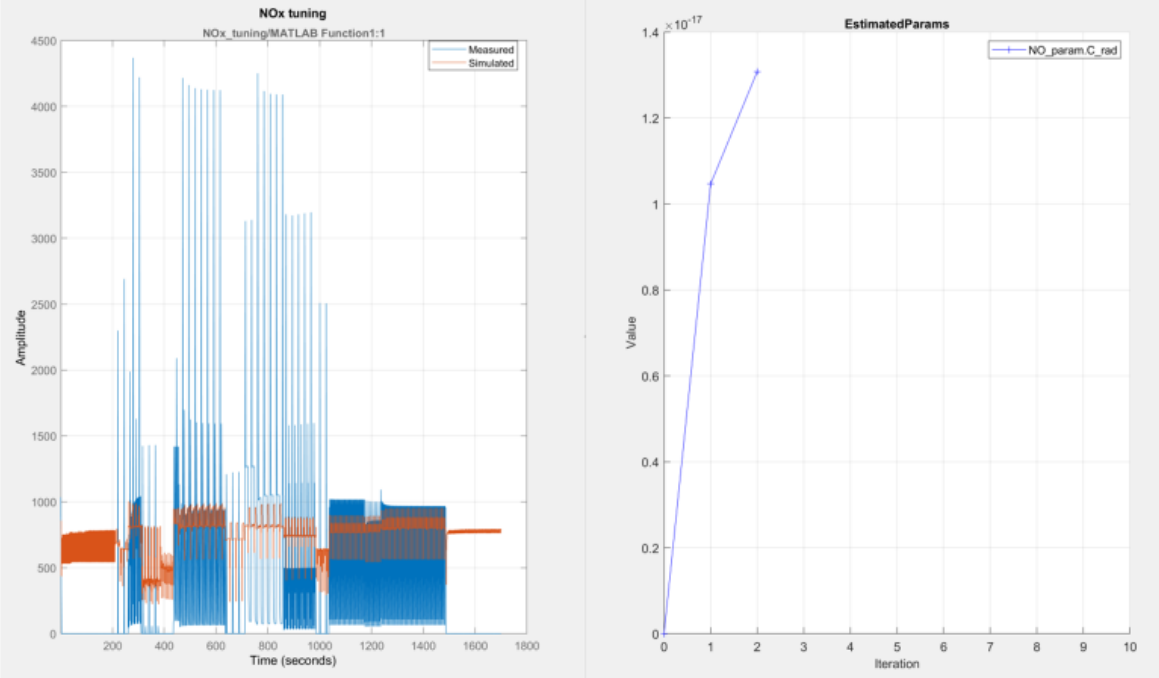

Figure 3.45. NOx Model Tuning for Heat Loss

Figure 3.46 shows validation of the NOx model for the WHSC. It is seen from the results; NOx prediction is capturing the dynamic changes in the cycle load and speeds.

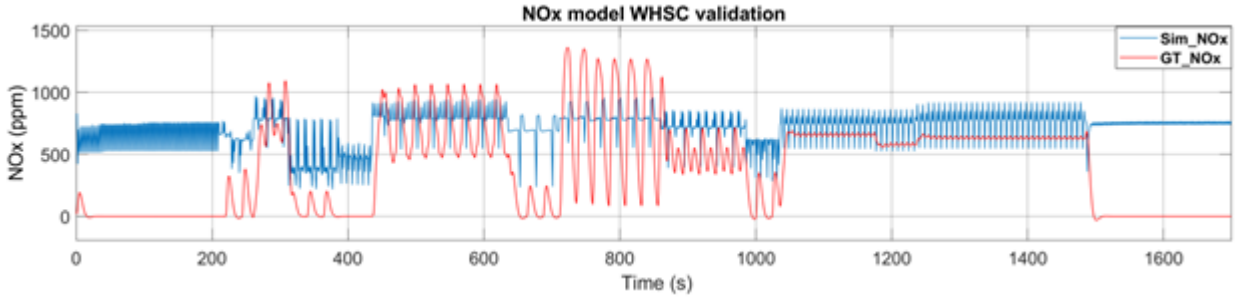

Figure 3.46. NOx Validation - WHSC

However, it is not capturing the trend for initial and final warm up and cool down phases of the cycle. This is due to errors in pressure and temperature estimation in cylinder. More-

over, it is seen that the radiative heat loss constant the mentioned phases is different based, and it is not estimated as an adaptive variable. Most important, combustion events like SOI to EOC are same for the entire cycler and are not changing that causes the peak pressure and temperature estimation. But model shows better estimates in cycle from 200s to 1500s capturing the changes in speed and load and within the experimental values. Total NOx produced is also analyzed and shown in Figure 3.47. It shows that almost twice the amount of total NOx was estimated as compared to the GT model. Note that, NOx prediction is done in this work for warm up and cool down cycle are not given by the GT-model. That indicates that the model is capable of predicting the NOx such conditions. But validation of this phase can only be achieved with the actual data from the test experiments.

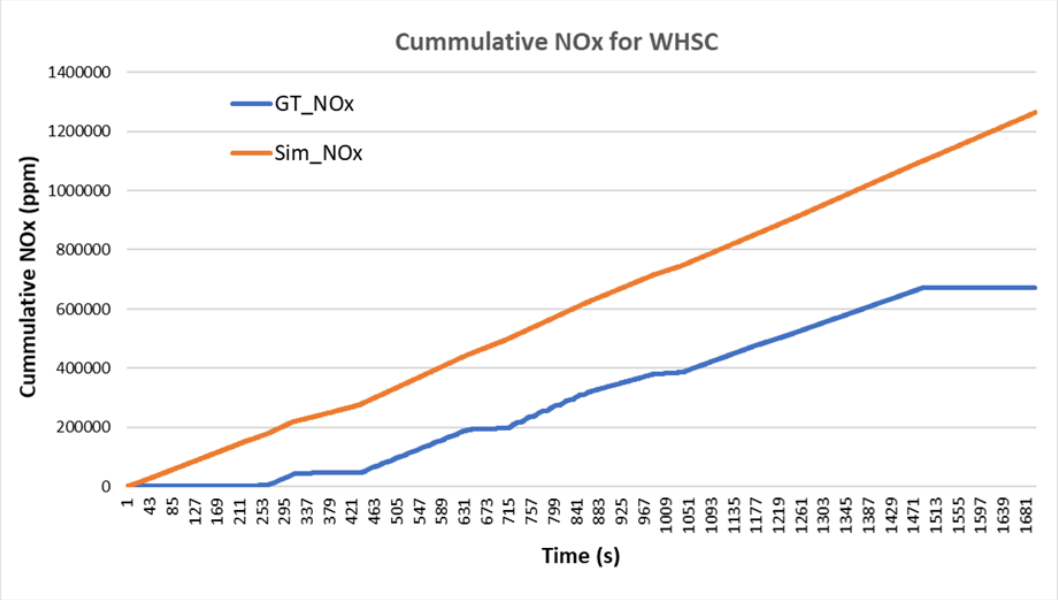

Figure 3.47. Total NOx in ppm for Complete Cycle

4. CONCLUSION AND FUTURE WORK

4.1 Conclusion

With the updated stringent regulations by the various environmental agencies across the world for emissions from the diesel engine has made the engine development process complex and challenging. To address the complexity of engine development and control, accurate estimation of in-cylinder parameters and engine out emission prediction is the key area of research. This thesis presents a method to develop the physics-based modeling, estimation, and validation to predict the in-cylinder states and emission for diesel engine. Cummins 6.7L turbo diesel engine virtual model in GT-power is considered as an application of interest for the bench-marking and validation. A physics-based model of a diesel engine equipped with EGR and VGT was adopted for further development of a CAD based combustion and NOx model to predict the in-cylinder parameters. CAD based combustion is developed using rate of heat release rates (ROHR) that are function of mass fractions burnt (MFB). A chemical equilibrium solver is developed to present the thermochemistry involved in the cylinder during combustion that predicts the adiabatic temperature and peak pressures. The Extended Zeldovich mechanism is used to predict EO NOx, that incorporates the reaction volumes zones for burnt masses and formation time and adiabatic temperature correction. The model and NOx function are developed in MATLAB and Simulink tool that depicts the behavior of dynamic equation involved. This model is then tuned for the unknowns using Least squared method in Parameter Estimator tool from MATLAB and Simulink's global optimization toolbox for model-based design. Model is tuned for both stationary and dynamic test points to achieve the accurate dynamic behavior. Considering a need for global strategies for engine testing, world harmonized stationary cycle is adopted for the validation using 13-point test procedure. Model tuning is done for individual systems as well as considering a complete model to account the overall modeling errors. Model is validated for both individual component and integrated system and showed promising accuracy of 88.4 percent in estimating the desired states such as cylinder temperature, pressure, and mass flow. The reduced accuracy is observed due to the cumulative effect of individual models accuracy. A few states have undesirable errors because of the turbine flow estimation, but

it does not affect the further EO NOx estimation. Finally, NOx estimation results are shown better accuracy in a particular operating phase. It is also noted that NOx developed here predicts the warm-up and cool down phase emission that are not validated because of the unavailability of actual engine test data. In conclusion, the detailed combustion and emission model developed in this work when integrated with the previously developed air-path model is able to estimate the desired in-cylinder variables required for the NOx prediction. In addition, model tuning method with both steady state and dynamic points is attempted with limited but significant portion of operating data. This method could successfully calibrate the model for WHSC validation against the virtual engine. Thus, reducing the high-volume data required and number experiments performed as adopted by the previous works mentioned in research gap. Therefore, this model development technique can be utilized for fast calibration and controller development for any engine equipped with EGR and VGT.

4.2 Future Work

There is an extensive potential in development of physics-based modeling for diesel engine in terms of making the models as detailed as possible by considering all possible dynamics involved. For example, there are many parameters such as various gas constant, time constants, combustion events (SOI, SOC, etc.), fractions, efficiencies, ambient conditions, specific heat capacities etc. are assumed to be constant here. These parameters can be modelled accurately to account for the real-time values. This work does not model the fuel injection system, which can be added to increase the model fitness. Parameter estimation of the unknown is done using the virtual engine. Using the actual test data for the tuning will be useful more accurate parameter estimation and validation. Consideration of actuator dynamics is needed in future to model the EGR and VGT actuator responses. This will increase the robustness of the model for controller development. Detailed NOx model considering the flame propagation and mixing of residuals will lead to the more accurate model. Detection of combustion events such as SOI to EOC can be estimated by online parameter estimation for better extraction of the cylinder variables. NOx controller developed based

on this model will lead to the in-cylinder NOx control by controlling fuel, EGR and VGT. In conclusion, accuracy and robustness of the model can be increased further by adding more degrees of freedom in modeling by including more detailed physics and chemistry involved in combustion phenomena.

REFERENCES

[1] *Transportation statistics annual report 2016 — bureau of transportation statistics*, https://www.bts.gov/content/transportation-statistics-annual-report-2016, (Accessed on 04/24/2021), Sep. 2017.

[2] *Federal highway administration (2017a), highway statistics—2016, washington DC: Federal highway administration, U S department of transportation.* https://www.fhwa.dot.gov/policyinformation/statistics/2016/pdf/hf10b.pdf, (Accessed on 04/23/2021), 2016.

[3] *Motorization rate 2015 – Worldwide, International Organization of Motor Vehicle Manufacturers — www.oica.net*, https://www.oica.net/world-vehicles-in-use-all-vehicles-2/, (Accessed on 04/23/2021), 2015.

[4] *Air pollutant emissions trends data — air emissions inventories — US EPA*, https://www.epa.gov/air-emissions-inventories/air-pollutant-emissions-trends-data, (Accessed on 04/23/2021), 2020.

[5] *Regulations for smog, soot, and other air pollution from commercial trucks & buses — regulations for emissions from vehicles and engines — US EPA*, https://www.epa.gov/regulations-emissions-vehicles-and-engines/regulations-smog-soot-and-other-air-pollution-commercial, (Accessed on 04/23/2021), Dec. 2016.

[6] V. Ahire, M. Shewale, and A. Razban, "A review of the state-of-the-art emission control strategies in modern diesel engines," *Archives of Computational Methods in Engineering*, pp. 1–19, 2021.

[7] H. He and L. Jin, "A historical review of the us vehicle emission compliance program and emission recall cases," *White paper*, 2017.

[8] *Highway statistics 2016 - policy — Federal Highway Administration*, https://www.fhwa.dot.gov/policyinformation/statistics/2016/pdf/vm1.pdf, (Accessed on 04/25/2021), 2016.

[9] J. Rissman and H. Kennan, "Advanced diesel internal combustion engines," *Case Studies on the Government's Role in Energy Technology Innovation, American Energy Innovation Council*, 2013.

[10] A. Al-Durra, "Survey of the state of affairs in diesel engine control," *J Appl Biotechnol Bioeng*, vol. 5, no. 4, pp. 279–285, 2018.

[11] X. Seykens, "Development and validation of a phenomenological diesel engine combustion model [ph. d. thesis]," *Eindhoven University of Technology, Eindhoven, The Netherlands*, 2010.

[12] N. Docquier and S. Candel, "Combustion control and sensors: A review," *Progress in energy and combustion science*, vol. 28, no. 2, pp. 107–150, 2002.

[13] P. Andersson, L. Eriksson, and L. Nielsen, "Modeling and architecture examples of model based engine control," in *Proceedings of the Second Conference on Computer Science and Systems Engineering. Linköping, Sweden*, Citeseer, 1999.

[14] R. Isermann and H. Sequenz, "Model-based development of combustion-engine control and optimal calibration for driving cycles: General procedure and application," *IFAC-PapersOnLine*, vol. 49, no. 11, pp. 633–640, 2016.

[15] M. Yao, H. Liu, and Z. Zheng, "Fuel chemistry and mixture stratification in hcci combustion control," *Green Energy and Technology*, p. 219, 2012.

[16] R. Stanglmaier and C. Roberts, "Homogeneous charge compression ignition (hcci): Benefits, compromises, and future engine applications," *SAE transactions*, pp. 2138–2145, 1999.

[17] N. Watson, A. Pilley, and M. Marzouk, "A combustion correlation for diesel engine simulation," SAE Technical Paper, Tech. Rep., 1980.

[18] I. Vibe, "Semi-empirical expression for combustion rate in engines," in *Proc. Conference on Piston Engines, USSR Academy of Sciences, Moscow*, 1956, pp. 185–191.

[19] H. Wolfer, "Ignition lag in diesel engines," *VDI-Forschungsheft*, vol. 392, pp. 621–436, 1938.

[20] G. Woschni and F. Anisits, "Experimental investigation and mathematical presentation of rate of heat release in diesel engines dependent upon engine operating conditions," SAE Technical Paper, Tech. Rep., 1974.

[21] H. C. Krijnsen, W. E. van Kooten, H. P. A. Calis, R. P. Verbeek, and C. M. v. d. Bleek, "Prediction of nox emissions from a transiently operating diesel engine using an artificial neural network," *Chemical Engineering & Technology: Industrial Chemistry-Plant Equipment-Process Engineering-Biotechnology*, vol. 22, no. 7, pp. 601–607, 1999.

[22] D. Lee and C. J. Rutland, "Probability density function combustion modeling of diesel engines," *Combustion science and technology*, vol. 174, no. 10, pp. 19–54, 2002.

[23] A. Parlak, Y. Islamoglu, H. Yasar, and A. Egrisogut, "Application of artificial neural network to predict specific fuel consumption and exhaust temperature for a diesel engine," *Applied Thermal Engineering*, vol. 26, no. 8-9, pp. 824–828, 2006.

[24] H. Hiroyasu, T. Kadota, and M. Arai, "Development and use of a spray combustion modeling to predict diesel engine efficiency and pollutant emissions: Part 1 combustion modeling," *Bulletin of JSME*, vol. 26, no. 214, pp. 569–575, 1983.

[25] G. Stiesch and G. P. Merker, "A phenomenological model for accurate and time efficient prediction of heat release and exhaust emissions in direct-injection diesel engines," SAE Technical Paper, Tech. Rep., 1999.

[26] H. Stebler, G. Weisser, H.-U. Horler, and K. Boulouchos, "Reduction of nox emissions of di diesel engines by application of the miller-system: An experimental and numerical investigation," *SAE transactions*, pp. 1238–1248, 1996.

[27] G. P. Merker, B. Hohlbaum, and M. Rauscher, "Two-zone model for calculation of nitrogen-oxide formation in direct-injection diesel engines," *SAE Transactions*, pp. 2043–2050, 1993.

[28] M. Andersson, B. Johansson, A. Hultqvist, and C. Noehre, "A predictive real time nox model for conventional and partially premixed diesel combustion," *SAE Transactions*, pp. 863–872, 2006.

[29] G. Bruneaux, "Mixing process in high pressure diesel jets by normalized laser induced exciplex fluorescence: Part i: Free jet," *SAE transactions*, pp. 1444–1461, 2005.

[30] F. G. Chmela and G. C. Orthaber, "Rate of heat release prediction for direct injection diesel engines based on purely mixing controlled combustion," *SAE transactions*, pp. 152–160, 1999.

[31] Y. B. Zeldovich, "26. oxidation of nitrogen in combustion and explosions," in *Selected Works of Yakov Borisovich Zeldovich, Volume I*, Princeton University Press, 2014, pp. 404–410.

[32] G. A. Lavoie, J. B. Heywood, and J. C. Keck, "Experimental and theoretical study of nitric oxide formation in internal combustion engines," *Combustion science and technology*, vol. 1, no. 4, pp. 313–326, 1970.

[33] C. Fenimore, "Formation of nitric oxide from fuel nitrogen in ethylene flames," *Combustion and Flame*, vol. 19, no. 2, pp. 289–296, 1972.

[34] J. Wolfrum, "Bildung von stickstoffoxiden bei der verbrennung," *Chemie Ingenieur Technik*, vol. 44, no. 10, pp. 656–659, 1972.

[35] D. R. Tree and K. I. Svensson, "Soot processes in compression ignition engines," *Progress in energy and combustion science*, vol. 33, no. 3, pp. 272–309, 2007.

[36] L. Guzzella and A. Amstutz, "Control of diesel engines," *IEEE Control Systems Magazine*, vol. 18, no. 5, pp. 53–71, 1998.

[37] C. Ericson, B. Westerberg, M. Andersson, and R. Egnell, "Modelling diesel engine combustion and nox formation for model based control and simulation of engine and exhaust aftertreatment systems," SAE Technical Paper, Tech. Rep., 2006.

[38] E. Klampfl, J. Lee, D. Dronzkowski, and K. Theisen, "Engine calibration process optimization.," in *ICORES*, 2012, pp. 335–341.

[39] S. Duraiarasan, R. Salehi, A. Stefanopoulou, S. Mahesh, and M. Allain, "Control-oriented physics-based nox emission model for a diesel engine with exhaust gas recirculation," *ASME Letters in Dynamic Systems and Control*, vol. 1, no. 1, 2021.

[40] L. Eriksson and A. Thomasson, "Cylinder state estimation from measured cylinder pressure traces-a survey," *IFAC-PapersOnLine*, vol. 50, no. 1, pp. 11 029–11 039, 2017.

[41] E. Rosseel, R. Sierens, and R. Baert, "Evaluating piezo-electric transducer response to thermal shock from in-cylinder pressure data," *SAE Transactions*, vol. 108, pp. 1431–1446, 1999, ISSN: 0096736X, 25771531. [Online]. Available: http://www.jstor.org/stable/44743470.

[42] A. Kalyankar, A. Munnannur, and Z. G. Liu, "Cfd modeling of tailpipe nox sensor accuracy," *SAE International Journal of Engines*, vol. 11, no. 4, pp. 435–446, 2018.

[43] B. Unver, Y. Koyuncuoglu, M. Gokasan, and S. Bogosyan, "Modeling and validation of turbocharged diesel engine airpath and combustion systems," *International Journal of Automotive Technology*, vol. 17, no. 1, pp. 13–34, 2016.

[44] J. Wahlström and L. Eriksson, "Modelling diesel engines with a variable-geometry turbocharger and exhaust gas recirculation by optimization of model parameters for capturing non-linear system dynamics," *Proceedings of the Institution of Mechanical Engineers, Part D: Journal of Automobile Engineering*, vol. 225, no. 7, pp. 960–986, 2011.

[45] P. Skogtjärn, P. Scania, C. Ab, R. Nr Lith-isy-ex, S. D. Elfvik, S. C. Ab, and J. B. Msc, "Modelling of the exhaust gas temperature for diesel engines," 2002.

[46] L. Eriksson, "Mean value models for exhaust system temperatures," *SAE Transactions*, pp. 753–767, 2002.

[47] J. E. Dec, "A conceptual model of dl diesel combustion based on laser-sheet imaging," *SAE transactions*, pp. 1319–1348, 1997.

[48] J. B. Heywood, *Internal combustion engine fundamentals*. McGraw-Hill Education, 2018.

[49] N. Savva and D. Hountalas, "Detailed evaluation of a new semi-empirical multi-zone no x model by application on various diesel engine configurations," SAE Technical Paper, Tech. Rep., 2012.

[50] X. Seykens, R. Baert, L. Somers, and F. Willems, "Experimental validation of extended no and soot model for advanced hd diesel engine combustion," *SAE International Journal of Engines*, vol. 2, no. 1, pp. 606–619, 2009.

[51] *Cummins 6.7l turbo diesel (2018) — cummins inc.* https://www.cummins.com/engines/67l-cummins-turbo-diesel-2018, (Accessed on 04/23/2021).

[52] M. Shewale, A. Razban, and V. Ahire, *Design & implementation of the engine out virtual nox and soot sensor for diesel engines*, https://www.gtisoft.com/wp-content/uploads/2020/11/, (Accessed on 04/26/2021).

[53] Cumminshub.com, *6.7l cummins isb turbodiesel specs*, http://www.cumminshub.com/67.html, (Accessed on 04/23/2021).

[54] H. Steven, *Vehicle regulations — UNECE*, https://unece.org/transport/vehicle-regulations, (Accessed on 04/25/2021).

PUBLICATIONS

1. V. Ahire, M. Shewale and A. Razban, "A Review of the State-of-the-Art Emission Control Strategies in Modern Diesel Engines. Archives of Computational Methods in Engineering," Archives of Computational Methods in Engineering, pp. 1-19, 2021, March 10, 2021